Norwegian University
of Life Sciences

Transfer of river-discharged Cs-137 in estuaries

- A case study from Vefsna river and the Vefsnfjord   in Norland, Norway.

Marie Larsen
Chemistry and biotechnology

Acknowledgements

Marie Larsen

December 15th 2021.

Abstract

Several decades after the Chernobyl accident, it is still detectable activities of Cs-137 in the environment. Norway was highly affected by radioactive fallout, where one of the locations that received the highest doses of Cs-137 was Nordland county. Recent studies have shown that the Vefsnfjord is amongst the fjords in Norway with highest activity of Cs-137. The Vefsna river feeds into the Vefsnfjord, creating an estuarine environment with a brackish surface layer, and an increasing salinity gradient outward the fjord. In this work, Cs-137 in the estuarine environment has been studied in water, sediments, and biota to identify changes in speciation, mobility, and bioavailability of Cs-137 outward the Vefsnfjord with increased salinity and distance to the river outlet.

The activity concentration of Cs-137 in water decreased as the salinity increased, from 4.0 ± 0.6 Bq/m^3 to 3.0 ± 0.2 Bq/m^3. By performing *in situ* fractionation of water and measuring activity of Cs-137 using HPGe-detector, it was reviled that the dominating specie was LMM in both freshwater and seawater, with low activity concentration of colloids ($<0.86 \pm 0.14$ Bq/m^3) and particles (0.55 ± 0.087 Bq/m^3) in freshwater. Cs-137 associated with river discharged colloids and particles was only identified in the lowest salinity in the estuary (5 PSU) and was lower than estimated by dilution. On the contrary, activity concentration of LMM species was slightly increased in low salinity seawater compared with the riverine water and, and higher than estimated by dilution, likely caused by remobilization from river transported colloids and particles.

Grain size analysis of surface sediments showed that the riverine sediments mostly consisted of sand (>90%), while silt (45-86%) was the dominating size fraction in marine sediments. The content of clay was generally low (0.03-2%). The mineral structure was established by performing XRD analysis, where the silt samples consisted mostly of quartz and albite, while clay contained muscovite. The activity concentration of Cs-137 in sediments increased with increased distance outwards the fjord (from 35 ± 1.5 Bq/kg to 152 ± 6.0 Bq/kg), which can be explained by reduced content of sand, while the content of silt increased. Results show that the activity concentration of Cs-137 in sand was low ($<66 \pm 7.3$ Bq/kg), while the activity concentration of Cs-137 in silt was higher, especially in the riverine sediments (529 ± 16 Bq/kg). However, the highest activity concentration of Cs-137 was found in riverine clay (3631 ± 28 Bq/kg). While it was no significant change activity concentration of Cs-137 in sand from

marine sediments compared to riverine sediments, a significant reduction in activity concentration was observed for silt and clay.

Sequential extraction of silt and clay from riverine- and marine sediments showed that Cs-137 was irreversibly bound to both silt and clay, as 42-58% of Cs-137 was extracted with 7 M nitric acid, while the remaining Cs-137 was left in the residue. Cs-137 bound to silt showed somewhat higher mobility than Cs-137 bound to clay, but it was no significant difference in mobility between riverine sediments and marine sediments. Apparent K_d values for Cs-137 showed an increasing trend for sediments (total) with increased distance out the fjord from $(7.4 \pm 0.99) \cdot 10^3$ L/kg to $(2.6 \pm 0.26) \cdot 10^4$ L/kg. The K_d was high for silt $((1.1 \pm 0.15) \cdot 10^5$ L/kg) and clay $((5.5 \pm 0.74) \cdot 10^5$ L/kg) from riverine sediments, but a significant decrease in K_d was observed for silt and clay in brackish water. However, based on the results from sequential extraction, it is unlikely that remobilization of Cs-137 from silt and clay is the cause of decreased K_d in marine sediments.

The biological uptake of Cs-137 was studied in seaweed (*F.vesiculosus, L.digitata*) and blue mussels (*M.edulis*) from various locations in the Vefsnfjord. However, the activity concentration in seaweed was low (0.65 ± 0.04 Bq/kg – 1.04 ± 0.04 Bq/kg), and under the detection limit (<0.17 Bq) in blue mussels. The BCF in seaweed (171 ± 21 L/kg - 247 ± 25 L/kg) was higher than reported in IAEA handbooks. The highest activity concentration and BCF was obtained in a mixed sample containing seaweed from the inner parts of the fjord, suggesting that the uptake was higher in low salinity water.

Based on the obtained results in this study, it can be established that the speciation of Cs-137 in freshwater from river Vefsna change upon mixing with seawater from the Vefsnfjord. LMM species is likely to have remobilized from suspended particles and colloids originating from the Vefsna river. Surface sediments, however, seems not to be a significant contributor to remobilisation of LMM species. Further, LMM Cs-137 was prone to biological uptake, such as seaweed. The results highlight the importance of obtaining knowledge about the processes affecting the speciation, mobility and biological uptake of radionuclides, in order to predict the transfer of radionuclides in estuaries and coastal areas.

Sammendrag

Flere tiår etter Tsjernobylulykken er det fortsatt målbare aktivitetsnivåer av Cs-137 in miljøet. Norge var sterkt påvirket av radioaktivt nedfall, og et av områdene som mottok de høyeste dosene var Nordland fylke. Nyere studier viser at Vefsnfjorden er en av fjordene i Norge med høyest aktivitet av Cs-137. Elven Vefsna munner ut i Vefsnfjorden og danner et estuar med et øvre brakkvannslag, og en økende saltgradient utover fjorden. I dette arbeidet har Cs-137 i vann, sedimenter og biota blitt undersøkt for å identifisere endringer i tilstandsformer, mobilitet og biotilgjengelighet med økt salinitet og avstand fra elvemunningen.

Aktivitetskonsentrasjonen av Cs-137 i vann viste en avtakende trend med økt salinitet, fra 4.0 ± 0.6 Bq/m^3 to 3.0 ± 0.2 Bq/m^3. Ved å utføre *in situ* fraksjonering av vann og ved å måle aktivitet av Cs-137 ved bruk av HPGe-detektor, fremkom det at LMM var den dominerende tilstandsformen, både i ferskvann og i sjøvann, og med lav aktivitetskonsentrasjon av kolloider (<0.86 ± 0.14 Bq/m^3) og partikler (0.55 ± 0.087 Bq/m^3) i ferskvann. Cs-137 assosiert med kolloider fraktet med elvevannet var kun identifisert i de laveste salinitetene i estuariet (5 PSU) og var lavere enn estimert med hensyn på fortynning. Derimot var aktivitetskonsentrasjonen av LMM -tilstandsformer noe forhøyet i sjøvann med lav salinitet sammenliknet med ferskvann, og høyere enn estimert med hensyn på fortynning. Dette er trolig på grunn av remobilisering fra kolloider og partikler fraktet med elvevannet.

Kornfordelingsanalyse av sedimenter viste at elvesediment hovedsakelig bestod av sand (>90%), mens silt (45-86%) var dominerende størrelsesfraksjon i sjøsediment. Det var generelt lavt innhold av leire (0.03-2%). Mineralstrukturen ble bestemt ved å anvende XRD analyse, der siltfraksjonen hovedsakelig bestod av kvarts og albitt, mens leire inneholdt muskovitt. Aktivitetskonsentrasjonen av Cs-137 i sedimentene økte med økt avstand utover fjorden (fra 35 ± 1.5 Bq/kg til 152 ± 6.0 Bq/kg), som kan forklares med redusert innhold av sand utover fjorden, mens andelen silt økte. Resultatet viste at aktivtetskonsentrasjonen av Cs-137 i sand var lav (<66 ± 7.3 Bq/kg), mens aktivitetskonsentrasjonen i silt var høyere, da særlig i elvesediment (529 ± 16 Bq/kg). Leire fra elvesediment hadde den høyeste aktivitetskonsentrasjonen av Cs-137 (3631 ± 28 Bq/kg). Det var ingen endring i aktivitetskonsentrasjonen av Cs-137 i sand fra sjøsediment sammenliknet med elvesediment. Derimot var det observert en betydelig reduksjon observert for aktivitetskonsentrasjonen i silt og leire.

Sekvensiell ekstraksjon av silt og leire fra elve- og sjøsediment viste at Cs-137 var irreversibelt bundet til både silt og leire, da 42-58% av Cs-137 ble utlekket ved anvendelse av 7 M salpetersyre, mens resterende fraksjon av Cs-137 ble gjenværende i bunnfallet. Cs-137 bundet til silt syntes å være noe mindre mobilt en Cs-137 bundet til leire, men det var ingen signifikant forskjell mellom mobiliteten i elvesediment sammenliknet med sjøsediment. Fordelingskoeffisienten (K_d) for Cs-137 viste en økende trend med økt avstand utover fjorden fra $(7.4\pm 0.99)\cdot 10^3$ L/kg til $(2.6\pm 0.26)\cdot 10^4$. Det var høy K_d for silt og leire fra elvesediment, men med en signifikant reduksjon i brakkvann. Basert på resultatene fra sekvensiell ekstraksjon er det dog usannsynlig at remobilisering av Cs-137 fra silt og leire er årsaken til reduksjonen av K_d i sjøsediment.

Biologisk opptak av Cs-137 ble undersøkt i tang og blåskjell fra varierende lokasjoner i Vefsnfjorden. Aktivitetskonsentrasjonen i tang var lav (0.65 ± 0.04 Bq/kg – 1.04 ± 0.04 Bq/kg), og under deteksjonsgrense (<0.17 Bq) i blåskjell. Biokonsentrasjonsfaktoren (BCF) i sjøgress (171 ± 21 L/kg - 247 ± 25 L/kg) var høyere enn rapportert i IAEAs håndbøker. Den høyeste aktivitetskonsentrasjonen og BCF ble oppnådd i en blandeprøve som inneholdt tang fra de indre delene av fjorden, noe som tyder på høyere opptak i vann med lavere salinitet.

Basert på de oppnådde resultatene i dette studiet, kan det konkluderes med at tilstandsformene av Cs-137 i ferskvann fra Vefsna gjennomgår endringer når ferskvannet blandes med sjøvann fra Vefsnfjorden. Det er sannsynlig at LMM tilstandsformer har remobilisert fra partikler og kolloider som stammer fra Vefsna. Overflatesedimenter derimot, syntes ikke å være en betydelig bidragsyter til remobiliseringen av LMM. Videre ble LMM Cs-137 tatt opp i biota, slik som tang. Resultatene belyser viktigheten av å innhente kunnskap om prosessene som påvirker tilstandsformer, mobilitet og biologisk opptak av radionuklider slik at transporten til radionuklider gjennom estuarier og kystområder kan forutsees.

Content

1 Introduction

1.2 Background

Since the beginning of the nuclear area contamination of radionuclides in the environment has been of great concern. Several sources throughout the years have contributed to high levels of anthropogenic radionuclides (Povinec et al., 2003). One of the most problematic radionuclides is the fission product Cs-137, a high energy γ-emitter with a half-life of 30.08 years (Atwood, 2010; Dietz et al., 1963; Fedchenko, 2015). Especially the marine environment has been affected as a result of the large geographical area of the earth that is covered by ocean(Avery, 1996). The three main sources of Cs-137 pollution in the northern European seas are the nuclear weapons testing mainly in the 1950's and 1960's, the Chernobyl accident in 1986, and discharge from reprocessing power plant La Hauge and Sellafield (section 2.1). Norway was amongst the most affected areas after the Chernobyl accident and received great amounts of radioactive fallout. As of today, this is still one of the main sources of Cs-137 in Norway, decades after the accident (Gjelsvik R & Jensen L, 2014). Cesium deposited in the terrestrial environment can enter rivers and freshwater reservoirs through run-off, which composes an important and persistent source of cesium to the aquatic environment (Garcia-Sanchez & Konoplev, 2009). Rivers and run-off compose a great source of radionuclides to coastal waters and estuaries, especially during heavy rains and flooding events (Buesseler et al., 2017). Contaminated sediments and soils might act as a secondary source of Cs-137 through remobilization (Otosaka & Kobayashi, 2013).

Cesium can exist in different physico-chemical forms, or species, in the aquatic environment, ranging from dissolved species (LMM) to colloids and suspended particles, or associated with bottom sediments (Salbu et al., 2004). The speciation of Cs-137 influence the behaviour, like transfer, mobility, and bioavailability (section 2.4-2.6). However, in dynamic systems like estuaries and coastal areas where high salinity seawater mixes with freshwater from river inputs, the distribution of species might undergo drastic changes resulting from changes in salinity, pH and temperature or interaction with other components in the systems (Mosley & Liss, 2020). It is crucial for risk assessment to understand the behaviour of radionuclides in the environment, and a lot of research has been carried out through the years. Although this is a well-studied topic, it suffers from some lack of knowledge regarding the physical and chemical transfer in dynamic environments such as estuaries (Salbu, 2016). Transfer data like sediment-water distribution coefficients (K_d) and bioconcentration factors (BCF) are based on thermodynamic

constants based on reversible, equilibrium conditions. However, this is usually not the case in dynamic estuaries. Numerical models exist that predicts the transport of radionuclides in the environment (Periáñez et al., 2016; Simonsen et al., 2017; Vives I Batlle et al., 2018). However, the different physico-chemical forms are usually not accounted for in the models and in estuaries where activity concentrations and speciation change rapidly with time, dynamic models must be used (Simonsen et al., 2019a). Therefore, there are some great uncertainties associated with these data (Salbu, 2016). Simonsen et al. 2019 developed a model for estuaries that included dynamic transformation of radionuclide species. However, limited data exists to validate this estuarine model.

1.2 Main objectivities and hypothesises

The goal of this thesis was to investigate the transfer of Cs-137 through a salinity gradient from a river system and throughout an estuary using methods to characterize the speciation distribution in water, activity concentration in sediments and the bioaccumulation in biota as a function of increasing salinity outwards the fjord. By utilizing *in situ* fractionation techniques, the speciation distribution between LMM, colloids, and particles were characterized as a function of salinity. As the fate of the different species largely depend on their mobility and potential uptake in biota, sediment and biota samples were studied. Remobilization from sediments poses a potential threat to the marine environment, and the tendency do desorb was considered with sequential extraction, along with water-sediment concentration factors (K_d-value). The potential for uptake in biota was analysed by collecting samples of seaweed and blue mussels at different locations in the fjord.

The hypothesises in this thesis are:

H1: Vefsna river is the main source of Cs-137 input to the Vefsnfjord.

H2: The size distribution of Cs-137 species in riverine water changes upon mixing with seawater in the estuarine zone.

H3: Changes in salinity in the estuarine zone will affect the distribution coefficient (K_d) of Cs-137.

H4: The uptake of Cs-137 in biota will be higher in low salinities close to the river outlet compared to high salinity water.

2 Theory

2.1 Sources of Cs-137

2.1.1 The Chernobyl accident

The Chernobyl accident, which took place in 1986 in a nuclear power plant in Chernobyl, Ukraine, is the greatest nuclear accident to have occurred to this point. 1100 PBq of debris from the reactor accident spread unevenly with wind currents to different locations around the globe. Out of this, approximately 85 PBq consisted of Cs-137 (Povinec et al., 2003). Particularly Scandinavia was highly affected by deposition of several radionuclides, including Cs-134 and Cs-137. Deposition of the Cs isotopes occurred partly as dry deposit and partly as wet deposit in the means of rainfall, in which the latter is known to be crucial for the amount deposited. Estimated total amount of Cs-137 deposited in Norway was 2300 TBq per May 15th, 1986 (Backe et al., 1986). The Gudbransdalen, Valdres, Trøndelag, and Nordland counties were the Norwegian areas that received the highest doses (Figure 2.1). As of today, Cs-137 is still contributing to radiation doses because of the long half-Life of the isotope (Liland et al., 2001).
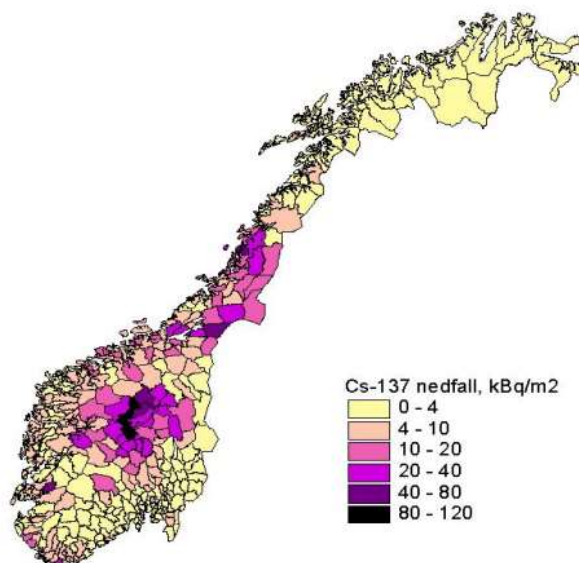
Figrue 2.1: *Deposition of Cs-137 in Norway after the Chernobyl accident (Liland et al., 2001).*

2.1.2 Nuclear weapons testing

Global fallout from nuclear weapons testing between 1945 and 1980 is the main contributor of Cs-137 released to the environment on a global scale, with a total of 453 tests carried out. It was especially in late 1950s and early 1960s that contributed the highest yields. The release of radionuclides from the tests was unrestrained, thus resulting in substantial quantities released into the environment (UNSCEAR, 2000). It was estimated that 102 PBq Cs-137 was released

in the North Atlantic Ocean, where 12 PBq was released to the Northern European Seas (Povinec et al., 2003). Radionuclides was transported over great distances and precipitated by rainfall. As a result, areas with frequent rainfall were affected more severely, such as in the western parts of Norway (Liland et al., 2001). However, most of the Cs-137 from the tests has now decayed after two half-lives has passed, thus only ¼ of the original activity.

2.1.3 Sellafield and La Hauge reprocessing power plants

Discharge containing radionuclides from the reprocessing plants Sellafield in England and La Hauge in France have also contributed to contamination of the marine environment. The total amount of discharge from Sellafield was estimated to be 41 PBq between 1952 to 1998, with a peak at the mid 1970's. The contribution of Cs-137 discharge from L Hauge to the Northern European Seas is smaller, with a total of 1 PBq from 1966 to 1998. Although the release of Cs-137 from both Sellafield and La Hauge have been significantly reduced over the years, it is still detectable levels in the seawater. Figure 2.2 illustrates how the activity of Cs-137 originating from Sellafield reprocessing plant has been reduced from 1976 to 1998. (IAEA, 2005; Povinec et al., 2003).
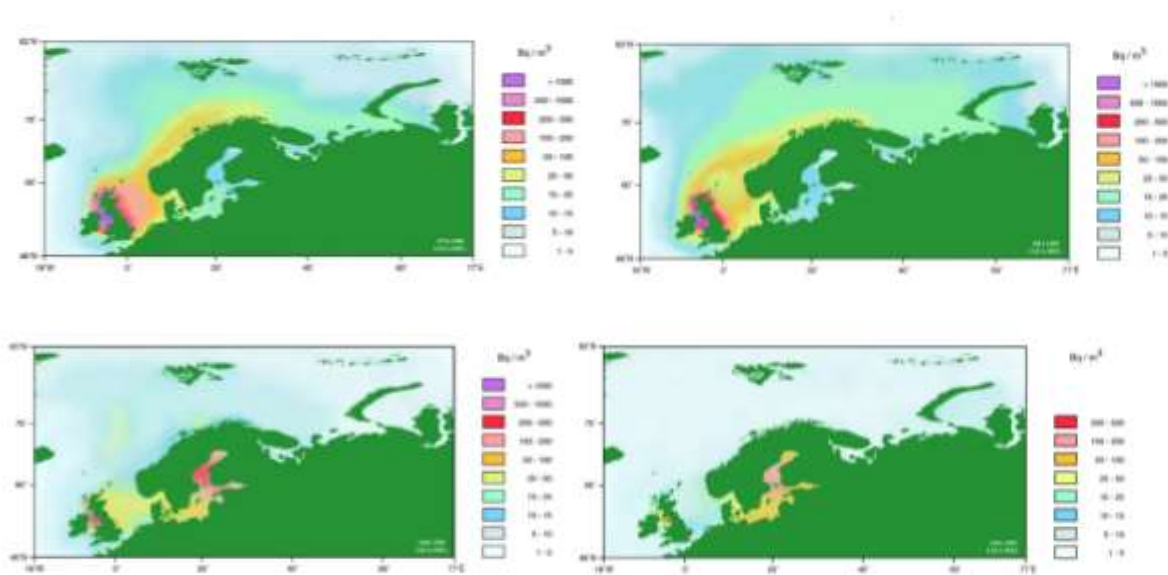
Figure 2.2: *Activity concentration of Cs-137 (Bq kg^{-1}) in the Northern European seas (1976-1995). (IAEA, 2005)*

2.2 Research location

The research sites for this thesis are the Vefsna river and Vefsnfjord, which are located in Nordland county. Vefsna with its surrounding catchment area was among the locations in Norway that was most affected by radioactive fallout from the Chernobyl accident.

The Vefsna river is 163 km long and runs into the Vefsnfjord. The Vefsnfjord is approximately 40 km long, counted from the river outlet to the orifice between Rødø and Tjøtta. At widest, the fjord is about 4 km, while it is approximately 1 km wide at the narrowest. The deepest point is at 485m. River Vefsna along with river Fusta are the main sources of freshwater to the Vefsnfjord, although there are also three smaller rivers (Drevja, Skjerva and Hundåla) which contributes to the freshwater supply. This thesis focuses on the Vefsna river, as this is the largest river and makes up most of the freshwater supply. The catchment area of Vefsnfjord is estimated to be 5100 km^2, of which 4119 km^2 makes up the catchment area surrounding Vefsna river (Molvær, 2010). There is a high degree of runoff from the terrestrial environment in Vefsna. A map over annual average runoff in Norway from the period 1961-1990 is presented in figure 2.3. According to the map, the catchment area surrounding the Vefsnfjord is contributing to a large amount of water runoff (up to >4000 mm per year) (Beldring et al., 2003).
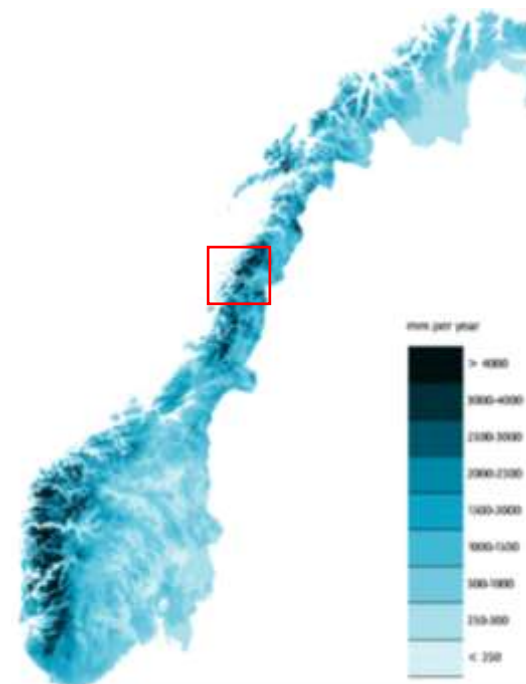
Figure 2.3: *Estimated annual average runoff in Norway between 1961 and 1990 (Beldring et al., 2003).*

The Vefsna watercourse is represented by multiple catchments and smaller rivers that mixes with river Vefsna. A selection of stations that all represents different catchments is presented in figure 2.4A. Eitårafoss, Svenningdalselva, and Joibakken are smaller tributaries that feeds into river Vefsna, and have separate catchments of 140, 474 and 2477 km^2, respectively. Station Laksfors is represented by a catchment of 3338 km^2. Mean runoff in the Vefsn watercourse is estimated to be approximately 50 L s^{-1} km^{-2}, with a variations between 140 L s^{-1} km^{-2} and 20 L s^{-1} depending on the area (Pettersson, 2004; Stenius, 2017). Figure 2.4 A-B shows a map over Vefsna river and the Vefsnfjord.

Figure 2.4: *Map over Vefsna river (A) and the Vefsnfjord (B).*

The mean water flow from the river outlet is estimated to be 170-175 m^3s^{-1}, although this estimate varies greatly due to flooding events and seasonal variation with a maximum flow rate of 1800 m^3s^{-1} (Molvær, 2010). Especially during autumn, the flooding events are more frequent due to rainfall. However, the highest waterflow is observed in May and June which is the snow melting season. The lowest flow rates are in the winter season, although occasional flooding event might occur (Pettersson, 2004; Stenius, 2017). The waterflow (m s^{-1}) out of Vefsna river into Vefsnfjord is illustrated in figure 2.5

Figure 2.5: *Simulation of the water flow in the brackish surface layer in the inner part of Vefsnfjord. Blue colour indicates highest velocity (1 m s^{-1}) while red represents 0 m s^{-1} (Molvær, 2010).*

Figure 2.5 shows how the Vefsna mixed with the Vefsnfjord, creating a brackish surface layer moving outward in the centre with some circulation towards the sides of the fjord. The flowrate of riverine freshwater determines the thickness of the upper layer of the saltwater wedge. The salinity will usually be between 0 - 5 PSU near the river outlet with waterflow over 130 m^{3}s^{-1} (Molvær, 2010). The salinity of the surface water is affected by the riverine water supply alongside tides and currents. The difference in density of freshwater and seawater creates a seawater wedge, where outflowing freshwater forms a layer on top of the seawater. This process is highly affected by tidal action (Uncles et al., 2015). A combination of low flooding events and high tide increases the salinity of the surface layer.

Activity concentration of Cs-137 in surface seawater from the Vefsnfjord have been reported to be in the range 2.3 - 4.4 Bq m^{-3}. The activity concentration of Cs-137 in surface sediments of Vefsnfjord have been reported to be in the range 137 - 268 Bq kg^{-1} (d.w) and among the highest collected along the Norwegian coast (Heldal et al., 2021; Skjerdal et al., 2015; Skjerdal et al., 2020).

2.3 Properties of cesium

Cesium is the rarest alkaline earth metal (Avery, 1996) and exists in the earth's crust at 2.6 ppm (Gad & Pham, 2014). Amongst the 40 known isotopes of cesium (Gupta & Walther, 2017), Cs-133 is the only naturally occurring isotope. One of the most concerning isotopes is the nuclear fission product Cs-137, as it emits high energy γ-radiation and has a relatively long half-life of 30.8 years (Atwood, 2010; Fedchenko, 2015).

Cs-137 disintegrates to Ba-137 or meta stable Ba-137m through β⁻ emission (figure 2.6). Ba-137m accounts for most of the total activity and is rapidly converted to stable Ba-137 by emitting γ-radiation as the half-life of Ba-137m is 2 minutes. The energy of the emitted γ-radiation is 0.662 MeV, which is used when measuring Cs-137 activity (Ashraf et al., 2014).
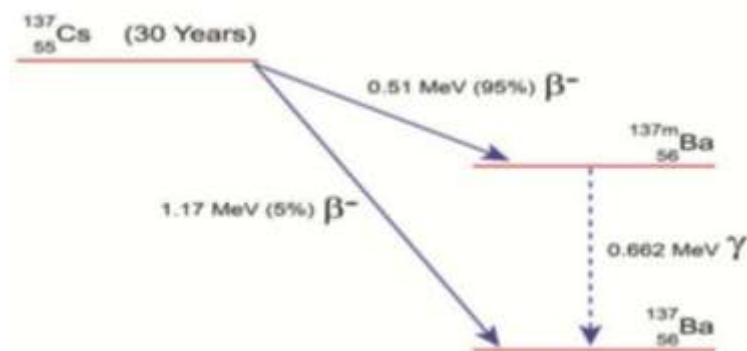
Figure 2.6: *Decay scheme of Cs-137 (Ashraf et al., 2014).*

Cs-137 can exist in different physico-chemical forms, also referred to as speciation. There are several aspects of the radionuclide behaviour that is included in the term speciation (von Gunten & Benes, 1994). Especially important in the distribution between dissolved, colloidal, and particulate species (figure 2.7), because it affects the mobility and bioavailability of the radionuclide. Ions, molecules, and complexes smaller than 1 nm in diameter is referred to as low molecular mass (LMM). High molecular mass (HMM) species includes mono- and polynuclear complexes, colloids and pseudocolloids, and have a size range between 1 nm and 0.45 µm. Particles are defined as the fraction <0.45 µm (Salbu et al., 2004; Salbu, 2007). Fractions between 10 *kDa* and 0.45 µm are operationally referred to as colloids.
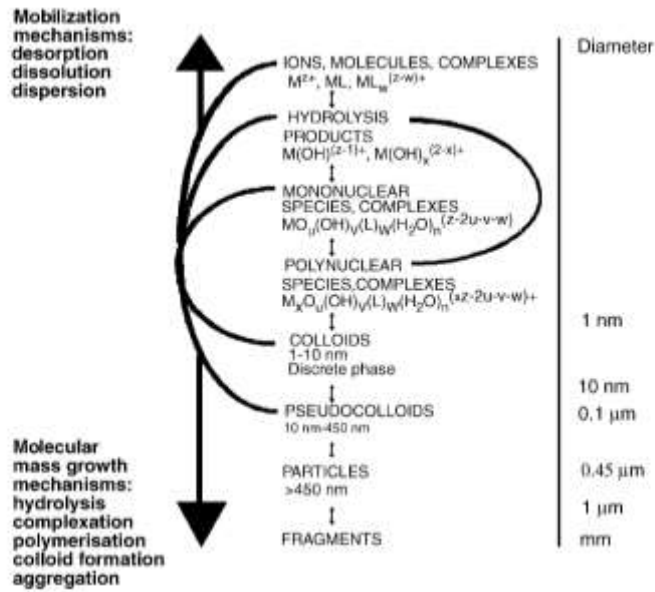
Figure 2.7: *Size fractions for the physico-chemical forms of radionuclides (Salbu et al., 2004)*

Cs is thought to be present as mobile LMM species in the marine environment (von Gunten & Benes, 1994). On the other hand, particles have been observed as the dominating species in rivers (Eyrolle & Charmasson, 2004; Kanivets et al., 1999).

All processes of transport, uptake, or surface adsorption are applicable for all isotopes of Cs. Thus, stable analogues (Cs-133) can be used in risk assessment to establish the transfer and fate of Cs-137. However, Cs being progressively fixed to soil and sediment often causes Cs-137 to be more mobile than Cs-133 which exists naturally in soils, thus having time to reach equilibrium conditions. On the contrary, Cs-137 is deposited by radioactive fallout and will use some time to reach equilibrium, resulting in faster uptake (Newman & Unger, 2003). Regardless, studies have shown correlations in transfer rates between Cs-137 and Cs-133, thus indicating that Cs-133 can be used as a stable analogue for the assessment of Cs-137 (Tsukada et al., 2002; Uchida & Tagami, 2007).

2.4 Processes in estuaries

Estuaries are coastal areas partly enclosed by land that is diluted by freshwater supply from rivers or water run-off. As a result of the seawater dilution in the estuary, a salinity gradient is created in the surface water (Kirk Cochran, 2014). The physics of the mixing of seawater and freshwater give rise to different classifications of estuaries based on the variation of salinity (figure 2.8). Like mentioned in section 2.1, will a fjord type estuary like the Vefsnfjord have a seawater wedge, with a brackish surface layer (Uncles et al., 2015). Radionuclides that enters

9

estuaries are likely to undergo dilution, as the concentration of substances are usually higher in rivers than in the sea as a result of erosion, and the water currents keeping particles and colloids from settling (Kakehi et al., 2016; Vives I Batlle, 2012). Naturally occurring Cs, however, will show the opposite trend, as seawater is a natural source of Cs-133 (Song et al., 2020).
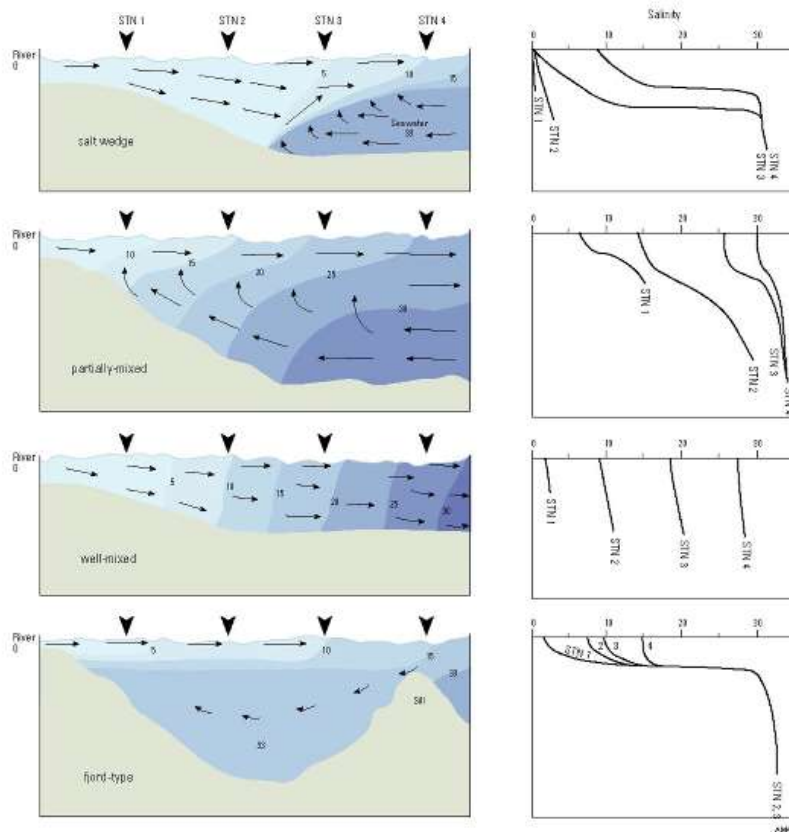
Figure 2.8*: Overview over different estuary types (Kirk Cochran, 2014).*

The dynamic nature of estuaries might induce drastic changes in the speciation of cesium. Initially, the speciation of cesium is strongly dependent on the source. The chemical properties of the environment will further influence behaviour of the radionuclide, such as variations in pH, salinity, and redox potential. Over time, interactions with available ligands or transformation processes might change the original distribution of species (Mosley & Liss, 2020; Salbu et al., 2004; von Gunten & Benes, 1994). LMM species can increase their size by growth mechanisms like hydrolysis, aggregation, or complexation (Salbu et al., 2004). The presence of monovalent and divalent cations in seawater will induce aggregation of particles and colloids by neutralizing the repulsive forces between the particles, causing them to stick together (Mosley & Liss, 2020; Portela et al., 2013). An increase of size will in turn reduce the

10

mobility as the settling velocity of particles is highly dependent on size, thus will aggregated particles settle rapidly, and become incorporated in bottom sediments. (Portela et al., 2013; Simonsen et al., 2019a).

On the other hand, HMM species can reduce their mass by desorption, dissolution, and dispersion processes, such as weathering of radioactive particles. By doing so, the mobility will increase, as LMM species mobilises from the HMM species (Salbu et al., 2004). A rapid increase in water salinity might cause remobilization of LMM species from colloids and particles by ion exchange as a result of increase of competing cations (Simonsen et al., 2019b; Teien et al., 2006).

2.5 Binding of Cesium to particles

Particles, in particular inorganic, prevail as effective carriers for cesium because of the high affinity to aluminium rich clay minerals. (Børretzen & Salbu, 2002; Cornell, 1993; von Gunten & Benes, 1994). Other sediment constituents like organic matter, quartz, carbonates, and Fe-, Mn-, and Al hydroxides do not adsorb Cs as strongly (Staunton et al., 2002).

The binding between Cs and clay can be reversible, slowly reversible or fixed. The degree of fixation depends on the locations where the Cs binds. Sorption to the clay mineral surface sites leads to exchangeable conditions, or reversible (figure 2.9). An example of cations exchange is between potassium and Cs. If Cs binds to the wedges on the sides of the mineral layers, the exchange is sterically limited to cations of similar size and charge. This results in slowly reversible binding. Interlayer binding results in a fixation that is non-reversible (Børretzen & Salbu, 2002). LMM species of cesium binds rapidly to particle surfaces through ionic exchange and tends to bind stronger to sediments over time. Cesium will get progressively fixed and bind stronger by accessing more unavailable sites on the sediments (Oughton et al., 1997).
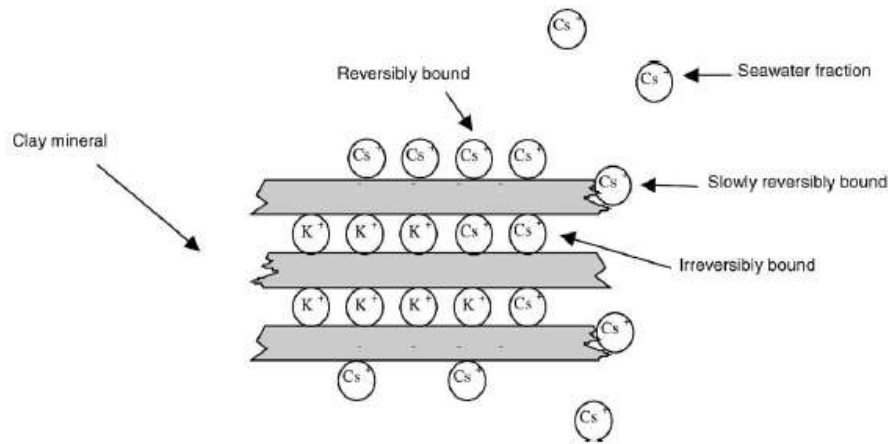
Figure 2.9: Binding of Cs to clays (Børretzen & Salbu, 2002).

Cesium also binds to the carboxylic functional group of organic (humic) matter. Dissociation of the functional groups creates a negative charge which allows accumulation of positively charged cesium ions around humic molecules. However, cesium does not become as strongly fixed to humic substance as it does to clay minerals (Lofts et al., 2002), and can easily be remobilized from organic matter by cation exchange reactions (Kvamme, 2019). The presence of organic matter might decrease the adsorption of Cs onto clay minerals (Staunton et al., 2002).

A quantitative description of the sorption of cesium on sediments is given by the distribution coefficient (K_d):

$$K_d = \frac{C_s}{C_{aq}}$$ (2.1)

Where C_s is the concentration adsorbed onto the solid phase, while C_{aq} is the equilibrium solution concentration (VanLoon & Duffy, 2017). The K_d value represents the relationship between the concentration of cesium in sediments compared to concentration in water. However, since this relationship is based on equilibrium conditions, it might not be relatable to the actual behaviour of cesium in a natural environment. Especially in estuaries where tides and river inputs give rise to constant changes in water properties (IAEA, 2004). In such cases, it is more appropriate to consider the apparent K_d (Standring et al., 2002). In more recent studies, dynamic models have been developed that accounts for kinetic rates rather than equilibrium conditions (Periáñez et al., 2018). For Cs, the recommended K_d in freshwater systems is $2.9 \cdot 10^4$ L/kg, but due to great variation in location, seasonal differences, and environmental factors, the reported range is $6.9 \cdot 10^3$ and $1.2 \cdot 10^5$. The reported K_d in open ocean seawater is $2 \cdot 10^3$ L/kg. (IAEA, 2004; IAEA, 2010).

2.6 Biological uptake of cesium

Due to the small size LMM species are considered bioavailable as they can be taken up by organisms by active transport through the sodium-potassium ATPase pump in the cell membrane (Keeran et al., 2021). As opposed to LMM, HMM species and particles are considered biologically inert as they are larger and less reactive The exceptions are filtering organisms, in which the particles might be retained (Salbu et al., 2004).

An organism's ability for uptake of a pollutant can be described by the relationship between concentration of the chemical in the organism and concentration in the ambient medium. This is referred to as bioconcentration factor (BCF), which can be affected by the bioavailability of the chemical, or the biochemistry of uptake in the organism (Walker et al., 2012). The BCF can be expressed as follows:

$$BCF = \frac{Concentration\ in\ organism}{Concentration\ in\ ambient\ medium} \tag{2.2}$$

Uptake of cesium is largely regulated by the concentration of similar cations, like potassium (K). This is a case of "chemical dilution", where higher concentration of competing cations results in lower uptake of cesium. Since cesium resembles potassium in size and valence, it will be incorporated in cells by the same mechanisms as those for potassium (Håkanson & Fernandez, 2001). Salinity is expected to affect the uptake, with more efficient uptake in freshwater than in seawater (Metian et al., 2019; Wada et al., 2019). The uptake might however be limited to local areas near the source (Periáñez et al., 2021).

Cs might undergo biomagnification in organisms, thus animals higher up in the food chain tend to have higher BCF. For instance, BCF for phytoplankton is 20L/kg, macroalgae (seaweed) is 50 L/kg, while fish has a BCF of 100 L/kg and muscle of pinnipeds (seals, sea lions) is 400 L/kg (IAEA, 2004).

2.7 Fractionation techniques

The most appropriate approach to separate the different size fractions (LMM, colloids and HMM) in an aqueous environment is fractionation *in situ*, as the microchemical conditions of radionuclides in the environment makes them prone to adsorption on container walls or aggregation by storage. Further, the speciation is sensitive to changes in pH and redox potential,

such that transfer to new containers and storage may alter the physical and chemical properties. Size fractionation techniques include membrane filtration, hollow fibre ultrafiltration, continuous centrifugation, and tangential cross flow, in which all techniques are feasible in the field (Salbu, 2009). Filtration using a 0.45 µm Millipore or 0,4 Nucleopore membrane is probably the most applied method for separating particles from LMM, colloids or pseudocolloids in solution. A disadvantage is the fact that particles or microorganisms may clog the membrane, causing a more inefficient filtering and that as species defined by the membrane size may not pass through the filter. Species associated with LMM can be retained from solution by using ultrafiltration, such as hollow fibre or tangential cross flow systems. This is beneficial for *in situ* filtration, as several hundred litres of water can be filtrated due to the efficient surface area of the membrane filter (Salbu, 2009).

Since the water samples often contain low concentrations of radionuclides, upconcentration from large amounts of sample might be necessary to determine the concentration of the radionuclide. Radiochemical separation methods can be useful to obtain the desired radionuclide from solution or remove unwanted interferences. A number of analytical techniques for radiochemical separation have been developed (Choppin et al., 2013). An example is separation by precipitation, a method that has been familiar to radiochemists for decades (Finston & Miskel, 1955). Precipitation is performed by forming a complex (scavenger) that binds to the radionuclide. Effective scavengers have large surface areas and low solubility product (K_{sp}) for the element precipitated, such as the gelatinous nature of hydroxyl complexes (Choppin et al., 2013).

2.8 Measurements and instrumental applications

2.8.1 X-ray powder diffraction (XRD)

Crystalline structures and minerals in particles can be studied using X-ray powder diffraction (XRD). It is a versatile analytical method, and can be used to determine phase composition, structure, texture and more in soil, sediments, rocks, or pollutants. Determination of the crystalline structure is based on Braggs law:

$$n\lambda = 2dsin\theta \qquad\qquad (2.3)$$

When X-ray photons pass through the mineral lattice they scatter in different angles, creating constructive and destructive interferences so that the direction of the X-ray beam affects the intensity of the signal registered at the detector. Figure 2.10 shows X-rays with wavelength λ

reflected off two parallel plans within the mineral, where the reflected angle is equal to incoming angle (θ). The spacing (d) between the parallel plans can be determined based on Braggs law (Ermrich & Opper, 2011).
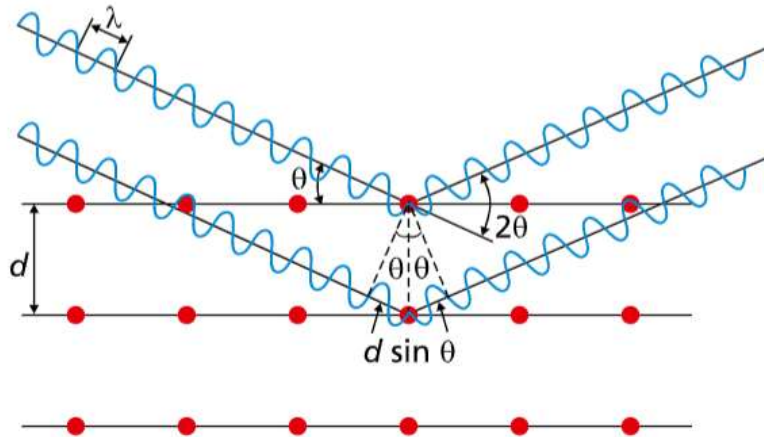
Figure 2.10: Reflection of X-ray beam on parallel mineral surfaces following Braggs law (Ermrich & Opper, 2011).

The measured intensity (counts) is presented in a diffractogram as a function of the 2θ angle (the Bragg angle). By comparing the intensity and placement of the peaks in the diffractogram with a reference pattern, the mineral composition of the sample can be determined (section 4.3.2).

2.8.2 ICP-MS

Inductively coupled plasma mass spectrometry is a method of analysis that allows the measurement of multiple elements simultaneously, and with low detection and quantification limits. This allows measurement of trace-level elements in biological and environmental samples. A liquid sample is introduced to a nebulizer, creating an aerosol that is further transferred to the plasma torch, that consists of argon plasma. The high temperature of the plasma ionises the sample, generating an "ion beam". The ion beam is guided into the quadrupole mass analyser by a set of electrostatic lenses referred to as the "ion optics". Elements are filtered in the quadrupole by their mass-charge ratio and registered by the detector. The most applied detector in ICP-MS is a photomultiplier that amplifies the signal so that the signal from a single ion is measurable (Skoog et al., 2014; Wilschefski & Baxter, 2019). Figure 2.11 provides a schematic description of the ICP-MS structure. Stable isotopes of elements are

usually determined by ICP-MS, but the concentration of radionuclides are often too low and radiochemical methods are commonly used.
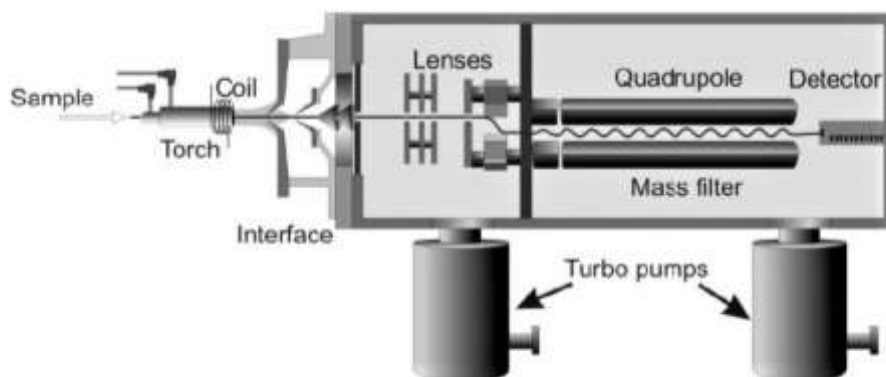
Figure 2.11: *schematic description of the ICP-MS structure (Wilschefski & Baxter, 2019).*

2.8.3 High Purity Germanium (HPGe) Detector

Radioactive Cs at low activity concentrations is commonly determined by γ-spectrometry using HPGe detectors. γ-rays must interact with matter in order to be measured. This interaction can occur through several mechanisms where electrons in the detector material are ionised. When γ-ray photons are partially or fully transferred to the electrons they are left in an excited state and can collide with other atoms. The mechanisms of γ-ray interaction with matter are: Coherent scattering, photoelectric effect, Compton scattering, and pair formation. Figure 2.12 illustrates these interactions.
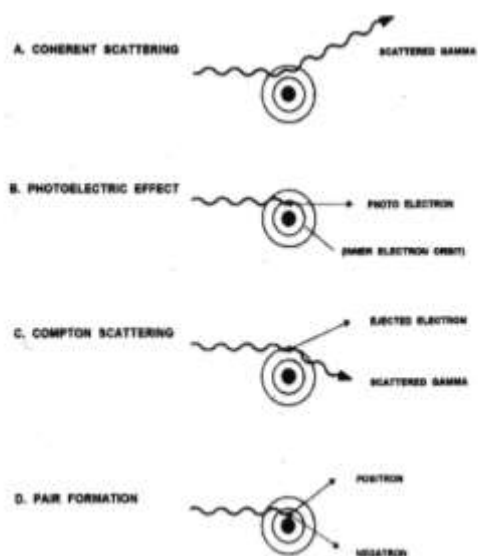
Figure 2.12*: The main processes of γ-ray interaction and absorption (Choppin et al., 2013).*

Although there is a wide range of detection and measurement techniques within radiochemistry, semiconductor detectors have become dominant for energy determination of nuclear radiation. A semiconductor, like germanium, have a small energy difference between the loosely bound valence electrons and the conduction band, where electrons can move readily. Nuclear radiation produces enough energy to transfer valence electrons to the conduction band. This leaves a vacancy in the valence band, producing a "electron-hole pair" that moves toward the anode as the electron moves towards the anode. As a result, a measurable current is produced where the electron-hole pairs and free electrons produced are proportional to the radiation energy of the radionuclide (Choppin et al., 2013).

The collected data is registered as counts or channels, although it is more useful when converted to activity (Bq). Such conversion is performed by several calibration parameters and is utilized by the software when energy- and efficiency calibrations are performed manually. By using user input, isotope libraries and energy spectra, relations like Full Width at Half Max (FWHM), count rate and activity (Bq) as well as spectrum channel numbers and energies can be defined. The different isotopes are recognized as peaks that appear at characteristic energies in a spectrum (ORTEC, 2020). A benefit from using HPGe-detectors is the high energy resolution (FWHM), meaning that the peaks obtained in the energy spectrum is distributed over a small area (Choppin et al., 2013). However, the peaks depend on correct energy data calibration to be reported correctly. The geometry of the container is important for good counting efficiency, and it is important to calibrate for the correct container (ORTEC, 2020).

3 Materials and methods

3.1 Sample locations

Vefsna river and the estuarine environment in the Vefsnfjord was the site of study in the present work (section 2.2). Water, sediments, and biota was sampled to study the distribution of Cs-137 at different locations in the Vefsna river, and after mixing with seawater in the Vefsnfjord, followed by an increasing salinity gradient along the fjord. The aim was to investigate if there were any changes in concentration and distribution of Cs-137 species in the brackish freshwater-seawater interface compared to the freshwater input. Surface freshwater was collected amongst five freshwater sampling sites (FW1, FW2, etc.), represented by different catchments in in the Vefsna watercourse, and six seawater sampling sites (SW1, SW2, etc.) which are shown in figure 3.1 A-C.
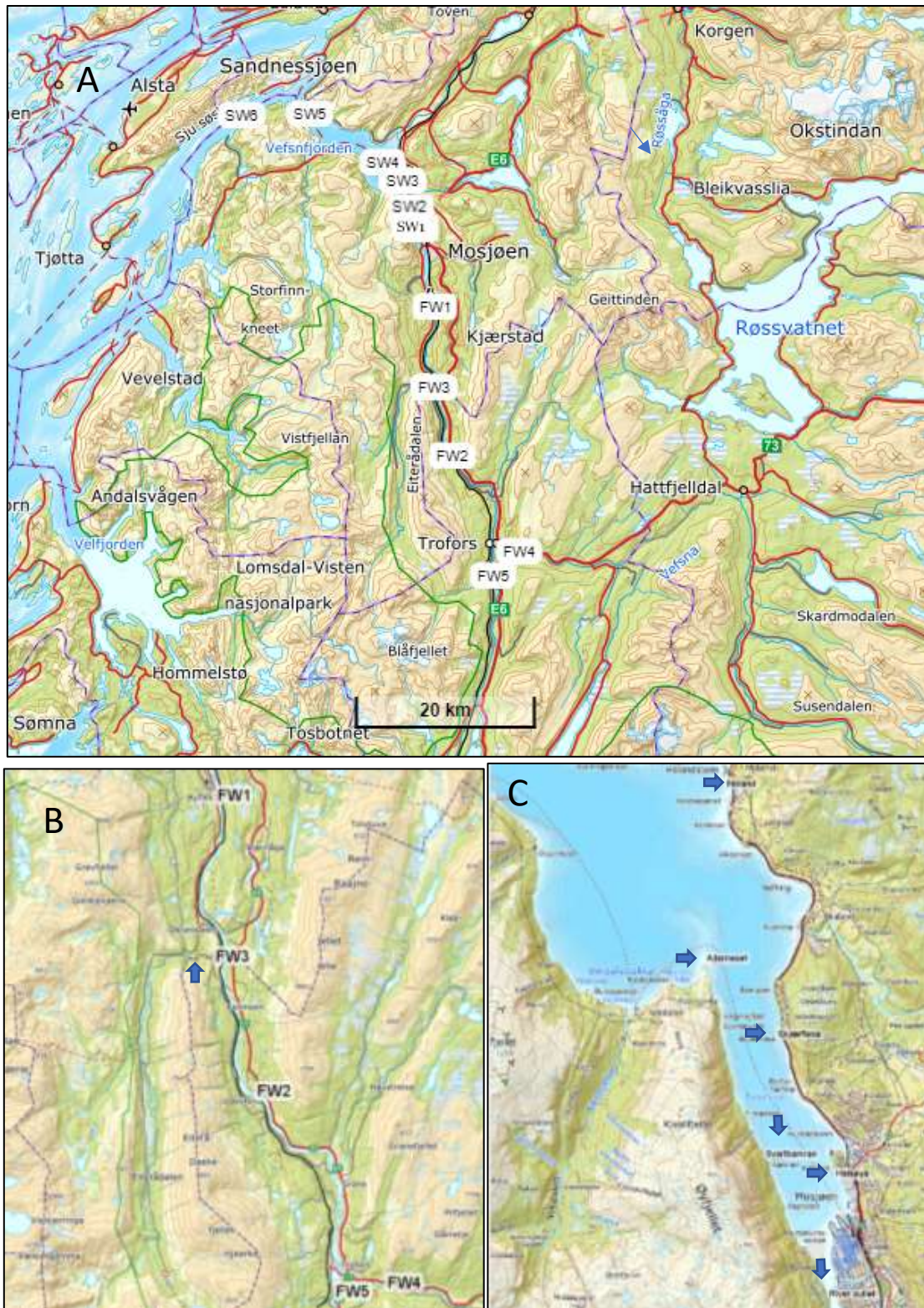
Figure 3.1: *Water and sediment sample sites in the Vefsnfjord and Vefsna river (A), freshwater sites in the Vefsna catchment (B) Biota sites in the Vefsnfjord. (www.norgeskart.no).*

Sample collection wat utilized during one week in late October 2020, between October 26th and October 31st. The weather was stable with sun and partly clouds without any rainfall during the week. The air temperatures ranged between 2°C and -3°C. There had not been any rain for the past weeks, therefore, the water flow in the Vefsna river was low and had been low a couple of weeks prior to the time of sample collection. Water flow (m³/s) is presented in figure 3.2.
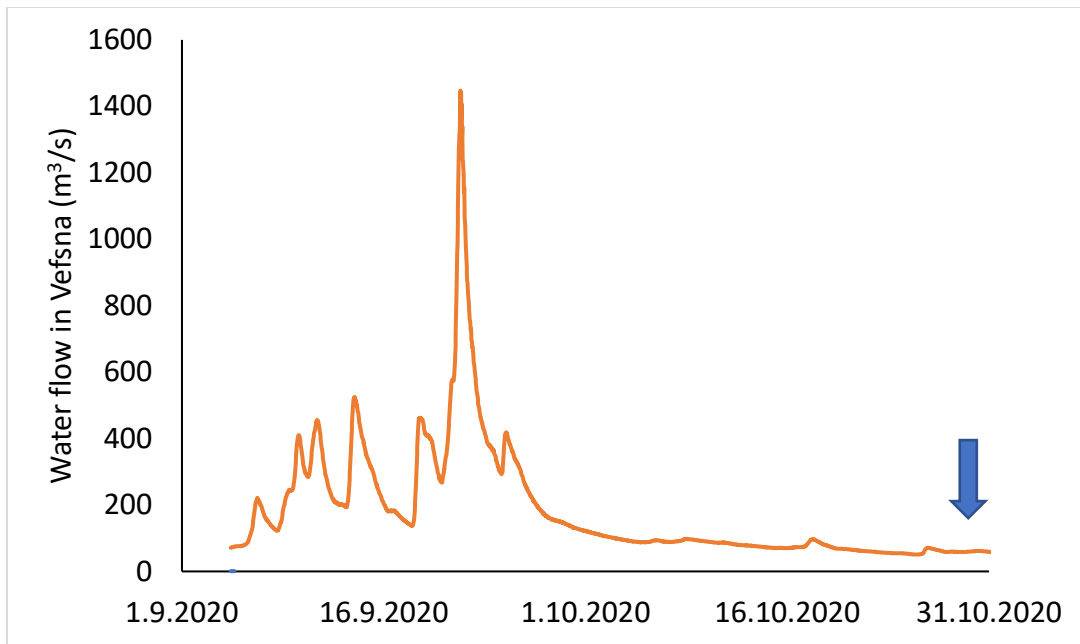
Figure 3.2: *Waterflow in river Vefsna form September 1st to October 31st, 2020. Blue arrow marks time for sample collection.*

An overview over collected water and sediment samples is presented in table 3.1. The table includes GPS-coordinates for each sample site, and which water fractions were collected, along with surface sediments and sediment cores.

Table 3.1: *Sampling sites with GPS-coordinates and samples collected.*

Site	Samples	GPS-coordinates
FW1	Water fractions: LMM, 0.45 µm, particles	65°46.25' N
	Surface sediments	13°13.57' E
FW2	Water fractions: LMM, 0.45 µm, particles	65°37.30' N
	Sediment core 0-7 cm	13°16.58' E
	Surface sediments	
FW3	Water fractions: 0.45 µm, particles	65°41.669' N
		13°14.096' E
FW4	Water fractions: 0.45 µm, particles	65°31.47' N
		13°27.17' E
FW5	Water fractions: 0.45 µm, particles	65°30.28' N
		13°23.28' E
SW1	Water fractions: LMM, 0.45 µm, particles	65°50.951' N
	Sediment core 0-5 cm	13°11.056' E
	Surface sediments	
SW2	Water fractions: LMM, 0.45 µm, particles	65°51.13' N
		13°10.618' E
SW3	Water fractions: LMM, 0.45 µm, particles	65°53.829' N
		13°8.718' E
SW4	Water fractions: LMM, 0.45 µm, particles	65°54.881' N
	Surface sediments	13°5.664' E
SW5	Surface sediments	65°54.78' N
		13°06.30' E
SW6	Surface sediments	65°57.38' N
		12°44.77' E

Biota samples were collected at six different locations in the Vefsnfjord, listed in table 3.2. The biota samples consisted of blue mussels (*Mytilus edulis*) and two different species of seaweed (*Fucus vesiculus*, *Laminara digitata*). The table includes which species are collected in the different locations, with name of location and GPS-coordinates.

Table 3.2: *Biota samples consisting of seaweed and blue mussels collected in the Vefsnfjord with sample collation and GPS-coordinates.*

Location same	Species	GPS
River outlet	*F.vesiculus*	65°50.2854′ N
		13°11.00346′E
Halsøya	*F.vesiculus*	65°51.576′ N
		13°11.1′ E
Svarthamran	*F.vesiculus*	65°51.7506′ N
		13°9.255′ E
Skjærflesa	*M.edulis*	65°53.0484′ N
	A.nodosium	13°9.46908′ E
	F.vesiculus	
Alterneset	*M.edulis*	65°53.63′ N
	L.digitata	13°7.369′ E
	F.vesiculus	
Holand	*M.edulis*	65°55.68′ N
	A.nodosium	13°7.974′ E
	F.vesiculus	

3.2 Water samples

3.2.1 Collection of water samples

To obtain information about the size distribution of Cs-137, samples were taken before and after the estuarine mixing zone. Surface water was sampled at site FW1-FW5 in the Vefsna river, and at site SW1-SW4 in the Vefsnfjord. The different locations in the fjord were selected based on salinity of the surface water, as a representative selection of salinities was required to investigate the trends in species distribution of Cs-137 as a function of salinity. Since it was a rapid change in salinity in the inner parts of the fjord, some sites were closer to one another. The riverine sites were determined based on obtaining information of sources of Cs-137, which were expected to originate from runoff. Therefore, the different FW-sites represent different river catchments (section 2.2).

Both information of Cs-137 species and general water quality (major cations, stable cesium) was gathered. The general water quality was determined by measuring unfiltered and filtered (LMM, <0.45 µm) water using ICP-MS (section 3.5.3), and measuring the pH, conductivity, turbidity, and salinity *in situ* (section 3.5.1). To determine stable Cs and trace elements, three parallels of 50 mL water sample from each fraction (LMM, <0.45 µm, and unfiltered sample) at each site were collected in sterile 50 mL centrifugal tubes (Sarstedt, 62.559).

The distribution of Cs-137 in water fractions was analysed with gamma-spectrometry using a HPGe-detector (section 3.5.4). To obtain information about the different size fractions, *in situ* filtration was performed. Desired fractions were LMM (<10 kDa), colloids/pseudo colloids (<0.45 µm), and particles (>0.45µm). Prior to sample collection, the amount of water that had to be filtered *in situ* to achieve detectable activities was estimated by filtering and measuring 50 L of water from Vefsna in the laboratory. Based on the measured activity, it was estimated that the required sampling volume had to be about 200L.

The water was pumped at site into 200 L plastic containers (Jula, art. No. 795994). Ultrafiltrated water was collected to determine the LMM species of Cs-137 using a large Microsa filtration hollow fibre membrane (PALL SLP-1053), coupled with a water pump (Gardena 3000). The volume of filtered water was recorded by pumping it into 25 L plastic cans (Europris, LK. Haaland, art. No. 125380), which was weighed. Likewise, the filtered fraction smaller than 0.45 µm was collected to determine colloidal, pseudocolloids, and LMM species of Cs-137 using a cellulose acetate membrane filter with a 0.45 µm pore size, while particles (> 0.45 µm) was retained on the membrane filters. To identify the Cs-137 fraction associated with particles, the filters with particles were collected and transferred to 20 mL Scintillation plastic (polyethylene) vials for further measurements. The filters were pre-weighed so the weight of particles could be calculated by subtracting the weight of the filters before and after filtration.

The setup at two of the locations are shown in figure 3.3. In the FW sites, filtrations were performed by the riverside, while for the SW sites, water filtration were performed from a boat. For practical reasons, some of the fractionation took place in a nearby workshop. Water was in these cases pumped directly into 25 L plastic cans and transported to the workshop before being filtered immediately.

Figure 3.3: *In situ fractionation of water with hollowfibre ultrafiltration and 0.45* μm *particle filtration at site FW1 (A) and SW3 (B).*

3.2.2 Radiochemical separation

To be able to determine Cs-137, concentration of Cs-137 from a large volume was necessary. Also, since the water samples contained large volumes between 100 L and 400 L, it would be impractical to transport over a long distance before determination of Cs-137. Therefore, LMM and colloids in the filtered water samples was precipitated using a scavenger in field. Radiochemical separation by precipitation was performed immediately after sample collection (the same day) and took place in a nearby workshop that was used as "laboratory" during the field trip (figure 3.4). Precipitation of Cs-137 was accomplished by qualitatively adding 15 mL 0.1 M k-hexacyanoferrate ($K_4Fe(II)(CN)_3$) and 15 mL 0.1 M cobalt chloride ($CoCl_2$) in large volume samples to form a scavenging complex with high affinity to the analyte. The mix was stirred using a plastic shaft, then was left for 10 minutes. This was enough time for the complexation of the scavenger, without risking reducing the yield. Thereafter, the water was pumped though a 0.45 µm cellulose acetate membrane filter. The precipitate was thus isolated on the filter and representing the total amount of Cs-137 in the sample. The filters were collected in 20 mL plastic vials.

The extent to which Cs-137 had adsorbed to the scavenger used in radiochemical separation was determined by the addition of a yield monitor. For this purpose, 100 µL (~185 Bq/mL) Cs-134 tracer was added quantitatively by using 10-100µL FinnPippette® automatic pipette with Finntip Flex (lot: 7033A0) disposable pipette-tips from ThermoFisher Scientific. Since all isotopes of Cs are assumed to have the same chemical behaviour, the yield of Cs-134 tracer would be the same as for Cs-137. Thus, the amount of Cs-137 lost during radiochemical

separation and filtration could be accounted for. Without a yield monitor, the possible loss of analyte would not be accounted for, hence underestimating the activity. Although it is worth mentioning that the chemical behaviour of some naturally occurring species are significantly different from the tracer species added, and might not be relevant (Salbu, 2009).

Figure 3.4: *Radiochemical separation of the water samples performed "in situ" at a local workshop. Adding yield monitor, k-hexacyanoferrate, and cobalt chloride (A), pumping water through 0.45 µm filter (B), and folding filter with precipitate containing Cs-137 and Cs-134 (C)*

3.3 Sediments

3.3.1 Collection of sediment samples

Surface sediments were collected at six different locations in Vefsna river and Vefsnfjord to investigate possible changes in Cs-137 distribution, as well as grain size distribution, from freshwater to seawater. In addition, two sediment cores were sampled (one from riverine sediments and one from marine sediments) to provide information about changes in Cs-137 activity with depth. Sediments from site FW1, FW2, and SW1 was collected by using a sediment core sampler (Figure 3.5). Riverine sediments were collected from the riverside, while the SW1 core was collected from a boat at approximately 40 meters depth. The cores were sliced with 1 cm thickness and collected in zip-lock bags, which were frozen immediately after the field work, and stored for about three months. The surface sediments were stored in plastic boxes. In addition, surface sediments from site SW4, SW5, and SW6 were collected by the ship R/V "Kristine Bonnevie" 26. October 2020 with a grab sampler at 446-, 485-, and 227-meters depth, respectively. The total weight of the sediment samples varied between 150 g and 3000 g (d.w), where the largest samples were collected in the river. Large samples were collected from the river because the riverine sediments were rather course and contained a lot of sand. Therefore, large samples were collected to obtain as much silt and clay as possible during grain size analysis (section 3.3.2).

Figure 3.5: *Sampling and slicing of sediment core.*

The sediments were freeze-dried using a Christ Epsilon 2-4 LSC freeze drier for about one week prior to measurement on Ge-detector to obtain activity in dry weight. The dry sediments were sieved with a 2.0 mm WWR test sieve (ISO 3310-1) to remove gravel from the sample.

3.3.2 Grain size analysis

The dried sediments containing fractions smaller than 2.0 mm in diameter were soaked in water overnight on a roller-table, as the samples were to be wet sieved. Seawater sediments were soaked in filtered seawater, while the freshwater sediments were soaked in freshwater from Vefsna river. Since it was not collected enough seawater from the Vefsnfjord for this preparation, filtered seawater (0.45 μm) form the Oslofjord collected at NIVA Research Facility Solbergstrand at proximately 40 meters below surface was used for soaking the seawater sediments. The purpose of using seawater was to prevent any changes in the properties of Cs-137 caused by changes in salinity. The seawater had a salinity of 33.5 PSU and was filtered with 0.45 µm high capacity in-line groundwater sampling capsule coupled to a water pump.

Sand was separated from silt and clay by washing the sample with riverine- or saline water through a 63 µm sieve. The sieve was washed with as little water as possible while still collecting sufficient silt and clay. The sand fraction was then collected in a pre-weighed glass beaker and set to dry in a drying oven from Termaks (NLS ISEM No. 1700040).

25

Clay was separated from silt based on settling velocity of the particles, determined by Stocke's law.

$$v = \frac{D^2 g (\rho_p - \rho_f)}{18\eta} \tag{3.1}$$

Where v is the settling velocity of the particle, D is particle diameter, ρ_p is the density of the particle (clay), ρ_f is velocity of water and η is the viscosity of water.

Within four and six hours, the silt fraction had sedimented 5,2 cm and 7,8 cm in freshwater, respectively. 1 L Nalgene bottles were marked at 5.2 cm (four hours) and 7.8 cm (six hours) hights, and the sample were then transferred to the bottles to the mark representing six hours, and the pottles were shaken vigorously. After 6 hours, the silt fraction had settled on the bottom of the bottle, while the clay fraction was still in the water fraction. Water containing clay was removed and collected in a large beaker using a water pump. As much water as possible was removed without stirring up the silt fraction. This procedure was repeated 3-6 times, until the water was clear and most of the clay had been separated from the silt. The remaining silt fraction was transferred to new plastic containers and freeze dried for approximately one week. Clay in water suspension had to settle to the bottom of the beaker before the remaining water was removed. Settling of clay took one week. The water was removed with a water pump, and the clay was transferred to new containers and freeze dried for approximately one week. The dry weight was reported.
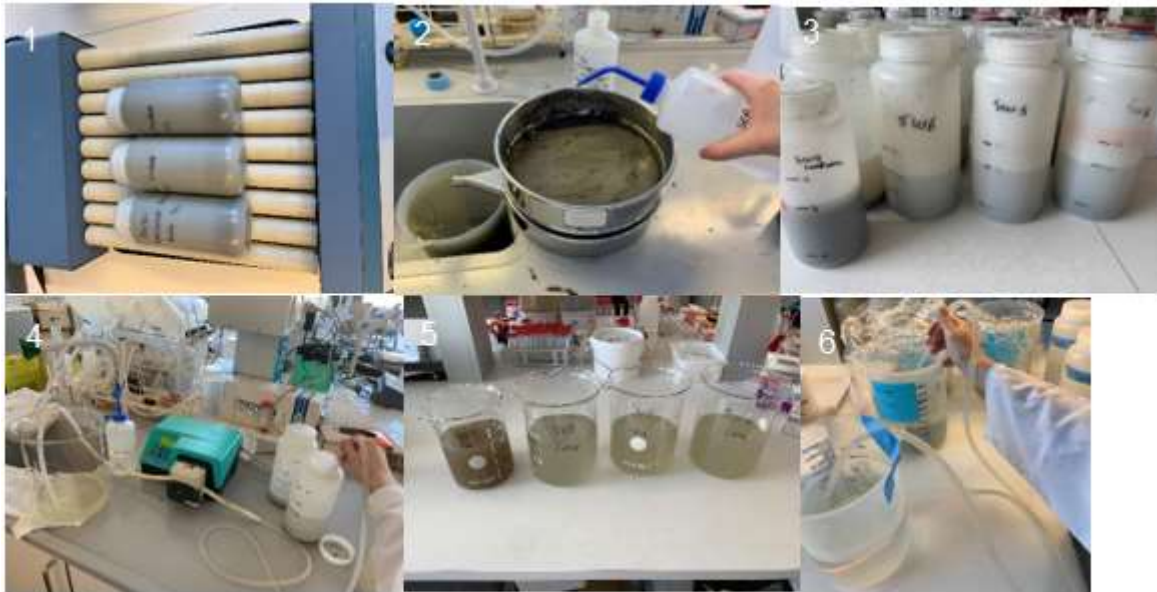
Figure 3.6: *Grain size analysis of surface sediments by wet sieving and sedimentation. Soaking sediments in water on roller table (1), wet sieving (2), separating silt from clay by Stoke's law (3), pumping off the clay fraction (3), settling of clay (5), removing water from the clay fraction (6).*

As the original protocol included wet sieving with Milli-Q water as opposed to saline water, the sedimentation rate of 5.2 and 7.8 cm per 4 and 6 hours, respectively, might not be correct. Stokes' law includes parameters such as viscosity and density, in which are not the same for fresh water and saline water. When correcting for standard values of density and viscosity of high salinity water, the sedimentation time is predicted to be somewhat longer compared to fresh water. However, observations indicated also that the sedimentation of clay in high saline samples was faster than in freshwater samples based on how much quicker the clay fraction turned clear. To correct for possible flocculation caused by the saline water, a sample of the separated silt fraction was added to freshwater from the Vefsna river, and a new separation was performed to investigate if more clay could be isolated from the silt. Approximately 20 g of silt from site SW4 was soaked in freshwater, and the procedure was repeated as previously.

After freeze-drying of the seawater sediments, a great amount of salt was left in the samples, especially in the clay fraction. Because of this, the weight of clay was uncertain. The approximate weight of clay was determined based on the volume of water left in each container prior to freeze-drying (~250 mL) and the salinity of water (33.5 g of salt per kg of water). Which gives approximately 8 g of salt in each clay sample. However, since the exact amount of water was not registered, there might be a higher salt content. Therefore, there is a high uncertainty regarding the weight of clay collected from seawater sediments.

3.3.3 Sequential extraction of silt and clay

The sequential extraction procedure was a modified version of (Tessier et al., 1979) and consisted of six steps. Due to low activity levels in the silt and clay seawater fractions, it was necessary with a larger amount of sample when performing sequential extraction. Therefore, the freshwater fractions were mixed, and the seawater fractions were mixed as presented in table 3.3, as opposed to performing sequential extraction each site separately. The table includes sample weight and volume of solutions used in sequential extraction.

Table 3.3: Mixed silt and clay fractions from freshwater- and seawater sediments with sample weights and volume of extracting solution used for sequential extraction.

Sample	Samples mixed	Sample weight (g)	Extraction volume (mL)
FW clay	FW1 clay, FW2 clay	1,91	20
FW silt	FW1 silt, FW2 silt	9,97	100
SW clay	SW1 clay, SW4 clay, SW5 clay, SW6 clay	10*	100
SW silt (n=3)	SW1 silt, SW4 silt, SW5 silt, SW6 silt	20.25, 20.79, 20.55	200

* Estimated weight of clay based on salt content. Weight with salt = 30.24g.

The first step extracts the water-soluble fraction of Cs-137. Milli-Q water was added to each sample, shaken, and put on a roller table for one hour. The samples were then centrifuged in a VWR Mega star 1.6R centrifuge for 20 minutes at 3000 rpm. After centrifugation, the supernatant was filtered through a 2.0 µm filter placed in a plastic funnel (Figure 3.8). The filtered supernatant was collected in suitable containers with a geometry that could be measured in the Ge-detector. The larger samples (<100 mL) were collected in blue cap bottles, while the small samples (20 mL) were collected in plastic vials. The same filter as for step one was used in the remaining steps (2-6).

Step two and three accounts for the reversible bound fraction of Cs and was utilized by adding 1 M Ammonium Acetate (CH_3COONH_4) with a pH value adjusted to 7 and 5, respectively. The bottles were shaken and left on a roller table for two hours. In a similar manner as for step one, the bottles were centrifugated at 3000 rpm for 20 minutes. The supernatant was filtered and collected in a new container. After step 3, a washing procedure was performed by adding Milli-

Q water to each tube, then shake vigorously and centrifuge as previously. The supernatant from the washing procedure was filtered through the same filter and collected in the same container as the extractant.

Step four accounted for the easily reduced components such as iron oxides and manganese, which were extracted with 0.04 M hydroxylamine hydrochloride ($NH_2OH \cdot HCl$) in 25% (v/v) acetic acid (CH_3COOH). The centrifuge tubes were put in a water bath at 80°C for 6 hours. The tubes were then centrifuged for 20 minutes at 3000 rpm and the supernatant was filtered and collected in a new container, followed by a washing procedure, preformed the same way as in step 3.

In step five was Cs associated with oxidised components such as organic matter was extracted. The samples were transferred to 250 mL Erlenmeyer flasks, which were added 30% hydrogen peroxide (80°C (Figure 3.7). The samples were then transferred from the Erlenmeyer flasks back to the centrifugal tubes with 3 x 5 mL, 25 mL and 50 mL 3.2 M ammonium acetate in 20% (V/V) nitric acid and 3 x 5 mL, 25 mL and 50 mL Milli-Q water to samples weighing 2 g, 10 g and 20 g, respectively. Thereafter, the centrifugal tubes were left on a roller table for 30 minutes, centrifuged at 3000 rpm for 20 minutes. The supernatant was filtered through the same filter as previously, and the filtered supernatant was collected in a new container. Lastly, the washing procedure was performed like in the previous steps.

The sixth and final step of the extraction procedure accounts for the acid dissolvable fraction, which corresponds to the irreversibly bound or non-exchangeable fraction. 7 M nitric acid was added to the remaining samples, before they were put in a water bath at 80 °C for 6 hours. The entire sample, both supernatant and residue, was filtered directly, without centrifugation. Filtered supernatant was transferred to a new container, while the filter with remaining residue was set to dry completely before transferring to another container. The weight of container with filtered and dried residue was registered to determine how much of the total sample was left as residue.
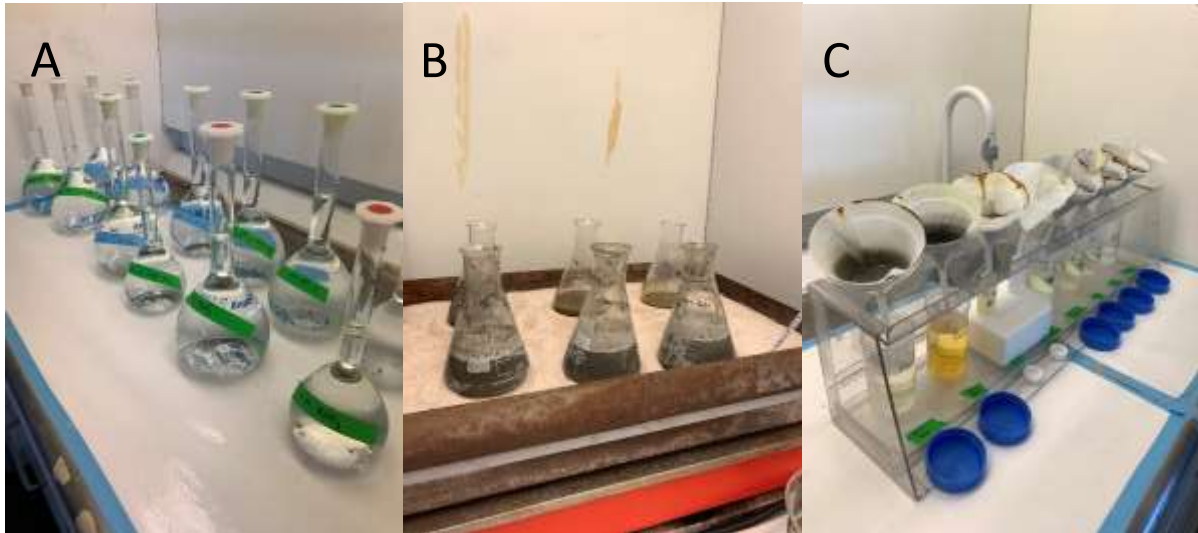
Figure 3.7: Solutions applied for the extractions (A), Heating of the sample on sand bath during step 5 (B), filtering of the supernatant (C).

Cs-137 extracted in each step was determined using Ge-detector (section 3.3.4). In addition, Cs-133 was measured with ICP-MS (section 3.3.3). Since the samples were to me measured on ICP-MS in addition to gamma spectrometry, some dilution was necessary prior to the measurement. As step 1 mostly contained Milli-Q water, no dilution was needed for freshwater clay and silt. However, seawater clay and silt contained a considerable amount of salt. Therefore, seawater clay and silt extracts were diluted 20 times by adding 0,5 mL extract to a new centrifugal tube and diluting to 10 mL. The diluted samples were acidified to 5% (V/V) with 65% ultrapure nitic acid. Step 2 to step 5 were all diluted 10 times, while step 6 was diluted 50 times.

3.4 Biota
3.4.1 Preparation of biota samples

Biota samples consisted of seaweed (*F.vesiculus, A.nodosium,* and *L.digitata*) and blue mussels (*M.edulis*) and were collected from the shore at different locations in the Vefsnfjord at increased distance from the outlet of Vefsna river. The inner parts of the fjord would have impact of freshwater, with increasing salinity outward the fjord. The size of the blue mussels ranged between 4 to

Figure 3.8: Collecting the entrails of blue mussels.

9 cm, approximately. Shortly after biota samples were collected, they were frozen. While still inn frozen condition, the entire entrails and muscle of the mussels were scraped out with a scalpel and collected in blue-cap and Nalgene-bottles (Figure 3.8). However, they were gradually thawed during this procedure. This procedure was performed in the local workshop, to reduce the amount of sample transported, as the shell would carry a lot of unnecessary weight. The samples of the soft tissues from the shells were then frozen again and kept in such condition for about three months.

Biota samples were freeze-dried using a Martin Christ Epsilon 2-4 LSC freeze drier prior to measurement on the Ge-detector, to obtain activity of dry weight. It took about one week for the sediment and biota samples to dry completely, as the samples had a relatively high water-content. After freeze-drying, the seaweed was crushed by using a Fritsch pulverisette cutting mill, then homogenized.

3.5 Measurement

3.5.1 pH, conductivity, turbidity, and temperature

The pH, conductivity, salinity, and temperature of the water was measured at site with WTW Multi 340i and WTW Multi 3420 multimeters coupled with a WTW SenTix 41 pH probe and TetraCon 325 conductivity probe. The probe pH was calibrated with pH 4 and pH 7 buffer solutions (Figure 3.10).

The turbidity was measured with a WTW VisoTurb® 900-P turbidity probe. Since the probe measured particles with infrared light at a 90° angle, it had to be measured in a dark container with appropriate size so light from the surroundings would not interfere. The probe was calibrated with a WTW 4000 FNU standard, diluted to 400 and 40 FNU (Figure 3.9).
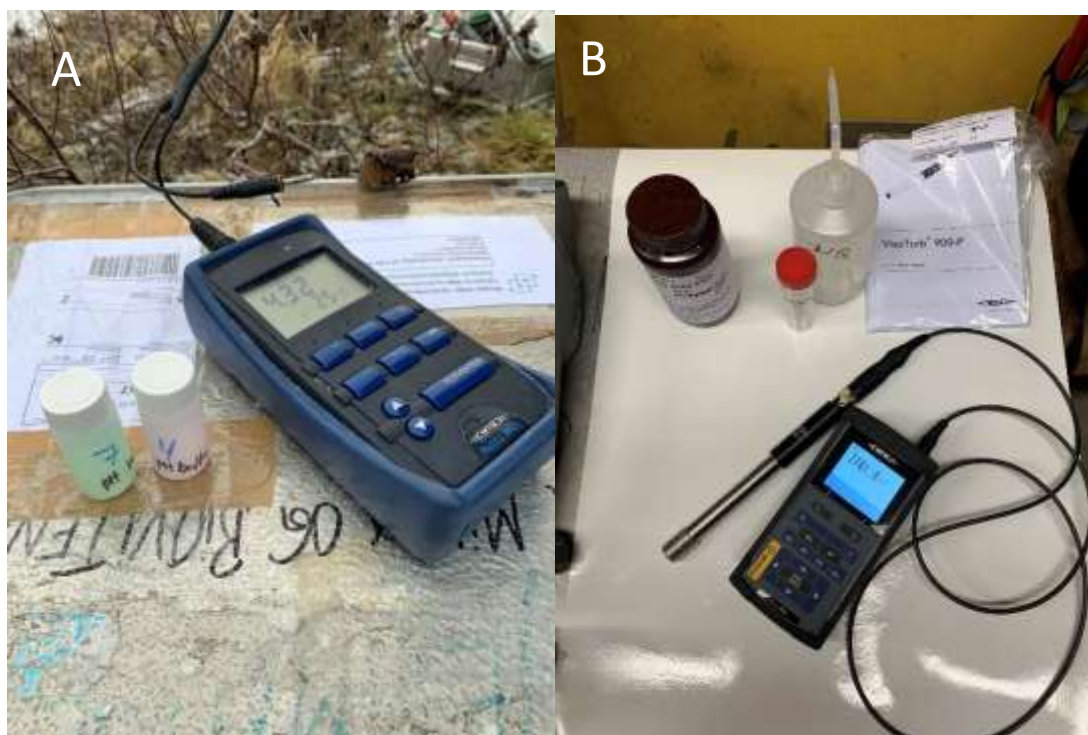
Figure 3.9: *Calibrating for (A) pH and (B) turbidity.*

The pH-value of the sediments was measured in the laboratory after the sediments had been soaked overnight in freshwater/seawater as described in chapter 3.2.2. The measurements were performed by twirling the probe in the water phase while measuring until the pH-value was stable.

3.5.2 XRD

The mineral composition of silt and clay fraction from freshwater and seawater sediments were determined by X-ray powder diffraction (XRD) using a Bruker D8 Advance X-ray diffractometer. The measured samples were silt from river sediments, silt and clay from marine sediments separated in seawater, and silt and clay from marine sediments separated in fresh water. The purpose of separating marine clay and silt in both freshwater and seawater, was to investigate whether the mineral composition was affected by separating in high salinity water as opposed to freshwater. The samples were freeze-dried for one week after separation by wet sieving and sedimentation. The dry samples were placed in the sample holders illustrated in figure 3.10 and scraped flat, leaving a smooth surface.

Figure 3.10: *Sample holders containing freeze dried sediments, for XRD analysis.*

The samples were analysed with the software DIFFRAC.COMMANDER, while the obtained diffractograms were further investigated with DIFFRAC.EVA, both of which are modules of the DIFFRAC.SUITE software platform by Bruker. DIFFRAC.EVA was used to determine the mineral composition of the samples by comparing the peaks of the diffractograms with reference patterns unique for each mineral from the library: "Crystallography open database". The diffractogram obtained from XRD analysis is a plot of intensity as a function of the Braggs angle (2θ), which is the angle between the incident beam and reflected beam (Ermrich & Opper, 2011). The reference pattern is represented by characteristic 2θ values that matches the intensity peaks appearing in the diffractogram. By using the software DIFFRAC.EVA, a selection of suggested minerals was provided. As a result of experimental error, some peak displacement might have occurred. Therefore, the 2θ value might variate some between the different samples.

3.5.3 ICP-MS
Acid digestion

Three parallels of either sediment sample or biota were were weighed into clean TFM-tubes with an accuracy of three decimals. Approximately 0.250 g (d.w) of sample was used. The TFM-tubes were acid washed for 48 hours with 50% (V/V) HNO_3 before use. Further, 100 µL of 10.0 mg/L and 1.0 mg/L Rh- solutions was added as an internal standard to the sediments and biota, respectively. Final concentration of the internal standard was determined to be 0.2 µg(Rh)/L. For digestion of the sediments, 5.0 mL of a 4+1 (V/V) mixture of
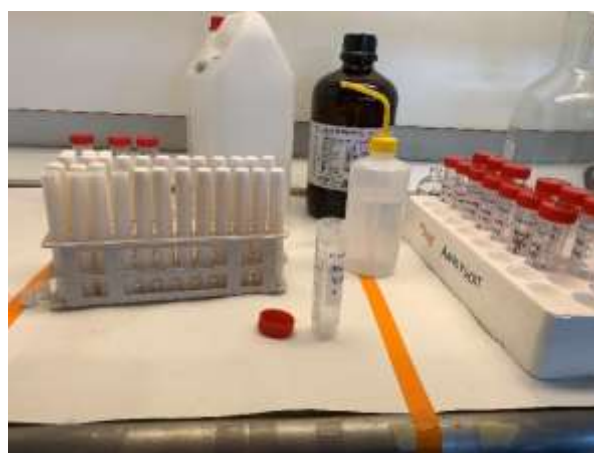
Figure 3.11: *Dilution of acid digested samples.*

HNO_3 and HF was added to the samples. As for the biota, the dry samples were soaked with 2.0 mL Milli-Q water (18.3 MΩcm^{-1}) for a few minutes, before 5.0 mL of concentrated 65% ultrapure HNO_3 was added. Furthermore, lids were placed on the TFM-tubes, which were shaken using a vortex for a brief moment. The tubes where then digested using a Milestone UltraWAVE microwave digestion system. The program lasted for about 1h40min with a maximum temperature of 260°C. After digestion, the solution was transferred quantitatively to 50 mL centrifugal tubes and was diluted with Milli-Q water to 50 mL (Figure 3.11). Since the digested solution matrix of the sediments contained high concentrations of major elements it

was diluted before analysis on the ICP-MS. This was utilized by adding 1.0 mL of digested solution to a new 15 mL centrifugal tube and then diluted with 9.0 mL of 4% (V/V) HNO_3 in Milli-Q water. In addition to the samples, five types of certified reference material and multiple blanks was included, which were prepared the same way as for the samples.

Calibration blanks and calibration standards were prepared for each sample matrix type (biota, sediments, sequential extraction). Calibration blank contained Milli-Q water with the same acid concentration as in the sample matrixes, while calibration standards in addition contained Cs-133 standard solution. Standard 1 was prepared by adding 100 µL of 0.1 mg/L Cs-133 standard solution, and diluted to 50 mL in a centrifugal tube, acidified to 5% (V/V) with ultrapure 65% nitric acid. Similarly, standard 2 was prepared by adding 100 µL of 1.0 mg/L Cs-133 standard. Final concentration of standards was 0.2 µg Cs/L and 2.0 µg Cs/L for standard 1 and standard 2, respectively.

Calibration blanks and calibration standards was prepared for each matrix solution from sequential extraction step 1-6 by diluting 20 mL of the solutions with Milli-Q water to 50 mL. 5 mL was then transferred from the diluted extracts to three new centrifugal tubes (calibration blank, standard 1 and standard 2), with 0,5 mL ultrapure 65% nitric acid and diluted to 50 mL with Milli-Q water. Standard solution was added like described above, to final concentrations of 0.2 µg/L and 2.0 µg/L.

The 50 mL water samples from each location in Vefsna river and the Vefsnfjord (section 3.2.1) were conserved to prevent any chemical change or microbial growth in the container. Conservation of water samples was achieved by acidifying with sub-boiled ultrapure nitric acid (HNO_3) to a final concentration of 5% (V/V). In addition, the seawater samples were diluted with Milli-Q water (18.3 $M\Omega cm^{-1}$), as too high salinity could lead to interferences while measuring the samples in ICP-MS. Final salinity was determined to be 2.5 PSU.

Measurement

Acidified water samples collected in 50 mL centrifugal tubes and digested sediment and biota samples were analysed for content of Cs-133 using the instrument Agilent 8800 Triple Quadrupole ICP-MS accompanied with the software "MassHunter" from Agilent Technologies. Ammonia (NH_3) was used as reaction gas introduced to the reaction cell when analysing sediments and biota, while oxygen (O_2) was used as reaction gas when analysing the water samples. One calibration blank and two calibration standards prepared as described above were used for calibrating the system and convert registered signal from counts to

concentration. Internal standard (Rh) was added before acid digestion to control dilution, while In was added on-line to check for drift during analysis.

Separate instrumental methods were developed for analysing the sediments, water, and biota. Additionally, it was developed one instrumental method for each sequential extraction step, as the sample matrix of the individual steps varied.

When determining which mass to be measured, the "relative isotopic abundance table" (Agilent Technologies, 2008) was used. Cs-133 was measured at mass equals to 133 amu, since there is a 100% abundance for this mass, and thus no interfering masses. Since this were the only analyte to be measured in the sediment and biota samples, there were no other interferences to consider. However, calcium (Ca) was also measured in the water samples as a control of salinity. Two different masses were measured: 42 amu $\rightarrow$ 58 amu, and 44 amu $\rightarrow$ 60 amu. The shift in mass is due to the reaction gas (O_2) introduced in the reaction cell, between the first and second quadrupole ($Q_1 \rightarrow Q_2$). Recommended mass for Ca based on relative isotopic abundance table was 44 amu, with 2.086% abundance (for normal plasma). A better abundance (96.94%) would be obtained if measured with cool plasma / Octapole Reaction System (ORS) on mass 40 amu. Since several elements were measured simultaneously, this would have been impractical. Furthermore, it was expected a high content of Ca, and thus measuring on 44 amu was sufficient in this analysis.

3.5.4 Gamma spectroscopy

Activity of Cs-137 in the samples were measured using Canberra and Ortec High-Purity Germanium (HPGe) coaxial detector with Gamma Vision V7 software. The sediment cores, surface sediments, and fractions (sand, silt, clay) were measured until counting uncertainty was lower than 5%. Time required for achieving desired counting uncertainty varied between one hour and over one week due to major differences in activity content and amount of sample available. As for the biota samples and fractions obtained from sequential extractions, there was not enough time to achieve an uncertainty of less than 5%, since these samples had rather low activities. Therefore, measuring time was determined beforehand. Biota samples were measured for one week, while each sequential extraction sample was measured for one day. The activity data from each sample was collected from the energy peak corresponding to the library value of Cs-137 at 661,66 kEV.

Energy and Efficiency calibrations were performed by laboratory staff, using a certified mixed radionuclide solution, and saved as files in the ORTEC software. When measuring the samples,

the calibration file corresponding to correct geometry of the sample container was selected. Three different geometries were used: 20 mL Scintillation plastic (polyethylene) vial, 180 mL "bluecap bottle" (Aseptic, polypropylene, from Kisker biotech, art. No.688281), and 1000 mL Marinelli beaker.

A standard reference material (Baltic Sea sediment, IAEA-300 (IAEA, 1993)) was measured as an indication for the accuracy of the method. However, there was only one geometry available for the reference material, which was 20 mL plastic vial.

3.6 Data handling and statistical analysis

All data handling and statistical analysis was performed using Microsoft Excel®. The measurements from ICP-MS are presented as the average value of n =3 parallels, where the standard deviation of the measurements accounts for the uncertainty, as well as indication the precision. The uncertainties for gamma measurements were given by the software in counts ($\pm$ counting uncertainty) and converted to becquerel by calculating the percentage. When adding or subtracting measurements, for example calculating concentration of the size fractions from fractionations of water (colloids and particles), absolute uncertainty was calculated from the following equation:

$$\sigma_{A+B} \; or \; \sigma_{A-B} = \sqrt{\sigma_A^2 + \sigma_B^2} \tag{3.2}$$

Where σ_A and σ_B are the uncertainties of each measurement.

The concentration of colloids and particles had to be calculated, as the <0.45 µm fraction contained both LMM and colloids. Concentration of colloids was obtained by subtracting the LMM fraction. Additionally, the particle fraction was calculated based on concentration in unfiltered fraction subtracting the concentration in the <0.45 µm fraction.

When percentage distribution of size fractions in water and sediment samples was calculated, the concentration or activity concentration of each fraction was divided by the total concentration or activity concentration. The uncertainty of the percentage distribution was calculated by using relative uncertainty:

$$\sigma_{A\times B} \; or \; \sigma_{A\div B} = \sqrt{(\frac{\sigma_A}{A})^2 + (\frac{\sigma_B}{B})^2} \tag{3.3}$$

Where σ_A and σ_B are the uncertainties of each measurement, and A and B are the concentrations or activity concentrations.

LOD and LOQ for the ICP-MS analysis was determined based on blank samples. For the sediments, there were 8 blanks, 5 blanks for the water samples, 6 blanks for the biota and 3 blanks for each step of the sequential extraction. Equation 3.4 and 3.5 were used when calculating the LOD and LOQ for the ICP-MS measurements:

$$LOD = 3 \cdot \sigma \tag{3.4}$$

$$LOQ = 10 \cdot \sigma \tag{3.5}$$

Where σ is the standard deviation of n blank samples.

LOD and LOQ for measurements Ge-detector was determined based on the background measurements, measured over a longer period of time (approximately one month) with the different geometries. Equation 3.6 and 3.7 were used when calculating LOD and LOQ.

$$LOD = 4.65 \cdot \sigma_B \tag{3.6}$$

$$LOQ = 14.1 \cdot \sigma_B \tag{3.7}$$

Where σ_B is the uncertainty of the background measurement.

Statistical analysis included students t-test (function "t.test"), and linear regression analysis. The t-test was used to obtain a p-value as an indication if the observed difference between the two mean values was significant. P-values are presented in the appendix (table A1). To look for any relationship or trends between datapoints, linear regression was used. The R^2-value of the regression line was used as an indication if a linear relationship seemed appropriate.

4. Results and discussion

4.1 Quality assurance

The accuracy of the gamma measurements of Cs-137 was validated for one of the geometries by measuring a certified reference material (IAEA 300, Baltic Sea sediment) containing Cs-137 with an activity of 0.704 Bq. Measurement of the certified reference material IAEA 300 in the 20 mL plastic vial geometry yielded an activity of 0.715 Bq $\pm$ 5.66%, which is within the acceptable range with a confidence interval of $\alpha=0.05$.

The obtained chemical yield of the Cs-134 tracer varied between 68% and 83% for LMM, <0.45 µm, and particles (appendix, table C1). When presenting the results of the Cs-137 measurements, the yields have been accounted for, as the loss of tracer is assumed to be equivalent to the loss off Cs-137.

LOD and LOQ for gamma measurements were calculated based on measured background over a longer time with different geometries. Table 4.1 presents the LOD and LOQ, which were 0.04 Bq and 0.12 Bq, respectively, for 20 mL plastic vial geometry. As for the geometry of 180 mL bluecap bottle, LOD was 0.04 Bq and LOQ was 0.17 Bq.

Table 4.1: *LOD and LOQ for Cs-137 (Bq) in different geometries.*

Detection and quantification limits for Cs-137 in Bq		
Geometry	20 mL plastic vial	180 mL Bluecap bottle
LOD	0.04	0.05
LOQ	0.12	0.17

The traceability and accuracy of the ICP-MS measurements was provided by measuring multiple certified reference materials. Results of these measurements are included in table 4.2. Nearly all the measured values of Cs-133 was within acceptable certified reference range, except for 2709a. In addition to accuracy, bias, given as a percentage, can also be calculated from these measurements. Since CRM 2709a was outside the given reference area, % bias can be used to decide if the difference from true concentration still is small enough to consider the accuracy of the method acceptable. The range for CRM 2709a is somewhat narrow, and the measured value is not very far from the stated value. The calculated bias for 2709a was 5.6%, which is lower than for DC773325 (11.9%) and DC7334a (7.0%). All the CRMs were relatively old, thus affecting the stability of the analytes. The CRMs ZC73007, DC773325. 2709a, DCT334a, and ZC73014 was from year 2003, 2004, 2009, 2010, and 2014, respectively. Therefore, the range might be somewhat larger than stated due to increased uncertainty. Although relative high bias, the measured values were within the CRM range and are thus assumed to be accurate.

Table 4.2: *Concentration (mg/kg d.w) of Cs-133 in certified reference materials measured with ICP-MS. n=3.*

CRM name	Sample	Measured (mg Cs-133/kg)	True (mg Cs-133/kg)	% bias
ZC73007	Soil	13.6	13.9 ± 0.7	2.3
DC773325	Soil	3.0	2.7 ± 0.8	11.9
2709a	Soil	5.3	5.0 ± 0.1	5.6
DC7334a	bush, twigs, and leaves	0.25	0.27 ± 0.02	7.0
ZC73014	Tea	0.31	0.32 ± 0.06	2.5

Blank samples were used to calculate the LOD and LOQ, as well as giving an indication whether there was some extent of contamination. Obtained LOD and LOQ is presented in table 4.3. LOQ of Cs-133 was 0.0006 mg/kg for sediment samples, 0.001 mg/kg for biota, and 0.001 µg/L for water.

Table 4.3: *LOD and LOQ for Cs-133 measured with ICP-MS in sediments, biota and water samples.*

Detection and quantification limits for Cs-133			
	Sediments (mg/kg)	**Biota (mg/kg)**	**Water (µg/L)**
LOD	0.0002	0.0003	0.0003
LOQ	0.00063	0.0011	0.0010

Since there were different matrixes in each sequential extraction step, different LOD and LOQ was obtained for each step (table 4.4). The LOQ varied between 0.000012 mg/kg and 0.00019 mg/kg.

Table 4.4: *LOD and LOQ for the different matrices of sequential extraction, measured on ICP-MS.*

Detection and quantification limits for Cs-133 in Sequential Extraction						
	Step 1 (mg/kg)	**Step 2 (mg/kg)**	**Step 3 (mg/kg)**	**Step 4 (mg/kg)**	**Step 5 (mg/kg)**	**Step 6 (mg/kg)**
LOD	0.000009	0.000004	0.000009	0.000007	0.00005	0.00006
LOQ	0.000031	0.000012	0.00003	0.000022	0.00018	0.00019

No blanks contained detectable values of Cs-133, thus indicating that there is no contamination in the samples that has occurred during sample preparation in the laboratory.

4.2 Water

4.2.1 Water chemistry

Water parameters measured *in situ* (temperature, pH, conductivity, salinity, and turbidity) are presented in table 4.5. As the salinity increased, temperature, pH, and conductivity also increased. This suggests that that the content of seawater is crucial for these parameters. Site FW1 and FW2 represent the main part of the river, while FW3, FW4 and FW5 are smaller tributaries. The water flow was different in the different tributaries, in addition, they represent different catchment areas.

Table 4.5*: Measured pH-value, conductivity, salinity, and turbidity of the water from the different sites in the Vefsna river and Vefsnfjord.*

Site	Temperature (°C)	pH	Conductivity (µS/cm)	Salinity (PSU)	Turbidity (FNU)
FW1	0.9	7.29	64	0	1.9
FW2	2.0	7.58	63	0	1.8
FW3	2.3	7.30	47	0	1.3
FW4	2.4	7.02	45	0	2.1
FW5	2.5	7.46	66	0	1.8
SW1	3.3	7.38	9340	4.9	1.2
SW2	5.6	7.94	22600	13.9	0.5
SW3	7.0	8.23	32900	22.0	0.5
SW4	8.1	8.49	46800	29.2	1.3

The pH-value ranged from 7.02 to 7.46 in the riverwater, and from 7.38 and 8.49 in the seawater. This is within normal pH-values in Norway, as previously reported pH-values from freshwaters and rivers in Nordland county have been reported to be in the range from about 6 and up to 8 in freshwater(Hindar et al., 2020 ; Walseng, 1989), and around 8 in the seawater of the Norwegian sea (Chierici et al., 2015).

Table 4.6 lists the concentration (µg/L) of major cations in the water samples (<0.45 µg/L). Ca^+ and Cs-133 were measured on ICP-MS, while K^+, Na^{2+} and Mg^{2+} were estimated based on representative concentrations of cations in standard seawater samples (Lienhard et al., 2012), by calculating the relationship between Ca^+ and K^+, Na^{2+}, and Mg^{2+}.

Table 4.6: *Major cations (µg/L) in river Vefsna and Vefsnfjord (<0.45 µm), measured with ICP-MS (n=3).*

Site	Ca^{2+} (µg/L)	K$^+$ (µg/L)*	Na$^+$ (µg/L)*	Mg^{2+} (µg/L)*	^{133}Cs$^+$ (µg/L)
FW1	9.9 ± 0.24	ND	ND	ND	0.009 ± 0.0001
FW2	9.9 ± 0.12	ND	ND	ND	0.007 ± 0.0001
FW3	4.7 ± 0.06	ND	ND	ND	0.010 ± 0.0001
FW4	2.3 ± 0.03	ND	ND	ND	0.015 ± 0.0001
FW5	11.5 ± 0.48	ND	ND	ND	0.017 ± 0.0001
SW1	74 ± 1.0	70 ± 1.0	1963 ± 28	234 ± 3.3	0.054 ± 0.0001
SW2	170 ± 3.2	161 ± 3.0	4487 ± 85	536 ± 10	0.123 ± 0.0001
SW3	277 ± 7.9	263 ± 7.5	7325 ± 208	875 ± 24	0.200 ± 0.0001
SW4	368 ± 9.8	349 ± 9.3	9717 ± 259	1161 ± 31	0.261 ± 0.0001

* Calculated based on Cs and the relationship in seawater (Lienhard et al., 2012).

The measured turbidity in water varied between 0.5 FNU and 2.1 FNU. These values are low, which is likely caused by low rainfall, and low waterflow in the river in the weeks prior to measurement. The turbidity measurements were somewhat higher in freshwater than in seawater, ranging between 1.3 FNU and 2.1 FNU. Variation in turbidity between the different sites in the river might be explained by differences in water flow. Additionally, they represent different catchment areas, so there might be some differences in erosion from the catchment or flooding. There will be an increase in particle content in the riverine water in periods of high erosion, causing an increase in turbidity (Vives I Batlle, 2012). In site FW4, samples were collected from a bridge using a bucket and a rope, thus causing bottom sediments to mix with the water. Therefore, measurements from this site are associated with high uncertainties.

In the seawater, there was a decrease in turbidity with increasing distance out the fjord, from 1.2 FNU in site SW1 to 0.5 FNU in site SW2 and SW3. However, at site SW4 there was an increase to 1.3 FNU. Turbidity tends to decrease with increased salinity in estuaries due to aggregation and flocculation effects, where the high salinity seawater causes particles to settle more quickly (Burgess et al., 2002). This phenomenon might explain the observed decrease in turbidity between salinities 5 and 22 PSU (SW1-SW3), however, it does not explain why there is a sudden increase at 29.3 PSU (SW4). A possible reason might be dilution of river transported particles as freshwater mixes with seawater.

Since the turbidity measurements were not performed in a laboratory, but in a workshop shortly after the sample collection, they might be associated with some uncertainty. The turbidity probe worked by measuring infrared light at a 90° angle from the bottom of the probe and required a light-proof container with appropriate conditions so that light from the surroundings and the

container walls did not interfere with the measurements (WTW, 2017). Moreover, the probe needed to be held steady to achieve as stable measurements as possible, although it did not become completely stable. As a sum of all these aspects, the results should be interpreted with caution.

4.2.2 Cs-133 in water

Although the main emphasis was to analyse Cs-137, the presence of Cs-133 is of interest as high concentrations might affect the binding of Cs-137 to suspended sediments, thus initializing competition between the two isotopes. In addition, Cs-133 might be used as a stable analogue for Cs-137, thus is it of interest to see if there are any correlations between the two isotopes.

The total concentration of naturally occurring Cs-133, and Cs-133 associated with particles and colloids + LMM (<0.45 µm) in Vefsna river is illustrated in figure 4. The figure presents concentration of Cs-133 from site FW5 to FW1, as this represents the locations in the river from furthest upstream to near the river outlet.
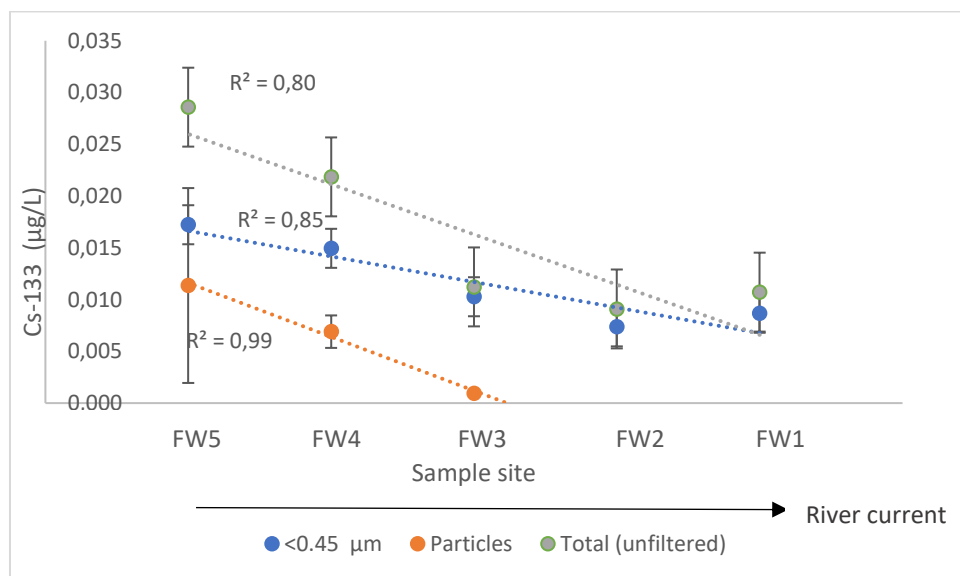
Figure 4.1: *concentration (µg/L) of Cs-133 in unfiltered water, particles, and <0.45µm in five different locations in the Vefsna river.*

The total concentration (fig. 4.1) of Cs-133 is less than 0.030 µg/L and low in all FW sites, although it seems to be a higher concentration further upstream the river. Cs-133 was fund in particles in site FW3, FW4, and FW5, although the particle fraction in site FW4 could be affected by the sampling technique. For FW1 and FW2, LMM and colloidal fraction were also determined. Table C2 in the appendix shows that Cs-133 in FW1 and FW2 predominantly

existed as LMM species, as the concentration of LMM made up 90% and 97% of the <0.45 μm fraction in site FW1 and FW2, respectively

The concentration of the <0.45 μm fraction was higher than the concentration of particles, whose concentration ranged between 0.001 ± 0.0003 µg/L and 0.01 ± 0.009 µg/L, while the concentration of the <0.45 μm fraction ranged between 0.007 ± 0.0002 µg/L and 0.02 ± 0.002 µg/L.

Error bars are included for all the datapoints in figure 4.1, however, the uncertainties for most of the datapoints for the <0.45 μm fraction is low and hardly visible. The uncertainties are high in site FW5, especially for particles. This suggests that the samples (n=3) are either inhomogeneous, or the precision of the method is poor. However, low uncertainties for the remaining samples indicated that the error is likely caused by inhomogeneous samples.

The concentration of Cs-133 in seawater as a function of salinity is presented in the appendix (figure B1). It is a linear relationship ($R^2 = 1$) between Cs-133 and salinity of water, with an increase in concentration of Cs-133 as the salinity increases. Cs-133 was predominantly represented as LMM species, although there was a low concentration of colloids in the inner part of the fjord, at 0-5 PSU. However, the concentration of colloids was barely above LOQ.

4.2.3 Cs-137 in water

The activity concentration of dissolved Cs-137 in the river is presented in figure 4.2. It was only in site FW1 (outlet of Vefsna) that the activity of particles was above LOQ, thus the total activity would be almost identical to dissolved concentration of Cs-137. Overall, the activity concentration was between 5.3 ± 0.3 Bq/m³ and 3.2 Bq/m³ $\pm$ 0.3 and relatively low, with small variations between each site.
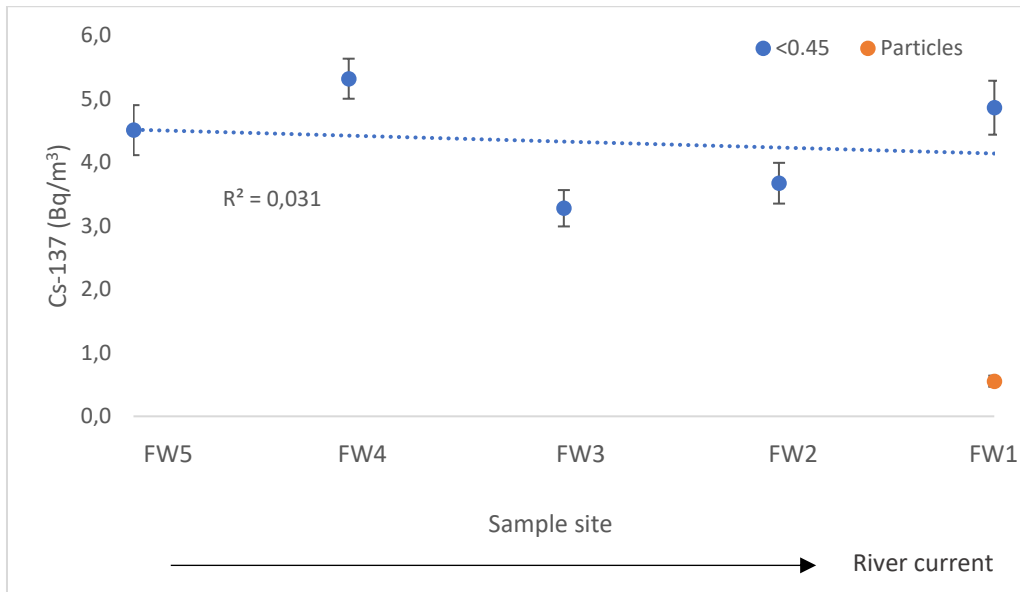
Figure 4.2*: Activity in particles (>0.45 µm) and the <0.45 µm fraction in the Vefsna river*

Cs-137 appears to be mainly represented as <0.45 µm, similar as for Cs-133. However, previous studies have reported that suspended particles usually account for the major fraction of the transport of Cs-137 in rivers (Eyrolle & Charmasson, 2004; Kanivets et al., 1999). The LMM fraction made up 82% and 92% (appendix, table C2) of the activity of the <0.45 µm fraction where it was measured (FW1, FW2). By comparing figure 4.1, it does not appear to be any correlation between Cs-133 and Cs-137 present as <0.45 µm in the river. The linear regression lines in figure 4.1 showed a relatively linear relationship (R^2=0.85) for the activity concentration of Cs-133 (<0.45 µm) with respect to the river current, which is not the case for Cs-137 (R^2=0.03). However, it must be noted that the linear regression in this case should be interpreted with caution, since the sites does not represent one continues river flow, as FW3, FW4, and FW5 feeds into the main river. Further, a plot of Cs-133 (µg/L) against Cs-137 (Bq/L) is presented in appendix C2, to look for ant relationship between the two isotopes. With an R^2 of 0.28 and a correlation coefficient of 0.49 does it not seem to be much correspondence. Thus, Cs-133 should not be used as a stable analogue for Cs-137 in Vefsna river.

The amount of Cs-137 associated with particles in site FW1 is about 0.55 ± 0.087 Bq/m^3 and approximately 10 times lower than for the <0.45 µm fraction. It might be worth noticing that the sites with presence of Cs-133 associated with particles are different from the site with Cs-137 associated with particles. As Cs-137 is only present as particles in site FW1, while Cs-133 is only present as particles in site FW3-FW5. A possible explanation for this observation is that Cs-133 are occupying the binding sites on the particles in site FW3-FW3, since the total concentration of Cs-133 also is higher in these sites. Alternatively, there might be a greater supply of Cs-137 in site FW1 causing more Cs-137 to bind to particles. However, since the activity concentration of particles are close to LOQ, it is more likely caused by uncertainties in the measurements.

Normally, it is expected that the major fraction of Cs-137 would be associated with the particle fraction in river discharge (Simonsen et al., 2019a). Cs-137 is mainly transported in rivers as particles because of its strong affinity to clay minerals, but also exists as LMM species and colloids (Delaval et al., 2020). The most apparent explanation for the low fraction of Cs-137 associated with particles was the low water flow in the river during sample collection, as erosion leads to higher content of suspended particles (Vives I Batlle, 2012). If the samples had been collected after or during a flooding event, it would likely result in a different size distribution. Particles are mostly transported with the currents and will settle rapidly in quieter waters (von Gunten & Benes, 1994).

Figure 4.3 (A) illustrates the change in total activity concentration of Cs-137 in surface water from the river outlet and out the Vefsnfjord, as a function of salinity. The activities were generally low both in freshwater and seawater, decreasing from 5.4 ± 0.5 Bq/m^3 to 3.0 ± 0.2 Bq/m^3 with increasing salinity. The data plot includes uncertainty bars based on counting uncertainty, which were approximately 10% for most data points. Since it is a relatively small difference in activity concentration between the different salinities, there are some overlapping values.
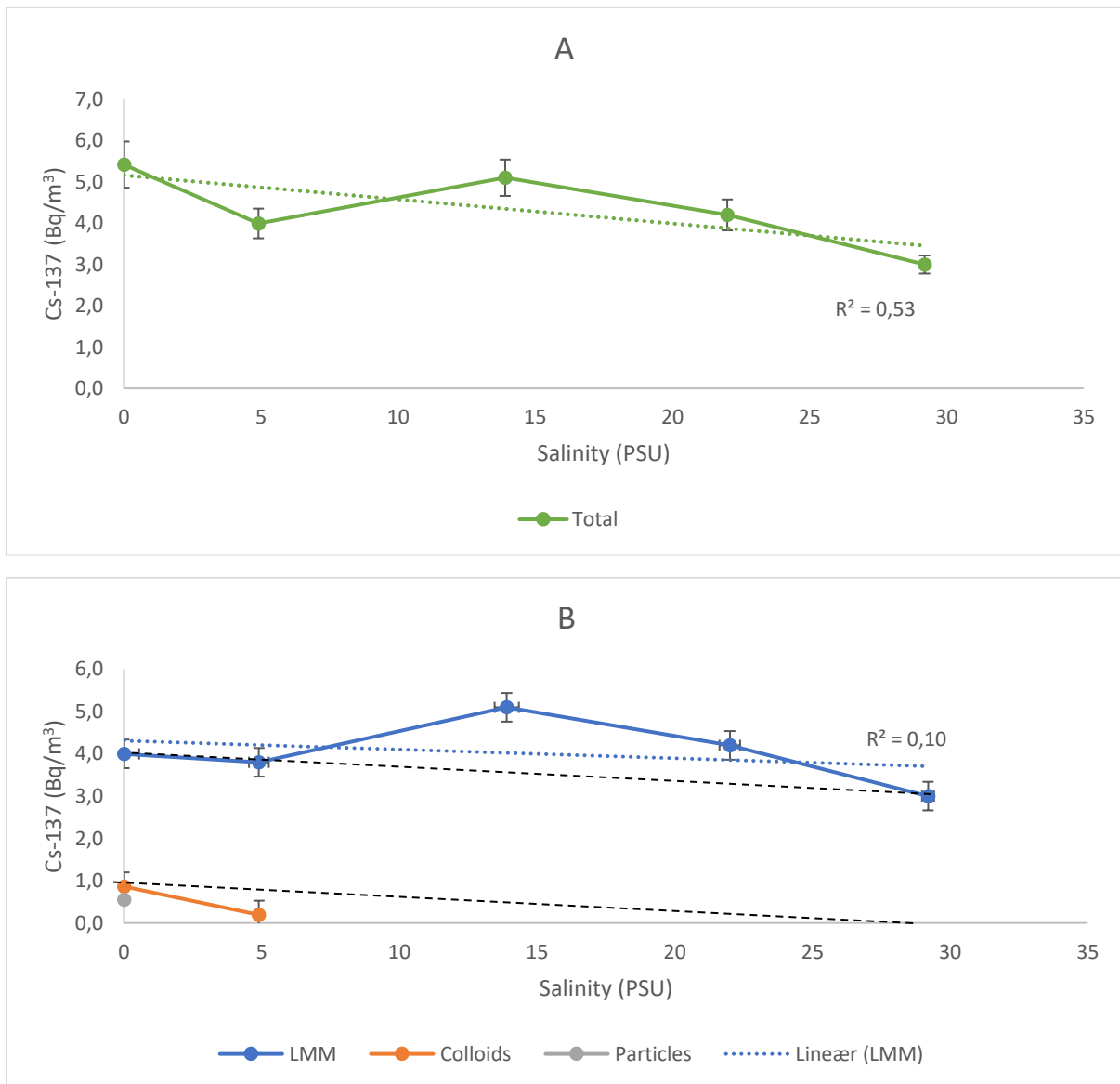
Figure 4.3: *Total measured activity of Cs-137 in water (A) and measured activity of Cs-137 in LMM, colloids and particles (B) at different levels of salinity. Dotted lines represent the dilution of LMM and colloidal species with increased salinity. Values above the estimated dilution indicates remobilization, while values below the estimated dilution indicates aggregation or remobilization.*

Activity concentration of LMM, colloids, and particles are presented in figure 4.3 (B). It was only in the river, at salinity 0 PSU (site FW1) that the activity concentration of particles was above LOQ. However, the activity was low (0.55 ± 0.09 Bq/m^3). Cs-137 was present as colloids at salinities 0 PSU and 5 PSU, but below detection limit at salinities above 5 PSU. The activity concentration of Cs-137 associated with colloids was reduced from 0.86 ± 0.14 Bq/m^3 at 0 PSU to 0.19 ± 0.26 Bq/m^3 at 5 PSU.

The major fraction of Cs-137 (74 – 100 %) was present as LMM in the water samples and had activity concentrations varying between 3.0 ± 0.2 Bq/m^3 and 5.1 ± 0.4 Bq/m^3. Since the major

fraction of Cs-137 exists as LMM species in seawater, the changes in total activity concentration (4.3A) is mostly dependent om the changes in the LMM fraction. Linear regression shows that there was an overall negative trend for activity concentration of LMM species with increasing salinity, although the decrease in activity concentration was minimal. There was a poor R^2 between the data points ($R^2 = 0.10$), meaning there was no linear relationship. The difference in activity concentration between colloids and LMM are significant, with a p-value of 0.002 calculated by using the mean values of each species in a two-sided t-test.

As the salinity increased from 0 to 5 PSU, the colloidal and particulate fractions was rapidly removed from the surface water. This might have occurred due to aggregation effects in the presence of cations in the seawater. Particles generally have a negatively charged surface, generating an electrostatic repulsing force. In the presence of monovalent (K^+, Na^+) or divalent (Ca^{2+}, Mg^{2+}) cations from the seawater, however, cations will interact with the surface of the particles, initiating van der Waals forces between adjacent particles, causing them to stick together (Mosley & Liss, 2020). Particle size changes settling velocity drastically, so that larger particles will settle more quickly (Simonsen et al., 2019a). Colloids typically remains in suspension and do not settle due to their small size. In estuaries however, colloids might aggregate from the destabilizing effect of seawater cations (Mosley & Liss, 2020).

Although there was a general decrease in concentration of LMM species which is supported by site SW1 (5 PSU) and SW4 (30 PSU), there was a slight increase in site SW2 (13 PSU). Since the Vefsna river is assumed to be the main source of Cs-137, it would be expected some dilution when the riverine water mixes with seawater in the estuarine zone causing a decrease in activity concentration, followed by a further decrease out the fjord. An explanation for the observed increase in LMM species is remobilization from colloids and particles caused by increased ionic strength in the inner parts of the fjord (Simonsen et al., 2019b). Based on the estimated dilution presented by the dotted line in figure 4.3, it does appear to be some degree of remobilisation of LMM species of Cs-137, as the activity concentration is higher than the estimate. Also, the reduced activity concentration of Cs-137 in colloids suggests either aggregation, or remobilization of LMM species from colloids.

Studies have shown that Cs-137 indeed does remobilize from particles when introduced to seawater (Takata et al., 2015). Remobilization is more rapid at low salinities up to 10 PSU, while there is lesser observed changes in desorption rates at higher salinities (10–35 PSU) (Delaval et al., 2020). This corresponds with the results of this experiments, where the incline

abates after 13 PSU, followed by a decrease in LMM activity concentration as the salinity increases from 13 PSU to the highest salinity point at about 30 PSU (SW4). On the other hand, other rivers that feed into the Vefsnfjord might have contribute to the elevated activity concentrations of LMM Cs-137 observed between 5 PSU and 13 PSU. The decrease in LMM activity concentration is likely to be caused by dilution form the seawater.

Since the concentration of Cs-133 in seawater was linearly correlated with salinity, it cannot be used as a stable analogue for Cs-137. The concentration of Cs-137 in seawater does not show the same correlation with salinity as Cs-133.

4.3 Sediments

4.3.1 Sediment characteristics

The composition of sand silt and clay in the sediments from the Vefsnfjord and Vefsna river was determined by wet sieving and sedimentation. The distribution of sand, silt, and clay in surface riverine- and marine sediments are presented in figure 4.4.
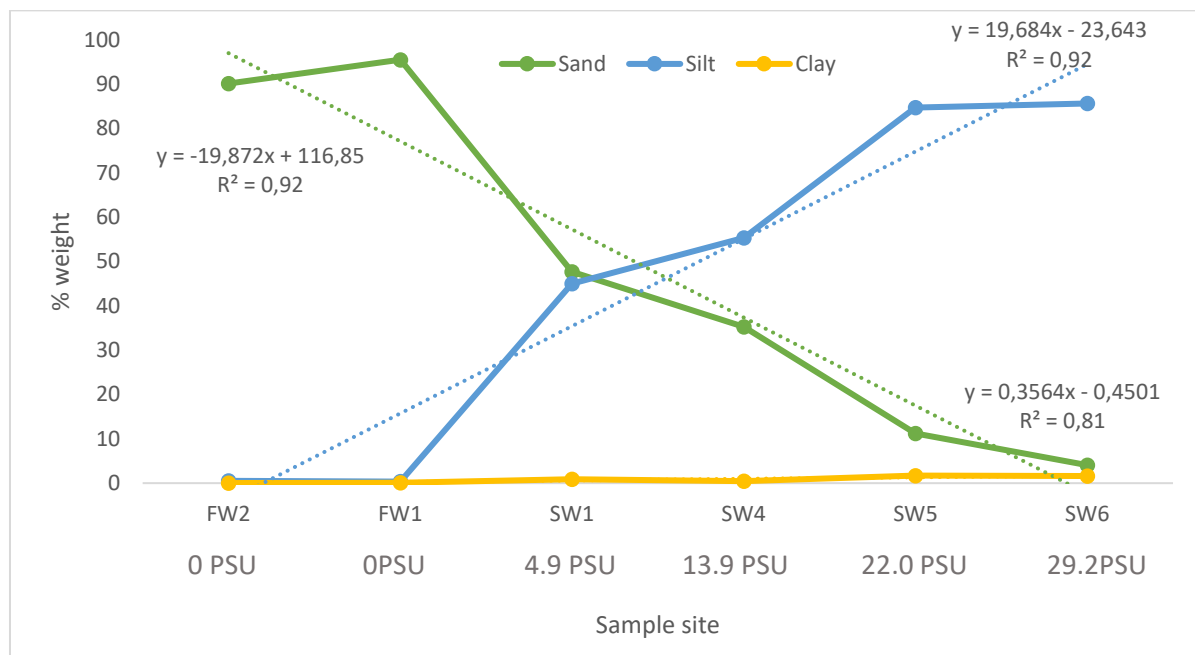

Figure 4.4: *Distribution (%) of Cs-137 associated with sand, silt, and clay from surface sediments at different sample sites in the Vefsna river and the Vefsnfjord. Site FW2 is displayed before site FW1 in the figure since it lays further upstream the river, thus representing the location of FW2 relative to the others.*

The riverine sediments consisted mostly of sand (<90%), while the weight of silt and clay made up <1% of the total mass each. At the river outlet, in the innermost part of the fjord (site SW1, at about 40 meters depth), there was a change in distribution of the size fractions compared to what was observed in the river, with 48% sand, 45% silt, and 2% clay. Coarse sediments is likely to be transported with the river current (Heldal et al., 2021), which explains why it was more sand in site SW1 than SW4-SW6. The distribution continued to change further out the fjord with increasing content of silt, while the sand fraction decreased. 85% of the sediments consisted of silt furthest out the fjord. Larger particles settle quickly when riverine water mixes with seawater in the river outlet, while smaller particles take longer time to settle and will remain in suspension for a longer period (Portela et al., 2013). Thus, are they transported for a longer distance. This might explain why the content of silt increased outward the fjord.

The fraction of clay remained low, however, the was a slightly increase in the outer parts of the fjord (SW5-SW6). Although, compared to the riverine sediments, the content of clay was more than a factor of 2 higher, at 2% in site SW4 and 5% in both site SW5 and SW6. The difference in distribution of Cs-137 between the riverine sediments and marine sediments was statistically significant, with a p-value of 0.01 for both sand and silt, and a p-value of 0.05 for clay (appendix, table A1). The p-value was determined by a two-sided t-test by comparing the mean value of the SW sediments and FW sediments for sand, silt, and clay.

Linear regression of the data points in figure 4.4 shows there was a linear relationship between percentage of silt and sand, and salinity, with R^2 values of 0.92 for both fractions. Clay has a small increasing trend with R^2 of 0.81. It is also observed a clear decreasing tendency for sand, while the silt fraction increases. The slopes of the curves have almost identical absolute values, with 19.8x for sand and 19.6x for silt. Based on the regression line, the majority of the sediment composition changes from sand to silt somewhere between in inner parts of the fjord, at site SW1 (PSU 5). The salinity was in the upper range of what is normal in the innermost part of the fjord as result of low waterflow (58 m^3/s). Normally, there is a higher waterflow in Vefsna (70 m^3/s) during late autumn with high flooding events during May-June, and thus lower salinity in station SW1. This might have an effect in distribution of sand, silt, and clay, as there seems to be a difference in sediment composition from freshwater to seawater.

A more recent study of sediments from the Vefsnfjord showed similar distribution of sand, silt, and clay in the locations corresponding to SW4, SW5 and SW6 (Heldal et al., 2021). In addition, the study showed that the sediments from the outermost parts of the fjord contained higher levels of TOC and carbonates than from the outer parts of the fjord, thus assuming the marine

sediments mostly consisted of biogenic materials. However, TOC was not measured in this experiment and can therefore not be compared. In the inner parts of the fjord however, the sediments were coarser, and thus was more likely a product of rock erosion (Heldal et al., 2021). The distribution of sediments in estuaries are dependent on several factors, like tidal discharge, freshwater river flow, and salinity of the water (Kendrick & Derbyshire, 1976). The interaction of tides, currents and the salinity causes the deposition of the finer fractions of the bottom sediments like silt and clay further out the fjord (Rainey et al., 2003), since increased salinity causes increased settling velocity of suspended clay and silt due to aggregation (Portela et al., 2013).

Since the separation of clay from silt in the marine sediments was performed in filtered seawater (33 PSU) rather than freshwater, the silt fraction might be overestimated. The purpose of performing the separation in seawater rather than freshwater was to avoid any change in distribution of sand, silt, and clay, simulating a natural environment. To see if it was possible to separate more clay from the seawater silt, a new round of separation was performed in riverine water. From approximately 20 g of silt from site SW4, 1.6 g of clay was isolated, which equals 8%. Compared to the low content of clay obtained from separation in seawater, it might make up a significant difference to separate in freshwater.

The chemical properties of clay minerals can explain why this may have occurred. Like mentioned in chapter 4.2.3, particles and colloids have a net negative charge initiating repulsive forces between the individual particles. Major cations in seawater induces coagulation of particles by compressing the electrical double layer of particles and colloids (Mosley & Liss, 2020). As the flocks of clay descend, other small particles are picked up, further increasing the size. The settling velocity will increase as a result of this due to the correlation with particle size. Larger particles descend faster than smaller particles The salt content is positively correlated with settling velocity for salinities up to 20 PSU, although these tendencies are mostly observed in brackish water with salinity between 5 to 10 PSU (Sutherland et al., 2015). Based on this information, it is likely that the separation of clay and silt indeed has been disrupted by the seawater. On the contrary, since these processes occur naturally in saline waters, it might be an accurate representation for the distribution after all. As a result, typical clay minerals might be found in the silt fraction, which can be investigated by determining the mineral composition of silt and clay.

4.3.2 Mineral composition

The diffractograms obtained from XRD analysis of silt fractions is presented in figure 4.5 A-C. The diffractograms are presented as intensity (counts) as a function of the 2θ angle. (A) shows the mixed (FW1+FW2) freshwater silt fraction from Vefsna river, (B) shows the mixed (SW1+SW4+SW5+SW6) seawater sediment sample, separated in seawater, and (C) shows the seawater sediment sample from site SW4 that has been separated in freshwater.
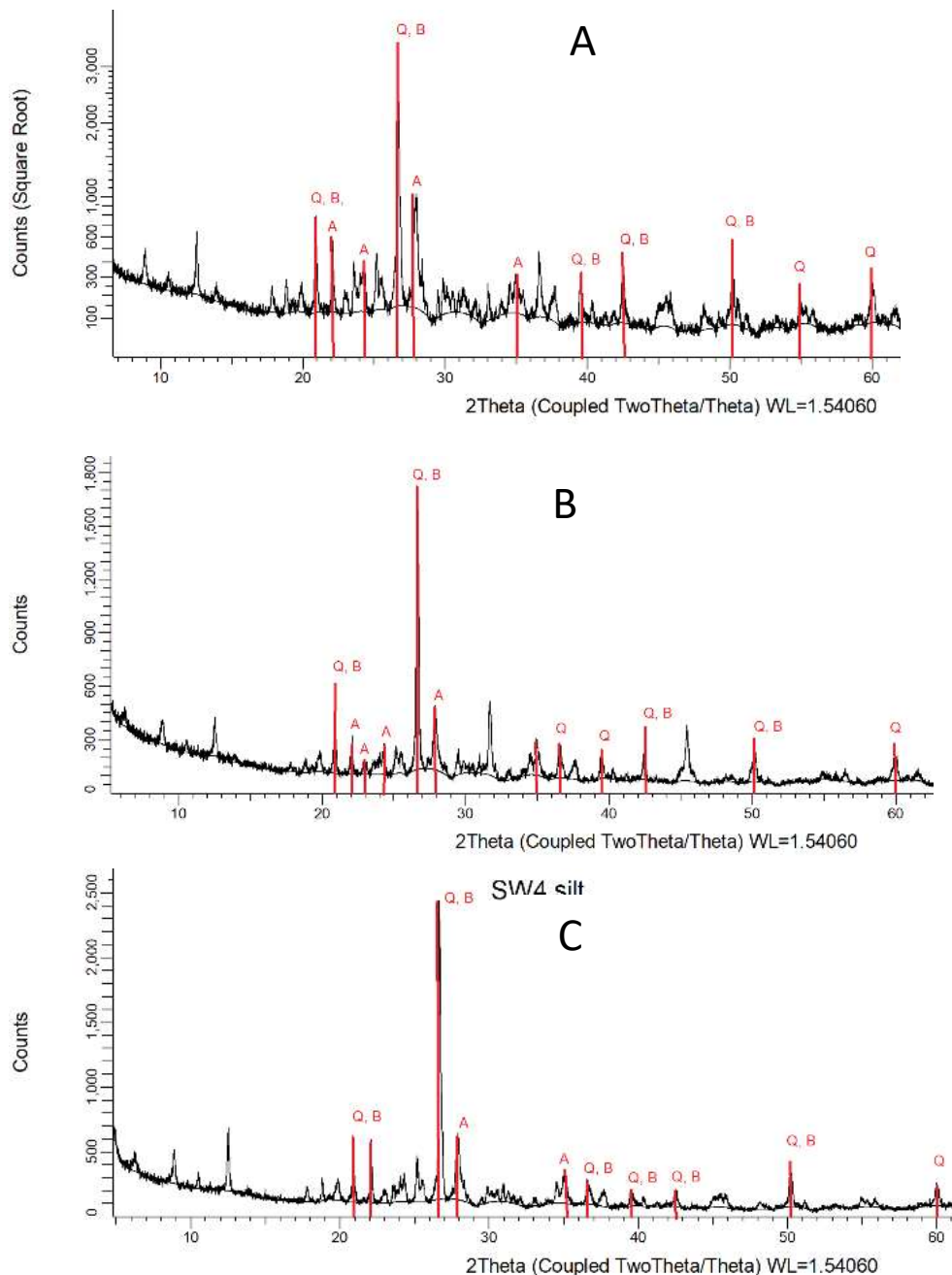
Figure 4.5: *Diffractograms of the silt fraction from mixed freshwater sediments (A), mixed seawater sediments (B) and seawater sediments from site SW4 separated in freshwater (C). Red lines represent the reference pattern for minerals recommended by the software. Q =quartz, B = berlinite, A = albite.*

The diffractograms for the silt samples both from freshwater and seawater (fig. 4.5 A-C) contains peaks that corresponds well with quartz and berlinite, with some lower intensity peaks that indicates content of albite as well. Berlinite has an almost identical chemical structure as quartz, where Si atoms are exchanged with Al and P atoms in an alternating manner (Tanaka et al., 2010). Therefore, it is difficult to differentiate between berlinite and quartz, as they will have a similar reference pattern. However, since berlinite is a rather rare mineral and quartz is quite commonly found in sediments, there might not be any berlinite present in the sample at all. Especially since quartz and berlinite share the same intensity peaks in all the diffractograms for the silt samples (Tanaka et al., 2010).

All the silt samples had relatively similar patterns, suggesting that the mineral composition does not change particularly from the river to the fjord. Since the seawater sediment sample (SW4, fig. 4.5 B) separated in freshwater have a similar pattern as the mixed seawater sediment sample (fig. 4.5 C), it appears that separation in freshwater did not alter the mineral composition greatly. However, there is a peak at $2\theta=31.5°$ in the mixed SW silt sample (B) that does not appear in SW4 silt (C) or FW silt (A). Although there were no mineral matches found for this peak, comparison with the diffractogram of SW clay (fig. 4.6 A) shows a high energy peak at approximately $2\theta=31.5°$ for halite (NaCl). Hence, the peak might be caused by salt from the SW silt sample.

Some peaks had rather low intensities, which can be explained by values that reaches LOD and LOQ. This leads to difficulties in determining whether the mineral is present in the sample or not, since intensities were not much higher than the background. In addition, background noise might reduce the intensity of the peaks. Uneven sample surface might lead to increased background, as well as too small or too large particle size. Preferred grain size for XRD ranges between 1 and 5 µm (Ermrich & Opper, 2011). The silt fraction in this experiment, however, ranged between 2 and 63 µm while the clay fraction was <2 µm. Therefore, this might have increased the intensity of the background.

The diffractograms obtained from clay are presented in figure 4.6 (A-B). Unfortunately, it was not enough clay from freshwater sediment to perform XRD, since the entire sample needed to be used in sequential extraction. As for the SW clay mixed sample (separated in seawater) (A) and SW4 clay (separated in freshwater) (B), the diffractograms turned out to be somewhat challenging to interpret. It was not possible to determine the mineral composition of SW clay due to the high salt content. The only match for SW clay was halite (NaCl), with high intensity

peaks. Clay minerals present in the sample would likely be closer to background level, based on the diffractogram for SW4 clay. As a result, the halite signal outcompetes any other signal.
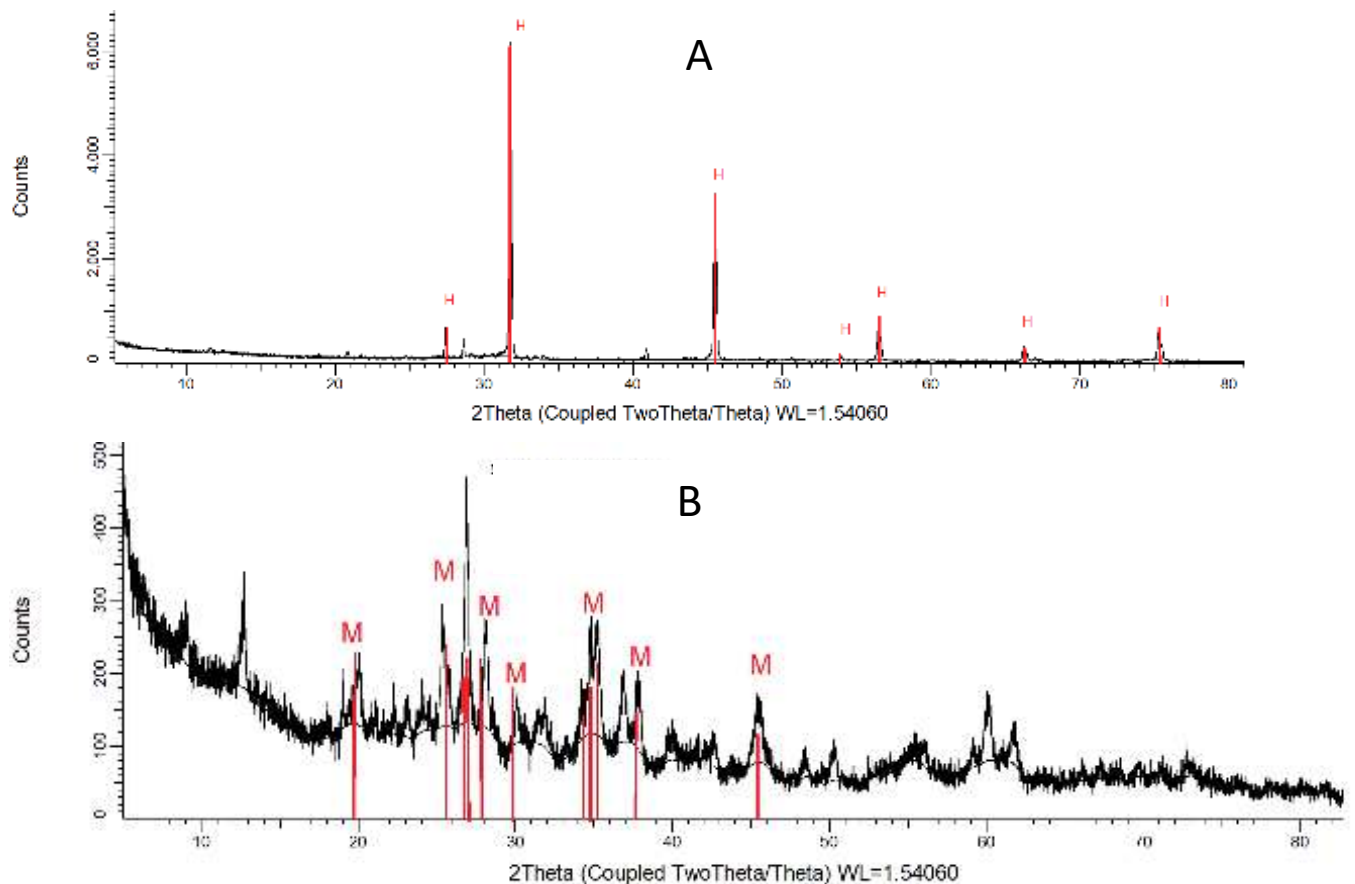
Figure 4.6: *Diffractograms of the clay fraction from seawater sediments separated in seawater (A), and SW4 sediments separated in freshwater (B). Red lines represent the reference pattern for minerals provided by the software. H = halite, M = muscovite.*

In the SW4 clay fraction that has been separated in freshwater, the only clay mineral that could fit the peak pattern provided by the crystallography open database was muscovite (fig. 4.6 B), however the reference pattern of muscovite did not appear as a very good match when compared with the peaks of the diffractogram. The high intensity peaks of the reference pattern for the mineral should appear in the diffractogram of the sample, or else, it is likely not a good match. However, this might be caused by the general low intensities reaching background levels making the diffractogram difficult to interpret. Since muscovite is defined as a clay mineral (VanLoon & Duffy, 2017), is it not unlikely that is a part of the clay sample.

Specific searching for typical clay minerals, especially illite which is the most abundant clay mineral and binds strongly with Cs (Rajec, 1999), yielded no matches. However, muscovite has a strong resemblance of illite with an almost identical mineral composition. In higher grade metasedimentary rocks, illite is replaced by muscovite (Hunziker et al., 1986). The same mineral search was performed for the silt samples to look for any clay minerals present in the silt fraction. If there were clay minerals present, it could be an indication that the silt fraction was indeed overestimated as a result of flocculation of clay minerals when separating clay from silt in seawater. However, there were no search matches, which might indicate that it was no clay in the silt fraction. Alternatively, it can be due to differences in intensity. While the silt fractions had intensities up to 3000 counts, was the highest peak in the SW4 clay (fig. 4.6 B) 600 counts, with a background level around 300 counts. In general, the various composition of clay minerals as well as the unique structures makes interpretation of the XRD diffractograms somewhat challenging (Zhou et al., 2018).

Studies has shown that Cs binds strongly to weathered, sand-sized muscovite particles in solution, with K_d-values comparable to that of illite. K_d-values obtained from the binding of Cs to muscovite was nearly one order of magnitude larger than observed K_d-value for relatively large illite particles (Kwong-Moses et al., 2020). However, the size of the illite clay particles is of importance, as binding of Cs to smaller illite particles had a much higher K_d-value than for muscovite. The muscovite in this study, however, is a part of the clay fraction (< 2.0 µm). Therefore, it might not be directly comparable with the result from Kwong-Moses et al., 2020. Muscovite has a higher cation exchange capacity (CEC) and K_d than quartz. The K_d-value of muscovite has previously been estimated to 591 L/kg, while quartz has a K_d value between 1 and 58 L/kg and albite has a K_d of 519 L/kg (Cornell, 1993). K_d values obtained from this experiment is presented and discussed in section 4.3.4.

4.3.3 Activity of Cs-137 in sediments

Results from the two core samples from the Vefsna river (site FW2) and Vefsnfjord (site SW1) are presented in figure 4.7 A and B, respectively. The riverine core from site FW2 was 7 cm deep, while the marine core from site SW1 was 5 cm deep. The figure shows activity concentration in sliced layers of 1 cm thickness. Therefore, the measured activity is represented as the mean value of each layer (i.e., 0.5 cm, 1.5 cm, etc.). The activity concentration in the core from the river (FW2) varied between 57 ± 1.7 Bq/kg to 93 ± 1.6 Bq/kg (d.w), while the activity concentration was higher in site SW1 and varied between 134 ± 6.3 Bq/kg and 197 ± 3.3 Bq/kg. Uncertainties varied between 1.2% and 4.6%.
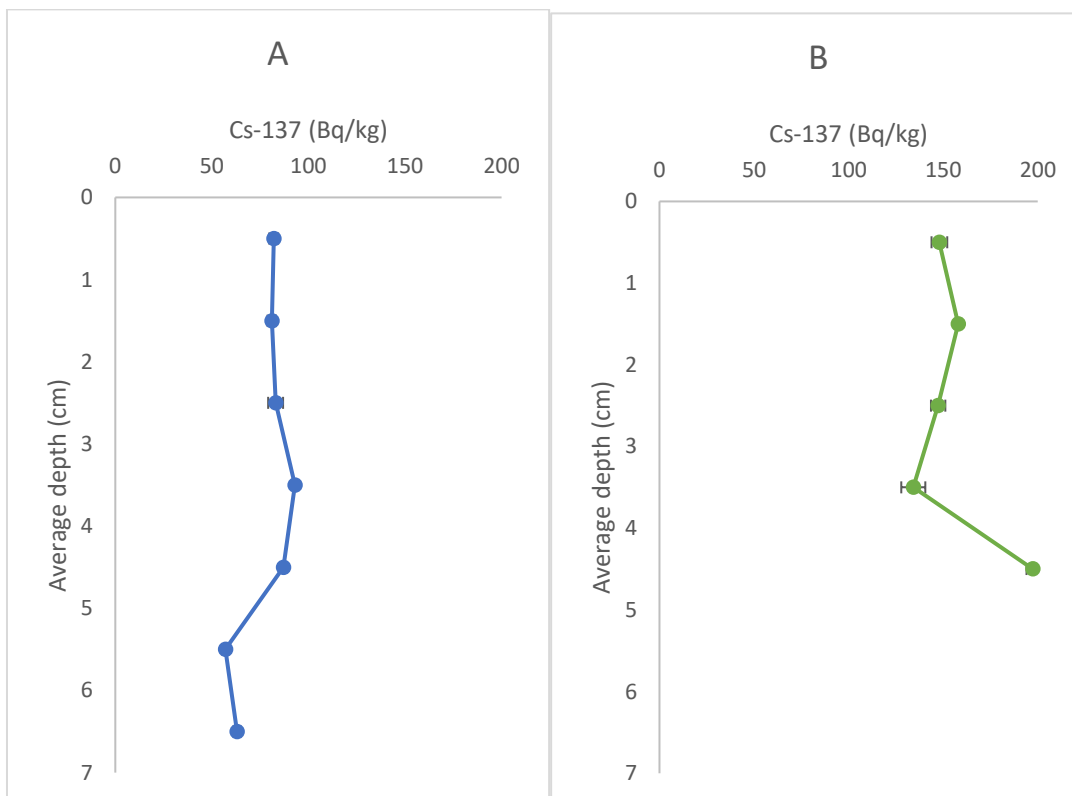
Figure 4.7: *Activity concentration (Bq/kg d.w) in cores from Vefsna river and the inner parts of the Vefsnfjord. A shows activity concentration from 0-7 cm in site FW2, while B shows activity concentration from 0-5 cm in site SW1.*

Unfortunately, sample collection with the corer was somewhat challenging as the corer would not dig deep enough into the sediments. As a result, the cores do not seem to be deep enough to observe any large differences in activity concentration. However, in the study of sediments from (Heldal et al., 2021), the cores seemed to have a activity concentration peak at 7-16 cm depths depending on location in the fjord. Regardless, the activity peaks were located deeper down the core than the 5 and 7 cm that was collected in this experiment. Further, those cores

were collected at different sites, with different sediment composition and salinity, and might not be comparable with the cores from the innermost part of the fjord.

The concentration of Cs-133 and activity concentration of Cs-137 of total sediment samples (before separation into sand, silt, and clay) are presented in figure 4.8 A and B. Cs-133 is included for comparison with Cs-137. Both isotopes show an increase in concentration and activity concentration with increased distance from the river and outward the fjord, with lowest concentrations in the river and highest concentrations furthest out the fjord (site SW6). In addition, linear regression shows R^2 values of both plots are relatively similar, with $R^2=0.82$ for Cs-133 and $R^2=0.78$ for Cs-137, which indicates a somewhat correspondence with the linear trendline.
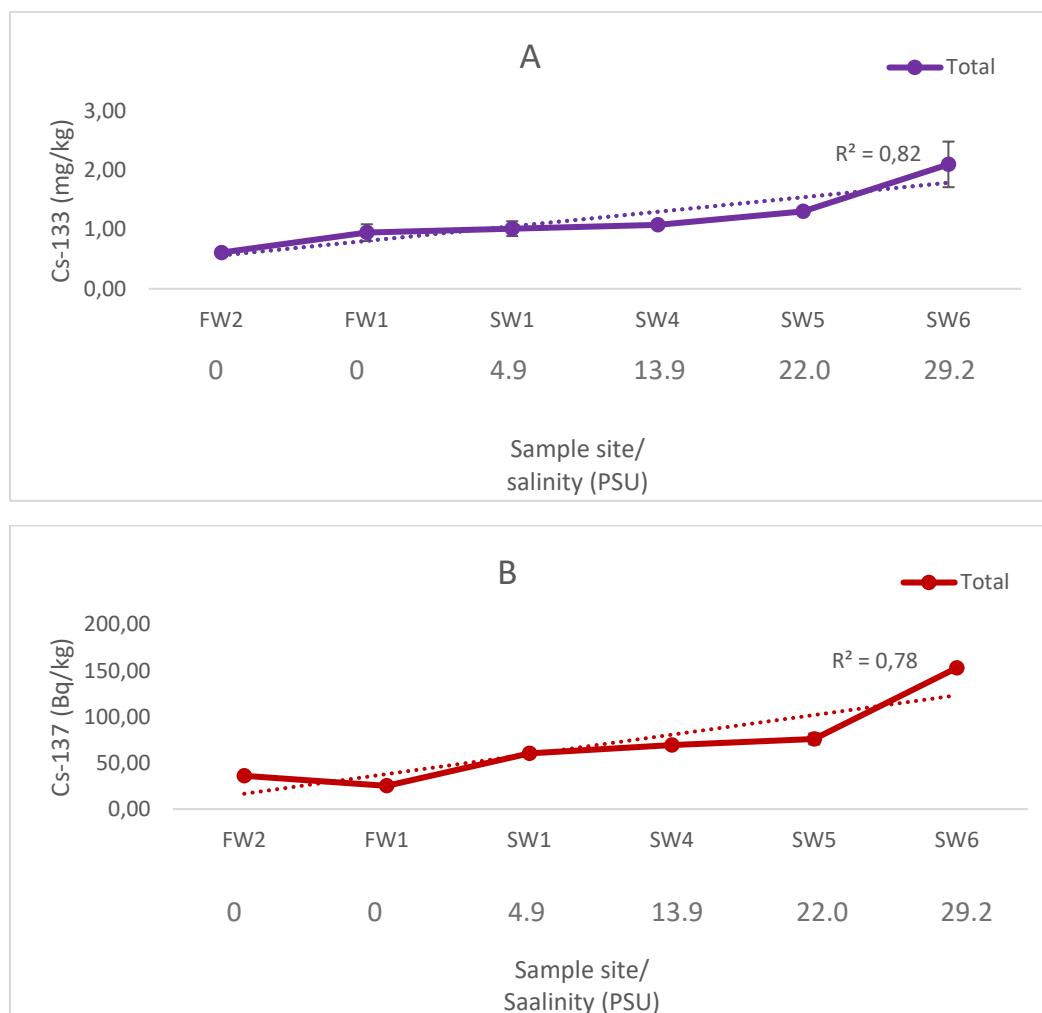
Figure 4.8: *(A) concentration (mg/kg d.w) Cs-133 and (B) activity concentration (Bq/kg d.w) in total sediment sample.*

For further comparison of Cs-133 and Cs-137, The concentration of the two isotopes is plotted against each other in Appendix, figure A1. The plot shows good correspondence with a linear model (R^2=0.90), indicating that Cs-133 might be used as a stable analogue for Cs-137.

The concentration (mg/kg d.w) of Cs-133 in sand, silt, and clay is presented in figure 4.9.
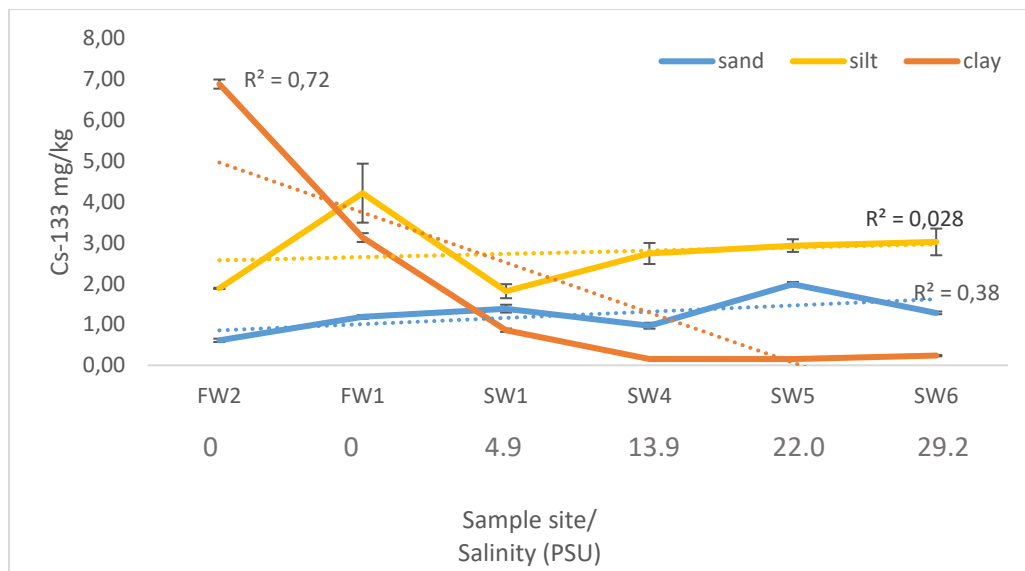
Figure 4.9: *Concentration of Cs-133 (mg/kg d.w) in surface sediments from river Vefsna and with increased distance outward the Vefsnfjord. Based on the mean value of n=3 parallels.*

As figure 4.9 shows, there were a higher concentration of Cs-133 in silt than in sand. However, it does not appear to be any correlation between the concentration of Cs-133 in riverine sediments and marine sediments for either sand or silt. This indicates that increased distance from the river outlet, and thus increased salinity, does not affect the concentration of Cs-133 in sand and silt. Although there are some variations in concentrations of Cs-133 in sand and silt, it does not follow any apparent trends. Linear regression provided R^2 values of 0.38 and 0.028 for sand and silt, respectively, which indicated poor correlation with a linear model.

While the main source of Cs-137 was the river, Cs-133 mainly originated from the seawater (section 4.2.1). However, it is the freshwater sites that has the highest concentrations of Cs-133 in clay. This might originate from runoff containing Cs-133 in soil and sedimentary rocks, as Cs gets strongly fixated to soils. The degree of fixation is dependent on inorganic content, especially clay minerals (Avery, 1996). The concentration would still be expected to increase with increased salinity because of the relatively high content of Cs-133 in seawater compared to freshwater. It is surprising that clay has the lowest concentration and might be explained by errors caused by uncertain weights, as there was a high content of salt in the samples like

mentioned previously. Therefore, the concentration is most likely higher than observed. The concentration of Cs-133 was higher in sand than in clay, strengthening the theory that there is some error in the obtained concentration of Cs-133 in clay.

Figure 4.10 (A-B) shows the activity concentration of Cs-137 in sand, silt, and clay from different locations the Vefsna river and with increased distance and thus increased salinity outward the Vefsnfjord.
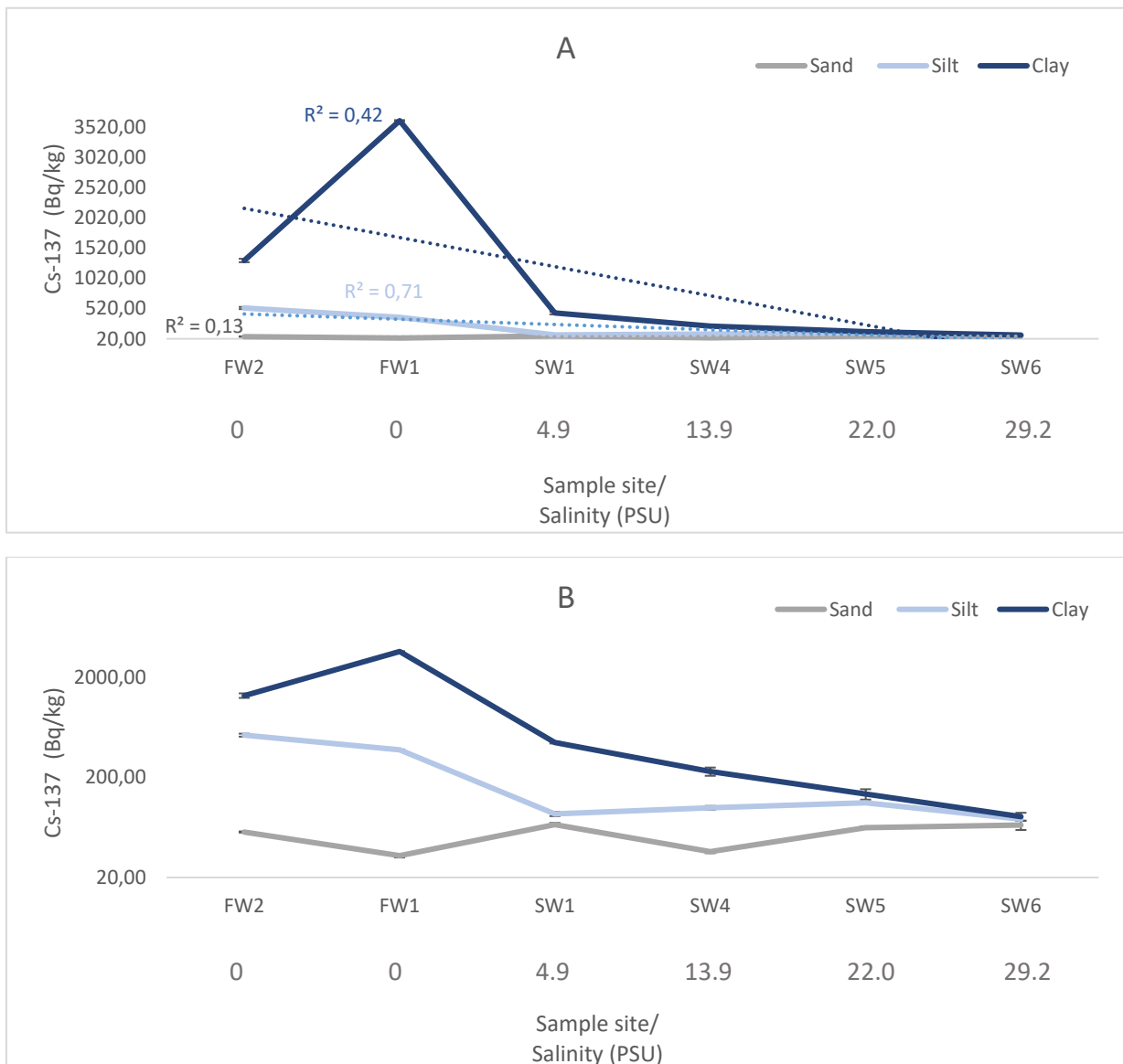
Figure 4.10*: Measured activity (Bq/kg) in Cs-137 in bottom sediments from six sample sites. (A) shows regular scale and includes linear regression. (B) shows logarithmic scale along the y-axis.*

Similar to the total concentrations of Cs-133 and Cs-137 in sediment (figure 4.8 A and B), there are some similarities regarding the low concentration of the two isotopes in sand. Linear regressions indicated poor correlation with a linear fit for sand ($R^2 = 0.13$). It essentially does

not appear to be any trends regarding the activity concentration of sand in riverine sediments compared to the marine sediments. The low concentration of cesium in sand (<66 Bq/kg) is expected, as cesium typically binds poorly to sand (Saiers & Hornberger, 1996).

The highest activity concentration of Cs-137 in silt is found in the riverine sediments (529 $\pm$ 16 Bq/kg) and decreases with increased salinity in a somewhat linear manner (R^2=0.71). The decrease in activity concentration of Cs-137 from riverine- to marine silt was significant with a p-value of 0.002. A possible explanation for the decreased activity with increased salinity might be remobilization of Cs-137, which does not bind particularly strong with quartz or albite, the main components of the silt fraction (section 4.3.2) (Cornell, 1993). However, a small increase in activity of Cs-137 is observed at higher salinities (SW4-SW5), which does not support this theory. Coagulation of clay particles with high affinity to Cs-137 might cause an increase of Cs-137 associated with the silt fraction. However, since the increase of activity in marine sediments is minor, it might be caused by error associated with the counting uncertainties.

The clay fraction in the riverine sediments had the highest activity concentration of Cs-137 (3631 $\pm$ 28 Bq/kg). It was a great decrease in activity concentration of Cs-137 in clay in the brackish water (SW1), where the activity concentration was about 8 times lower than in the riverine clay (FW1). The decrease in activity of Cs-137 from riverine- to marine clay is significant within a 96% confidence interval (p-value of 0.04).

The loss of activity observed in clay might be caused by remobilization of Cs-137 as the salinity increases (Cornell, 1993; Morris et al., 2000). Since it was such a significant decrease in activity concentration from site FW1 to SW1, it is not unlikely that a remobilization has occurred. However, Cs tend to bind irreversibly to clays and are typically not easily mobilized, but high salinity water might lead to remobilization over time. As the salinity of the Vefsnfjord increases, the activity concentration of clay continues to decrease, but less rapidly. Increased concentration of K^+ and Na^+ in seawater leads to cation exchange with Cs, thus increasing the degree of remobilization. Since Na^+ has a higher hydration energy than K^+, it can exchange Cs within the interlayers of clay minerals. K^+ hoverer, has a lower hydration energy, and will mostly affect the reversible bound fraction of the surface sites of clays. In addition, K^+ has a collapsing effect on clays that will inhibit cation exchange (Delaval et al., 2020; Mukai et al., 2018; Onodera et al., 2017).

The activity of the total sediment samples is mostly affected by the relative content of clay, as cesium is known to bind strongly to clay minerals. However, the current results demonstrated that Cs-137 was highly associated with silt. Although the activity concentration of Cs-137 in silt and clay showed a decreasing trend with increased salinity, the total activity concentration is increasing. The reason for this is the distribution of sand, silt, and clay within the sediments. Since there is <1% clay + silt in the riverine sediments (FW1 and FW2), the total activity concentration is lower than the marine sediments with higher content of silt.

The distribution of the concentration of Cs-133 and the activity concentration of Cs-137 is presented in figure 4.11 A-B.
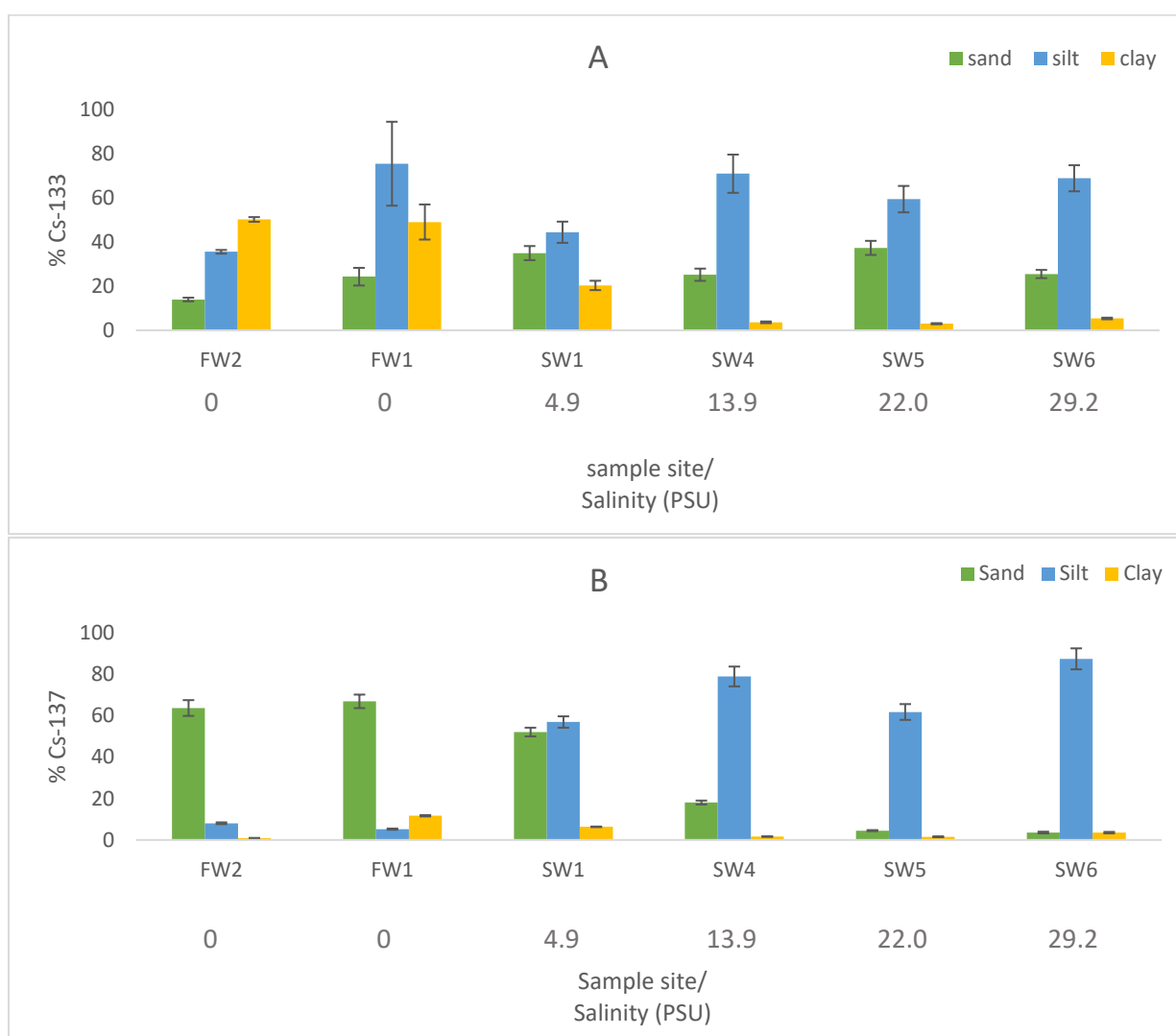
Figure 4.11: *Distribution of Cs-133 (A) and activity distribution of Cs-137 (B) in sand, silt, and clay from riverine- and marine sediments.*

It does not appear to be any observable trends in the distribution of Cs-133 in silt and sand, as the percentages varies between each site with no apparent pattern. On the contrary, it appears to be a clear trend in distribution of Cs-133 in clay. The major fraction of Cs-133 is associated with clay in site FW2, and remains high in site FW1, followed by a decrease in the SW sites.

As for Cs-137, there is a clear trend in activity distribution of the different size fractions of the sediments, and the distribution clearly resembles the size distribution with a change in distribution between sand and silt with increased salinity. Most of the Cs-137 was associated with the sand fraction in the riverine sediments, as these sediments mostly consisted of sand. However, because of the high activity concentration in clay (fig. 4.10), $11 \pm 2\%$ of Cs-137 is associated with clay in site FW1, while the clay fraction makes up 0.3% of the total weight of the sediments. In a similar manner, silt contains $5 \pm 5\%$ of the total activity in site FW1, while 0.5% of the sediments consist of silt. Cs-137 was highly represented by the silt fraction in higher salinities, as a result of silt composing the main fraction of the total seawater sediments.

4.3.4 Mobility of Cs

The binding properties of Cs-137 an Cs-133 was investigated by performing sequential extraction of silt and clay. Since the activity concentration was relatively low for some of the samples, or there were not enough sample, freshwater sediments of similar fraction (FW1 and FW2) were mixed together, and seawater sediments of similar fraction (SW1, SW4, SW5, and SW6) were mixed together, like presented in table 3.3 section 3.3.3. Ideally, clay and silt from each individual site would have been extracted separately to observe possible differences. However, it was more important to obtain as high activities as possible to improve the uncertainties of the measurements and overcome the detection and quantification limit. For this same reason, there were only enough sample to perform sequential extraction on one parallel of FW clay, FW silt and SW clay, and still have enough sample to achieve measurements over LOD and LOQ. For SW silt however, there was sufficient sample to perform three parallels. Therefore, the precision of the method could only be accounted for with the SW silt samples.

Figure 4.12 shows the percentage of Cs-133 extracted in each step. The residue was not measured on ICP-MS, therefore, the total value used to determine each percentage is based on the sum of all extraction step rather than a measured total value.
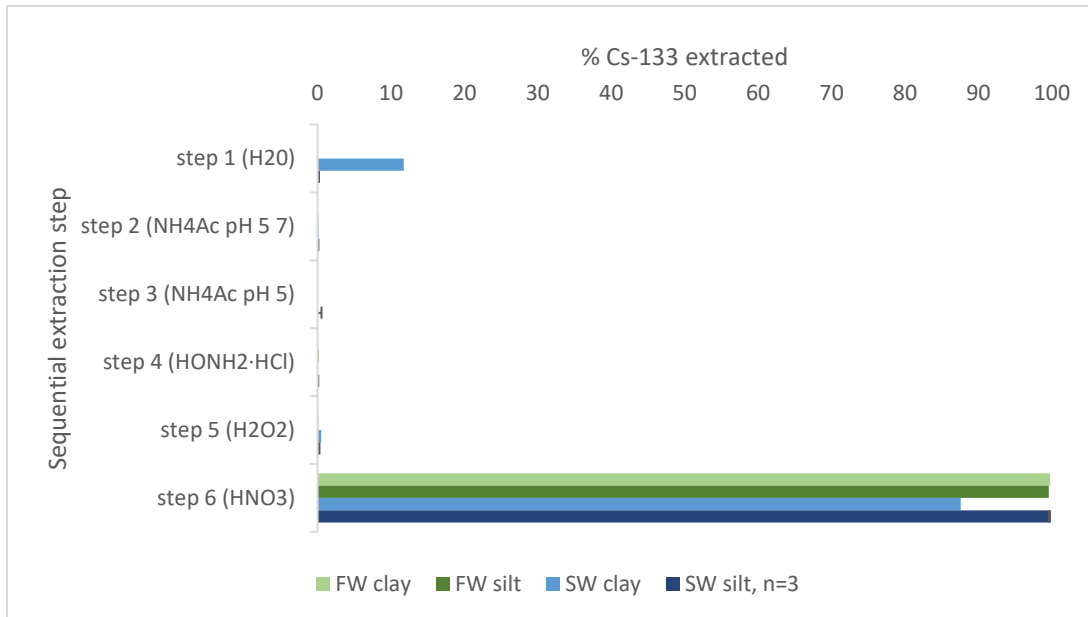
Figure 4.12: *Percentage Cs-133 extracted from each extraction step after sequential extraction. n=3 for SW silt, n=1 for FW clay, FW silt and SW clay.*

Figure 4.12 shows that most of the Cs-133 was remobilized with 7 M nitric acid. However, 11% of the Cs-133 in seawater clay was extracted with clean water (step one). The explanation for this is the high content of salt in the clay samples originating from seawater, which contained relatively high concentrations of Cs-133.

The results of Cs-137 extracted from seawater and freshwater silt and clay is presented in figure 4.13. The figure shows percentage Cs-137 extracted with 7 M nitric acid (step 6) and activity left in the residue, as the activities of Cs-137 extracted in step 1-5 was below LOQ (0.17 Bq). The percentages are calculated based on the sum of measured activity from each extraction step.
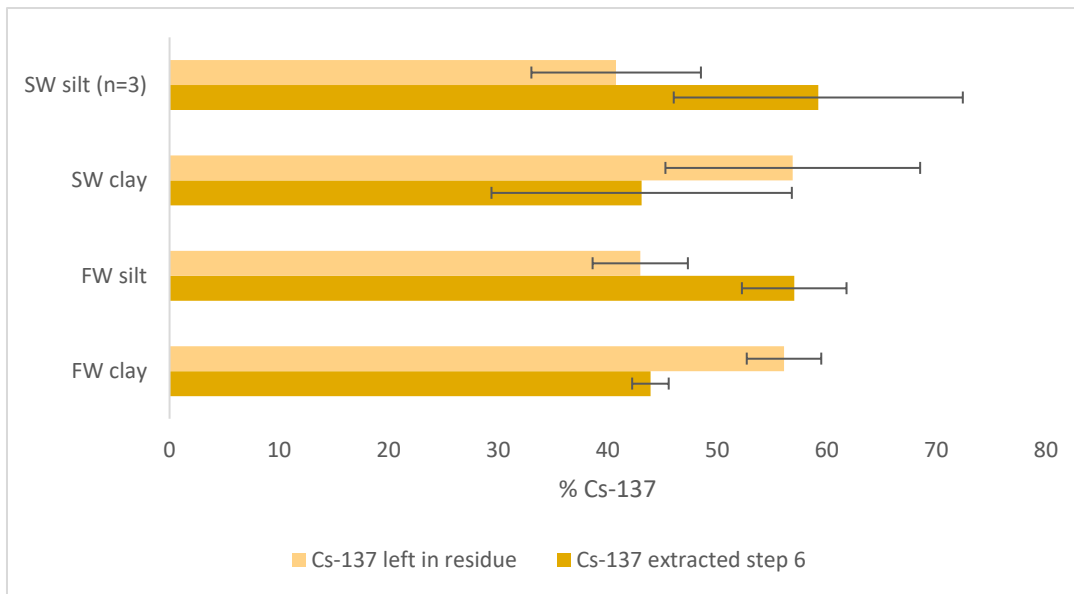
Figure 4.13: Results from sequential extraction of silt and clay from Vefsna river and Vefsnfjord, presented as % Cs-137 measured in extractant and residue based on sum of measured Cs-137 in residue and extractant.

Based on figure 4.13, there seems to be a difference between the binding properties of Cs-137 to clay compared to silt. For both FW and SW silt, more Cs-137 was extracted with 7 M nitric acid than what remained in the residue. Results showed the opposite observation for clay, which seemed to retain Cs-137 somewhat stronger. This agrees with literature, as Cs in known to bind strongly with clays (Børretzen & Salbu, 2002; Oughton et al., 1997; von Gunten & Benes, 1994). Although the uncertainties are relatively large. The difference between measured activity of Cs-137 in extract from silt compared to clay had a p-value of 0.07, which is significant with a 93% confidence interval. There was no significant difference between seawater and freshwater sediments, with a p-value of 0.7.

The results of sequential extraction revealed that Cs-137 in both silt and clay from riverine and marine sediments was irreversibly bound, and thus associated with the unavailable fraction (Børretzen & Salbu, 2002; Oughton et al., 1997). This disproves the previous theory regarding remobilization of Cs-137 from sediments with increased salinity. For remobilization by cation exchange to occur, Cs-137 must be reversibly bound to the particle surface or onto the wedge sites of clay minerals. As a strong solution (7 M nitric acid) was necessary to extract Cs-137 from sediments, it is unlikely that seawater would cause remobilization.

The maximum activity of Cs-137 extracted from step 1-5 can be determined based on LOD (0.04 Bq). The total activity measured in step 6 and in the residue was between 0.53 ± 0.15 Bq and 2.30 ± 0.12 Bq. Thus, the possible concentration of Cs-137 extracted in the first five steps

compose between 1.0% and 3.1% of the total activity, which is low compared to Cs-137 extracted in the last step (between 43% and 59%) and suggests that the amount of Cs-137 remobilized in the first five steps was insignificant.

The measured activity concentration from figure 4.10 (section 4.3.3) was initially used to determine estimated total activity in each sample prior to extraction (Appendix, figure G1). However, it was a significant difference between estimated total activity and measured activity in step 6 + residue. Therefore, the result of extraction is presented as the sum of measured activity from each extraction step.

Apparent K_d values were calculated from measured activity concentration of the sediment samples and activity of the <0.45 µm water fraction to further investigate the mobility of Cs-137 in the river and in brackish water with increased distance from the river outlet. Estimated K_d-values for Cs-137 in total sediment, sand, silt, and clay from different locations (FW2+FW1, SW1 and SW4) are presented in figure 4.14 A and B. Since FW1 and FW2 are both located in Vefsna river and represent salinity 0 PSU, they are presented together as the mean value of the two sites. Since it is surface water that has been used to calculate the apparent K_d, the obtained values are highly uncertain. Optimally, bottom water close to the sediments should have been used.
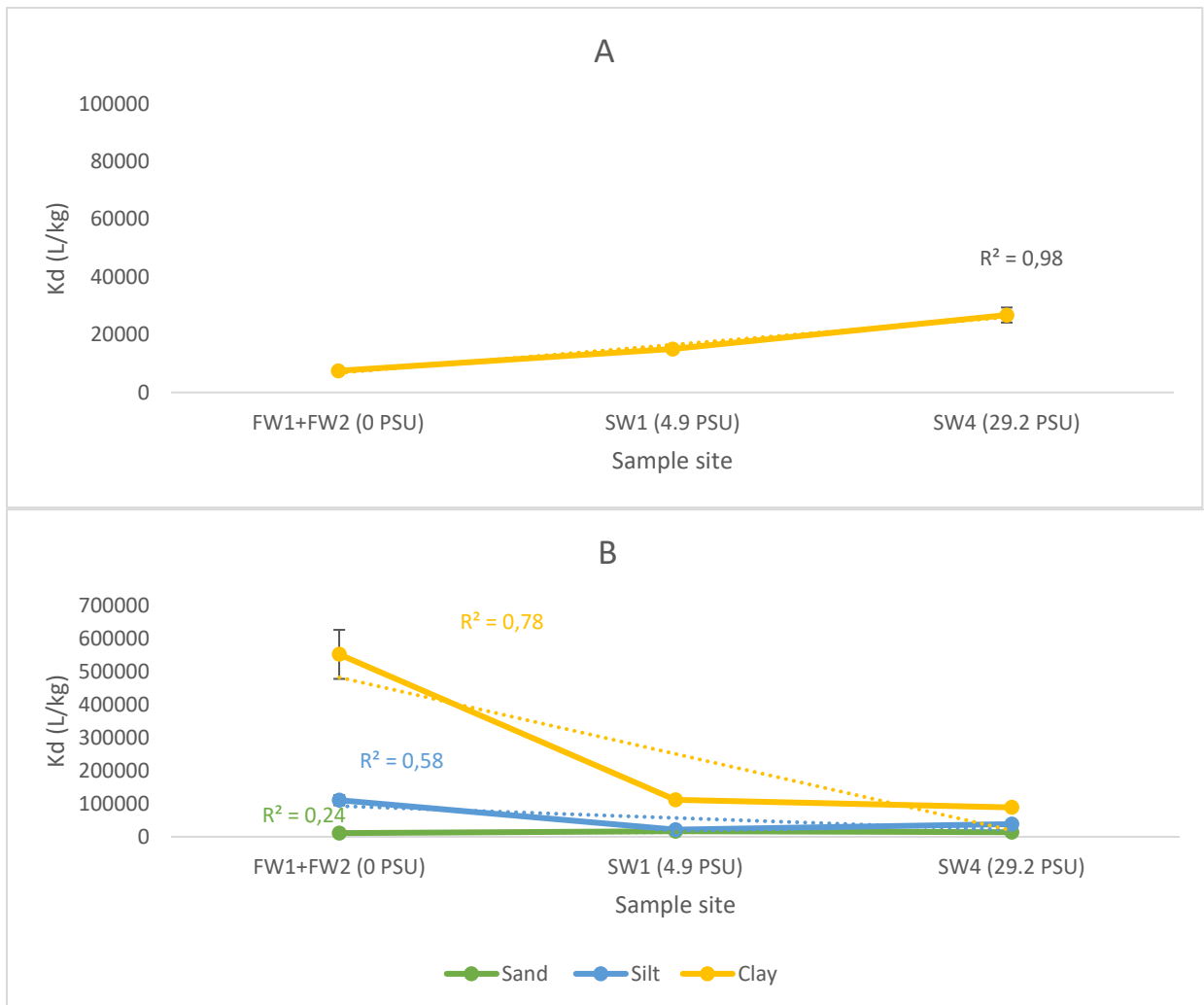
Figure 4.14: *K_d values for surface sediments from site FW1+FW2, SW1 and SW4 based on activity concentration of Cs-137 in different sediment fractions and <0.45 μm water filter. (A) shows K_d in total sediment samples, while (B) shows K_d in sand, silt, and clay. Error bars are included, though hardly visible due to low uncertainties. Note the different scales on the y-axis.*

The K_d value of total sediment sample is increasing with increasing distance from the river outlet, and thus increasing salinity (figure 4.14A). However, this is a very atypical tendency for cesium, as the sorption of Cs-137 onto sediments are expected to decrease with increased salinity because of competing ions in the marine environment (Periáñez et al., 2018). The K_d ranged between $(7.4 \pm 0.99) \cdot 10^3$ L/kg to $(2.6 \pm 0.26) \cdot 10^4$, which are more similar to reported K_d ($2.9 \cdot 10^4$ L/kg) in freshwater. The open ocean K_d is reported to be $2 \cdot 10^3$ L/kg and lower than observed in Vefsnfjord (IAEA, 2004; IAEA, 2010).

The estimated K_d values of sand, silt, and clay from Vefsna river and the Vefsnfjord is presented in figure 4.14 (B). The figure shows resemblance with activity concentrations in sediment fractions (fig. 4.10), which is expected since the differences in activity of water (fig.4.3) is less

significant. Sand has the lowest K_d and seem so follow the trend of total sediment K_d (fig. 4.3A), as it has a low increase as the salinity increases. However, there is no linear correlation for sand (R^2=0.24), like there is for total sediment (R^2=0.98).

For silt, the K_d decreased from $(1.4 \pm 0.15) \cdot 10^5$ L/kg in the river (FW1+FW2) to $(2.1 \pm 0.21) \cdot 10^4$ L/kg in brackish water in site SW1. However, there is slightly increase in site SW4. The decrease in activity from freshwater to seawater is as expected, based on the recommended K_d for freshwater and seawater. However, the increase from site SW1 to site SW4 is not as expected. The sorption of cesium ions onto quartz mineral, the main component of the silt samples, is highly dependent on ionic strength and pH. Previous research has shown that the K_d of Cs sorption onto quartz increased as the ionic strength, or salinity, decreased (Kitamura et al., 1996). Therefore, it would be expected to observe a reduction in K_d for silt with increased distance out the fjord. Like mentioned in 4.3.2, the K_d value of quarts has been reported in the range 1 to 58 L/kg, while albite has a K_d of 519 L/kg, which are the main components of the silt fraction. However, the presence of clay in the silt fraction will increase the sorption strength of Cs-137. This can explain the increased K_d in site SW4, provided that the assumption that the amount of clay minerals in the silt fraction was overestimated holds.

The highest K_d are found in riverine clay at $(5.5 \pm 0.74) \cdot 10^5$ L/kg. The effects of salinity on K_d was expected to be most abundant near the river outlet in the mixing zone of freshwater and seawater (Simonsen et al., 2019a), which applies for the clay fraction, as a significant decrease in K_d in brackish water (4.9 PSU) is observed. The difference between the K_d value of clay from 4.9 PSU (SW1) to 29.2 PSU (SW4) was minimal, however slightly decreasing. Based on literature, the decreased K_d could be caused by increased salinity, where significant reductions of K_d in sediments have been observed in estuaries (Delaval et al., 2020; Kakehi et al., 2016), although the results from sequential extraction revealed that Cs-137 is not very mobile.

The K_d is highly affected by the differences in activity in the sediments, and the total sediment samples is dependent on sediment characteristics. For instance, activity of clay (Bq/kg d.w) is much higher in site FW1, causing the K_d to be higher as well.

4.4 Biota

4.4.1 Uptake of Cs in biota

To investigate potential uptake in biota, samples of blue mussels(*M.edulis*) and seaweed (*F.vesiculosus* and *L.digitata*) from different locations in the Vefsnfjord was collected and measured for Cs-133 and Cs-137. In addition, the bioconcentration factor (BCF) was estimated. Figure 4.15 A and B shows the concentration (mg/kg d.w) and BCF (L/kg) of Cs-133, while figure C and D shows activity concentration of Cs-137 (Bq/kg) and BCF.
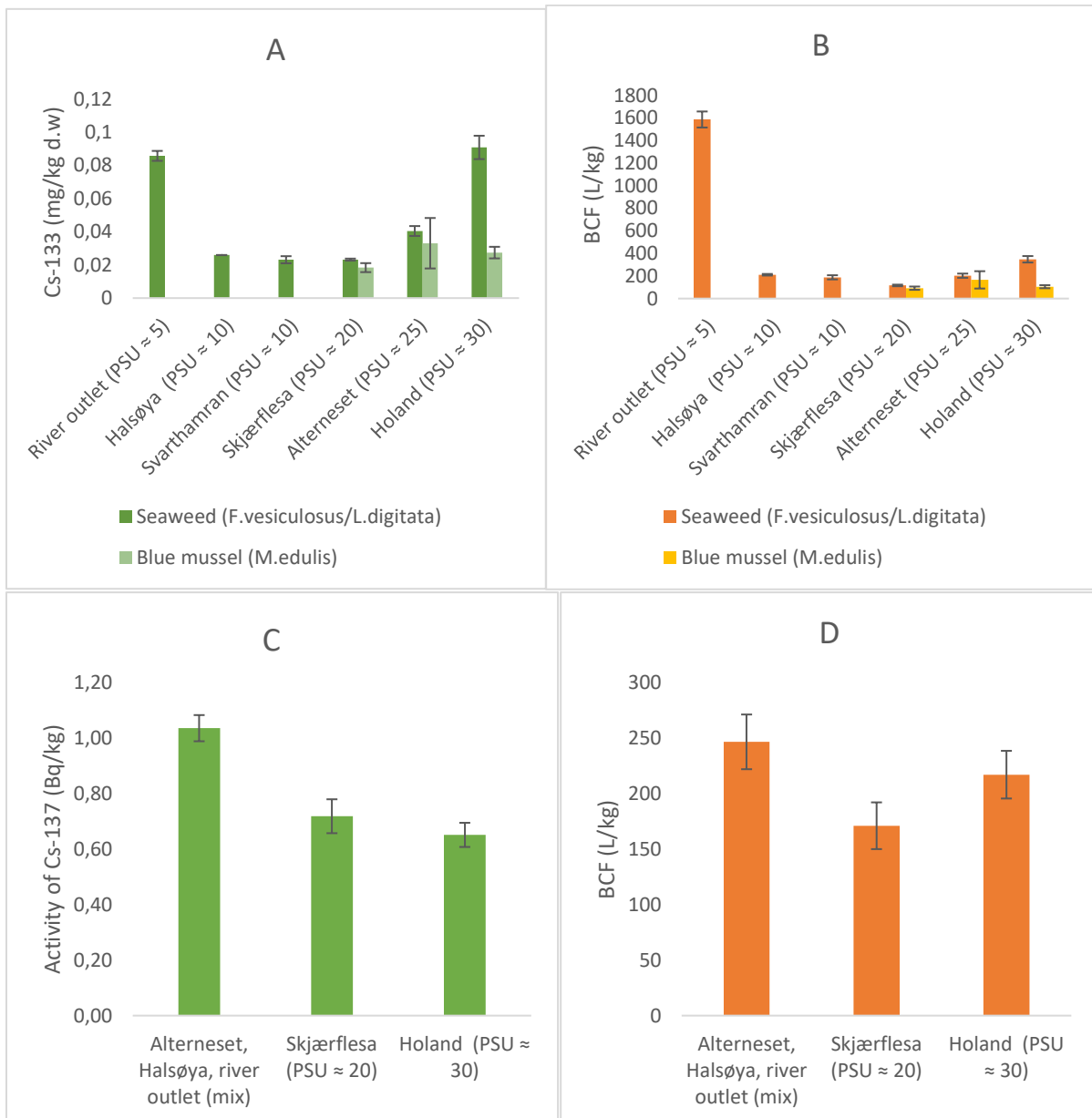
Figure 4.15: *Concentration (mg/kg d.w, n=3) of Cs-133, activity (Bq/kg d.w, n=1) of Cs-137, and BCF (L/kg) in seaweed (F.vesiculosus and L.digitata) and blue mussels (M.edulis) from different locations Vefsnfjord, with different salinities.*

The concentration of Cs-133 (fig. 4.15A) was highest in seaweed from the river outlet, where it was brackish water with a salinity of approximately 5 PSU. The lowest concentration was observed at Halsøya, Svarthamran, and Skjærflesa, with salinities of 10 PSU, 10 SPU, and 20 PSU, respectively. Further out the fjord, where the salinity increases to 25 PSU (Alterneset), it is a small increase. There were no significant differences in concentration in blue mussels between sites. The uncertainty for blue mussels from Alterneset (30 PSU) was relatively large, thus leading to overlapping concentration range with that of Skjærflesa (20 PSU) and Holand (30 PSU).

The BCF of Cs-133 in seaweed is generally low in most of the sites, except for the river outlet (fig. 4.15 B). Uptake of cesium in biota is dependent on salinity, with most efficient uptake in low salinities (Carlson & Erlandsson, 1991; Topcuoğlu, 2001). BCF illustrates the effect of uptake in low salinity water. It is a significant difference in BCF in seaweed from the river outlet (5 PSU) compared to the other samples. The concentration of Cs-133 is highest in seaweed from Holand (30 PSU), but does not have the highest BCF, hence the uptake is more efficient near the river outlet despite lower concentrations of Cs-133 in the water. The increased uptake at high salinities is most likely caused by increased concertation of Cs-133 in seawater further out the fjord.

BCF for uptake of Cs-137 in mussels based on literature ranged between 42 to 600 L/kg (Baumann et al., 2013; Friday et al., 1996; Ke et al., 2000), which compares well with the BCF for Cs-133 obtained in the present. Although most of the results in this thesis has showed that Cs-133 cannot be used as a stable analogue for Cs-137 because of the high content of Cs-133 in seawater. Therefore, is it uncertain if the BCF for Cs-137 from literature can be used for comparison.

The low detection limits obtained for Cs-133 from ICP-MS made it possible to present uptake in both seaweed and blue mussels, as well as in individual sites. However, the measured activity of Cs-137 blue mussels was <LOQ. Therefore, only the activity and BCF of seaweed is displayed. Site Holand and Skjærflesa consisted of samples from two different locations, while it was not enough sample to measure from each of the three locations Alterneset, Halsøya and river outlet, where Halsøya and river outlet are closest to the outlet of river Vefsna. Thus, Alterneset, Halsøya, and river outlet were mixed together in order to fill a 1000 ml Marinelli beaker. The mixed sample had the highest activity concentration (1.04 ± 0.04 Bq/kg). Since the different seaweeds in the mixed sample originated from different locations, it is not clear which of the sites are the main contributors to the activity. However, based on the knowledge that

Cs-137 tend to have higher uptake in lower salinities, it is not unreasonable to assume that it is the samples collected closer to the river outlet that contributed most to the activity of the mixed seaweed sample.

It does not appear to be any major difference in activity concentrations of seaweed from Skjærflesa (20 PSU, 0.72 ±0.06 Bq/kg) and Holand (30 PSU, 0.65 ± 0.04 Bq/kg) when the uncertainties are considered. Previously measured activities of Cs-137 in seaweed (*F.vesiculosus*) in Norway showed activity concentrations of 0.1 Bq/kg to 2.6 Bq/kg dependent on locations, and 1.8 Bq/kg close to Vefsna (Skjerdal et al., 2015). This is slightly higher than the activities obtained in this experiment. Monitoring of the concentration in *F.vesiculosus* has shown a relatively stable activity over the years, but with a slightly decreasing trend.

The BCF of Cs-137 in seaweed was highest in the mixed sample (247 ± 25 L/kg), and lowest in Skjærflesa (171 ± 21 L/kg), although the differences in BCF between the three locations are insignificant when considering the uncertainties. Competing ions like K^+ and Cs-133 has the possibility to affect the uptake of Cs-137 in higher salinities, although this does not seem to have contributed greatly. Recommended BCF for seaweed is 50 L/kg, which is about four times lower than the BCF obtained in this study, although the there are some variation between different species (IAEA, 2004). BCF also depend on concentration of Cs-137 in water (Baumann et al., 2013), hence biota from locations in close proximity to a source might have higher BCF. The difference in observed BCF compared to recommended value by IAEA, 2004 is likely caused by higher uptake of Cs-137. Like mentioned previously, it is usually a higher waterflow in river Vefsna, causing the salinity to be lower in the inner parts of the fjord, especially closer to the river outlet. Further, since the river is assumed to be the main source of Cs-137, higher waterflow leads to increased input of Cs-137 to the fjord. The combination of increased input of Cs-137 and low salinity will likely increase the uptake. Cs-137 have competition from K^+ in seawater, thus lower concentration of K^+ leads to higher uptake of Cs-137 (Friday et al., 1996).

Like mentioned in section 2.6 are the uptake of Cs-137 in biota dependent on the speciation, where LMM species are most bioavailable. Remobilization of LMM species from HMM species can increase the BCF while decrease the K_d (Salbu, 2016). The decrease in K_d for silt and clay observed in brackish water accompanied with an increase of LMM species might contribute to more efficient uptake of biota.

5 Conclusions and assessment of hypothesises

5.1 Conclusions

In this study, it has been observed that the estuarine environment induces changes in speciation, sediment characterization, and biological uptake, which all are highly dependent on the change in salinity. The increase in competing ions from seawater in the estuary increase the remobilization of Cs-137 from river discharged particles, as well as creating flocs that sediments faster.

Cs-137 was mostly represented as LMM species in the river, and a small fraction was shown in the particulate fraction in the riverine water before the outlet to the Vefsnfjord. In the freshwater-seawater interface by the outlet of river Vefsna, Cs-137 associated with particles was not identified. However, a minor fraction of Cs-137 was associated with colloids at 0-5 PSU although the activity concentration was lower than estimated by dilution. As the activity concentration of Cs-137 in colloids and particles was reduced, the concentration of LMM species was slightly elevated, suggesting remobilization of LMM species.

The activity concentration in sediments showed an increasing trend from the riverine sediments, during the estuary, and outwards the Vefsnfjord. However, both clay and silt had higher activity concentration of Cs-137 in the river than in seawater. The change in grain size of sediments seems to be the main reason for the increase of Cs-137 in the marine sediments compared to the riverine sediments. Grain size analysis of sand, silt, and clay revealed that the riverine sediments consisted mostly of sand, with a change in composition in the fjord where the silt fraction was dominating. As the sand fraction decreased, the silt fraction increased with increasing distance from the river and out the fjord. The clay fraction had the highest activity concentration of Cs-137 in the river, while the silt fraction had the highest activity concentration of Cs-137 in the seawater. XRD analysis did not show any clay minerals present in the marine silt fraction, which consisted mostly of quartz and albite. Thus, the increased activity observed in marine silt was not due to aggregated clay containing Cs-137 minerals. In clay, only muscovite was detected, which binds strongly to Cs-137.

The mobility of Cs-137 was determined by sequential extraction of silt and clay from freshwater and seawater sediments. Sequential extraction reviled that Cs-137 was irreversibly fixed to both silt and clay, as it was only 7 M nitric acid that was able to release Cs-137 from the sediment fraction, while a great amount of Cs-137 was left in the residue, thus being unavailable. This indicated that the remobilization of Cs-137 by seawater was low and sediments might act as a permanent sink for Cs-137, making it unavailable for other organisms. Thus, the observed

increase in mobility of Cs-137 is probably from other particulate and colloidal river transported material, such as organic matter.

K_d for the sediment samples as well as the sediment fractions sand, silt, and clay were calculated from measured activity of Cs-137 in surface water and the activity of sediments. The results revealed that the total sediment sample showed a slightly increase with increasing salinity. The same was observed for sand, but for silt and clay there was a reduction. The most apparent change occurred in brackish water with low salinity (5 PSU), where especially clay had significant decreased K_d. The reason for the observed reduction in K_d for clay and silt could be explained by remobilization induced by seawater, however, sequential extraction disproved this theory as Cs-137 was irreversibly bound to clay and silt.

Measurements of the activity of Cs-137 in seaweed and blue mussels revelated that the concentration was low (0.65 – 1.04 Bq/kg), and large samples was necessary to achieve detectable activity concentrations. Even though 1000 mL Marinelli beaker was used, the activity of blue mussels was <LOQ (<0.17 Bq/kg). Although concentrations of Cs-137 in seaweed was low, the BCF was still four times higher than reported value in handbooks by IAEA, which means that the uptake was high although the concentration was low.

The results provided in this study show that the distribution of species, mobility, and bioavailability of radionuclides such as Cs-137 change in the interface of freshwater and seawater. Therefore, knowledge of the processes of radionuclides in estuaries and coastal areas are crucial for estimating the transfer and risk assessment.

5.2 Assessment of hypothesises

H1 was supported, although the low water flow in Vefsna river might have resulted in lower concentration of Cs-137 than usual, however, since the activity concentration decreased further out the Vefsnfjord, it does not appear to be other major sources of Cs-137. Therefore, it is assumed that the Vefsna river was the main source of Cs-137. However, analysis of Cs-137 in water from other rivers near the Vefsnfjord are needed for confirmation.

H2 was supported, as the colloidal and particulate species of Cs-137 decreased more than estimated by dilution when the salinity increased, further the LMM fraction increased slightly. However, the concentrations were low, and changes were minor. Further experiments should be conducted to confirm these observations. Preferably when the transport of colloids and particles is higher, such as during high waterflow in river Vefsna.

H3 was supported, as the K_d of Cs-137 in surface sediments changed with increased salinity. However, different trends were observed for total, sand, silt, and clay. While the total K_d increased with increased salinity, a decrease in K_d was observed for clay and silt. The difference in trends between the fractions illustrates the importance of obtaining information about the sediment characterization.

It was not sufficient data to support H4. The highest activity concentration and BCF was observed in the mixed seaweed sample, assumably due to increased uptake in the brackish water in the river outlet. However, more data is needed to support the hypothesis.

References

Ashraf, M. A., Akib, S., Maah, M. J., Yusoff, I. & Balkhair, K. S. (2014). Cesium-137: Radio-Chemistry, Fate, and Transport, Remediation, and Future Concerns. *Critical Reviews in Environmental Science and Technology*, 44 (15): 1740-1793. doi: 10.1080/10643389.2013.790753.

Atwood, D. A. (2010). Cesium. In Atwood, D. A. (ed.) *Radionuclides in the environment*. United kingdom: John Wiley & sons ltd. .

Avery, S. V. (1996). Fate of caesium in the environment: Distribution between the abiotic and biotic components of aquatic and terrestrial ecosystems. *Journal of Environmental Radioactivity*, 30 (2): 139-171. doi: https://doi.org/10.1016/0265-931X(96)89276-9.

Backe, S., Bjerke, H., Rudfjord, A. J. & Ugletveit, F. (1986). *Nedfall av cesium i Norge etter Tsjernobylulykken*. Østerås, Norway: National Institute of Radiation Hygiene.

Baumann, Z., Casacuberta, N., Baumann, H., Masqué, P. & Fisher, N. S. (2013). Natural and Fukushima-derived radioactivity in macroalgae and mussels along the Japanese shoreline. *Biogeosciences*, 10 (6): 3809-3815. doi: 10.5194/bg-10-3809-2013.

Beldring, S., Engeland, K., Roald, L. A., Sælthun, N. R. & Voksø, A. (2003). Estimation of parameters in a distributed precipitation-runoff model for Norway. *Hydrology and Earth System Sciences*, 7 (3): 304-316. doi: 10.5194/hess-7-304-2003.

Buesseler, K., Dai, M., Aoyama, M., Benitez-Nelson, C., Charmasson, S., Higley, K., Maderich, V., Masqué, P., Morris, P. J., Oughton, D., et al. (2017). Fukushima Daiichi–Derived Radionuclides in the Ocean: Transport, Fate, and Impacts. *Annual Review of Marine Science*, 9 (1): 173-203. doi: 10.1146/annurev-marine-010816-060733.

Burgess, H. M., Mitchell, S. B. & Pope, D. J. (2002). The Influence Of Tides And Wind Speed On Fine-sediment Transport In A Semi-enclosed Natural Harbour (Pagham Harbour, UK). *Coastal Environment*. doi: 10.2495/cen.

Børretzen, P. & Salbu, B. (2002). Fixation of Cs to marine sediments estimated by a stochastic modelling approach. *Journal of Environmental Radioactivity*, 61 (1): 1-20. doi: 10.1016/s0265-931x(01)00107-2.

Carlson, L. & Erlandsson, B. (1991). Effects of salinity on the uptake of radionuclides by Fucus vesiculosus L. *Journal of Environmental Radioactivity*, 13 (4): 309-322. doi: https://doi.org/10.1016/0265-931X(91)90004-Y.

Chierici, M., Skjelvan, I., Norli, M., Lødemel, H. H., Lunde, L. F., Sørensen, K., Yakushev, E., Bellerby, R., King, A. L., Lauvset, S. K., et al. (2015). *Havforsuringsovervåking i norske farvann i 2014 /Monitoring ocean acidification in Norwegian seas in 2014*: Havforskningsinstituttet, Uni Research, Norsk institutt for vannforskning.

Choppin, G., Liljenizin, J.-O., Rydberg, J. & Ekberg, C. (2013). *Radiochemistry and nuclear chemistry*. Fourth ed.: Academic Press.

Cornell, R. M. (1993). Adsorption of cesium on minerals: A review. *Journal of Radioanalytical and Nuclear Chemistry Articles*, 171 (2): 483-500. doi: 10.1007/bf02219872.

Delaval, A., Duffa, C. & Radakovitch, O. (2020). A review on cesium desorption at the freshwater-seawater interface. *Journal of Environmental Radioactivity*, 218: 106255. doi: 10.1016/j.jenvrad.2020.106255.

Dietz, L. A., Pachucki, C. F. & Land, G. A. (1963). Half Lives of Cesium-137 and Cesium-134 as Measured by Mass Spectrometry. *Analytical Chemistry*, 35 (7): 797-799. doi: 10.1021/ac60200a011.

Ermrich, M. & Opper, D. (2011). *XRD for the analyst - Getting acquainted with the principles*: PANalytical GmbH.

Eyrolle, F. & Charmasson, S. (2004). Importance of colloids in the transport within the dissolved phase (<450 nm) of artificial radionuclides from the Rhône river towards the Gulf of Lions (Mediterranean Sea). *Journal of Environmental Radioactivity*, 72 (3): 273-286. doi: 10.1016/s0265-931x(03)00178-4.

Fedchenko, V. (2015). *New nuclear Forensics - Analysis of nuclear materials for security purposes*: Oxfrd University Press.

Finston, H. L. & Miskel, J. (1955). Radiochemical Separation Techniques. *Annual Review of Nuclear Science*, 5 (1): 269-296. doi: 10.1146/annurev.ns.05.120155.001413.

Friday, G. P., Cummins, C. L. & Schwartzman, A. L. (1996). *Radiological Bioconcentration Factors for Aquatic, Terrestrial, and Wetland Ecosystems at the Savannah River Site (U)*. Westinghouse Savannah River Co., Aiken, SC (United States).

Gad, S. C. & Pham, T. (2014). Cesium. In Wexler, P. (ed.) *Encyclopedia of Toxicology (Third Edition)*, pp. 776-778: Academic Press.

Garcia-Sanchez, L. & Konoplev, A. V. (2009). Watershed wash-off of atmospherically deposited radionuclides: a review of normalized entrainment coefficients. *Journal of Environmental Radioactivity*, 100 (9): 774-778. doi: 10.1016/j.jenvrad.2008.08.005.

Gjelsvik R, K. M., Brittain J, Eikelmann IM, Gaare E, Gwynn J, Holmstrøm F, Kiel & Jensen L, K. J., Møller B, Nybø S, Steinnes E, Solberg EJ, Stokke S, Ugedal O, Veiberg V. (2014). *Radioaktivt cesium i n*, 9. Østerås, Norge: Norwegian Radiation Protection Authority.

Gupta, D. K. & Walther, C. (2017). Preface. In Gupta, D. K. & Walther, C. (eds) *Impact of Cesium on Plants and the Environment* Switzerland: Springer Nature.

Heldal, H. E., Helvik, L., Haanes, H., Volynkin, A., Jensen, H. & Lepland, A. (2021). Distribution of natural and anthropogenic radionuclides in sediments from the Vefsnfjord, Norway. *Marine Pollution Bulletin*, 172: 112822. doi: 10.1016/j.marpolbul.2021.112822.

Hindar, A., Garmo, Ø., Austnes, K. & Sample, J. E. (2020). Nasjonal innsjøundersøkelse 2019 *Norsk institutt for vannforskning (NIVA)*.

Hunziker, J. C., Frey, M., Clauer, N., Dallmeyer, R. D., Friedrichsen, H., Flehmig, W., Hochstrasser, K., Roggwiler, P. & Schwander, H. (1986). The evolution of illite to muscovite: mineralogical and isotopic data from the Glarus Alps, Switzerland. *Contributions to Mineralogy and Petrology*, 92 (2): 157-180. doi: 10.1007/bf00375291.

Håkanson, L. & Fernandez, J. A. (2001). A mechanistic sub model predicting the infuence of potassium on radiocesium uptake in aquatic biota. *Journal of*

Environmental Radioactivity, 54 (3): 345-360. doi: 10.1016/S0265-931X(00)00180-6.

IAEA. (2004). *Sediment distribution coefficionets and concentration factors in the marine environment*, 422. Vienna, Austria: International Atomic Energy Agency.

IAEA. (2005). *Worldwide marine radioactivity studies (WOMARS) Radionuclide levels in oceans and seas.* Vienna: International Atomic Energy Agency.

IAEA. (2010). Handbook of Parameter Values for the Prediction of Radionuclide Transfer in Terrestrial and Freshwater Environments. *TECHNICAL REPORTS SERIES No. 472, International Atomic Energy Agency*.

Kakehi, S., Kaeriyama, H., Ambe, D., Ono, T., Ito, S.-I., Shimizu, Y. & Watanabe, T. (2016). Radioactive cesium dynamics derived from hydrographic observations in the Abukuma River Estuary, Japan. *Journal of Environmental Radioactivity*, 153: 1-9. doi: 10.1016/j.jenvrad.2015.11.015.

Kanivets, V. V., Voitsekhovitch, O. V. & Rkhrystyk, B. (1999). Riverine transport of Cs-137 and Sr-90 into the black sea after Chernobyl accident (Data analysis and methodological aspects of monitoring). *IAEA*: 44-51.

Ke, C., Yu, K. N., Lam, P. K. S. & Wang, W.-X. (2000). Uptake and depuration of cesium in the green mussel Perna viridis. *Marine Biology*, 137 (4): 567-575. doi: 10.1007/s002270000373.

Keeran, N. S., Usha, B. & Ganesan, G. (2021). *Metal and Nutrient Transporters in Abiotic Stress*: Academic Press.

Kendrick, M. P. & Derbyshire, B. V. (1976). FACTORS INFLUENCING ESTUARY SEDIMENT DISTRIBUTION. *Coastal Engineering Proceedings*, 1 (15): 120. doi: 10.9753/icce.v15.120.

Kirk Cochran, J. (2014). Estuaries. In: Elsevier.

Kitamura, A., Yamamoto, T., Moriyama, H. & Nishikawa, S. (1996). Analysis of Adsorption Behavior of Cesium onto Quartz Using Electrical Double Layer Model. *Journal of Nuclear Science and Technology*, 33 (11): 840-845. doi: 10.1080/18811248.1996.9732018.

Kvamme, B. B. (2019). *The transfer of radiocesium in coastal waters -Radiocesium tracer to investigate mixing zone processes in brackish waters*. Ås, Norway: Norwegian University of Life Sciences.

Kwong-Moses, D. S., Elliott, W. C., Wampler, J. M., Powell, B. A. & Avant, D. M. (2020). Sorption and desorption of radiocesium by muscovite separated from the Georgia kaolin. *Journal of Environmental Radioactivity*, 211: 106074. doi: 10.1016/j.jenvrad.2019.106074.

Lienhard, J., Antar, M. A., Bilton, A., Blanco, J. & Zaragoza, G. (2012). Solar Desalination. *Annual Review of Heat Transfer*, 15 (15): 277-347. doi: 10.1615/AnnualRevHeatTransfer.2012004659.

Liland, A., L., S., Bergan, T., Forseth, T., Gaare, E. & Hellstrøm, T. (2001). *monitoring of radioactive contamination in food and the environment 1986-1998 (in Norwegian)*. StrålevernRapport 2001:1. Østerås, Norway: Norwegian Radiation Protection Authority.

Lofts, S., Tipping, E. W., Sanchez, A. L. & Dodd, B. A. (2002). Modelling the role of humic acid in radiocaesium distribution in a British upland peat soil. *Journal of*

Environmental Radioactivity, 61 (2): 133-147. doi: 10.1016/s0265-931x(01)00118-7.

Metian, M., Pouil, S. & Fowler, S. W. (2019). Radiocesium accumulation in aquatic organisms: A global synthesis from an experimentalist's perspective. *J Environ Radioact*, 198: 147-158. doi: 10.1016/j.jenvrad.2018.11.013.

Molvær, J. (2010). *Vefsnfjorden. Beskrivelse av hydrofysiske forhold i fjordens indre del.* Oslo, Norway: NIVA.

Morris, K., Butterworth, J. C. & Livens, F. R. (2000). Evidence for the Remobilization of Sellafield Waste Radionuclides in an Intertidal Salt Marsh, West Cumbria, U.K. *Estuarine, Coastal and Shelf Science*, 51 (5): 613-625. doi: 10.1006/ecss.2000.0705.

Mosley, L. M. & Liss, P. S. (2020). Particle aggregation, pH changes and metal behaviour during estuarine mixing: review and integration. *Marine and Freshwater Research*, 71 (3): 300. doi: 10.1071/mf19195.

Mukai, H., Tamura, K., Kikuchi, R., Takahashi, Y., Yaita, T. & Kogure, T. (2018). Cesium desorption behavior of weathered biotite in Fukushima considering the actual radioactive contamination level of soils. *Journal of Environmental Radioactivity*, 190-191: 81-88. doi: 10.1016/j.jenvrad.2018.05.006.

Newman, M. C. & Unger, M. A. (2003). *Fundamentals of Ecotoxicology, Second Edition*. Second ed.: Lewis Publishers.

Onodera, M., Kirishima, A., Nagao, S., Takamiya, K., Ohtsuki, T., Akiyama, D. & Sato, N. (2017). Desorption of radioactive cesium by seawater from the suspended particles in river water. *Chemosphere*, 185: 806-815. doi: 10.1016/j.chemosphere.2017.07.078.

ORTEC. (2020). *GammaVision® Maestro-PRO® Gamma-Ray Spectrum Analysis and MCA Emulators for Microsoft® Windows®7, 8.1, and 10 Professional. A66-BW, A66SV-BW, A66MP-BW, Software User's Manual. Software Version 9.*: Advanced Measurement Technology, Inc.

Otosaka, S. & Kobayashi, T. (2013). Sedimentation and remobilization of radiocesium in the coastal area of Ibaraki, 70 km south of the Fukushima Dai-ichi Nuclear Power Plant. *Environmental Monitoring and Assessment*, 185 (7): 5419-5433. doi: 10.1007/s10661-012-2956-7.

Oughton, D. H., Børretzen, P., Salbu, B. & Tronstad, E. (1997). Mobilisation of 137Cs and 90Sr from sediments: potential sources to arctic waters. *Science of The Total Environment*, 202 (1-3): 155-165. doi: 10.1016/s0048-9697(97)00112-5.

Periáñez, R., Bezhenar, R., Brovchenko, I., Duffa, C., Iosjpe, M., Jung, K. T., Kobayashi, T., Lamego, F., Maderich, V., Min, B. I., et al. (2016). Modelling of marine radionuclide dispersion in IAEA MODARIA program: Lessons learnt from the Baltic Sea and Fukushima scenarios. *Science of The Total Environment*, 569-570: 594-602. doi: 10.1016/j.scitotenv.2016.06.131.

Periáñez, R., Brovchenko, I., Jung, K. T., Kim, K. O. & Maderich, V. (2018). The marine kd and water/sediment interaction problem. *Journal of Environmental Radioactivity*, 192: 635-647. doi: 10.1016/j.jenvrad.2018.02.014.

Periáñez, R., Qiao, F., Zhao, C., De With, G., Jung, K.-T., Sangmanee, C., Wang, G., Xia, C. & Zhang, M. (2021). Opening Fukushima floodgates: Modelling 137Cs

impact in marine biota. *Marine Pollution Bulletin*, 170: 112645. doi: 10.1016/j.marpolbul.2021.112645.

Pettersson, L.-E. (2004). *Flomberegning for Vefsna og Skjerva*. Oslo, Norway: Norges vassdrags- og energidirektorat.

Portela, L. I., Ramos, S. & Teixeira, A. T. (2013). Effect of salinity on the settling velocity of fine sediments of a harbour basin. *Journal of Coastal Research*, 165: 1188-1193. doi: 10.2112/si65-201.1.

Povinec, P. P., Bailly Du Bois, P., Kershaw, P. J., Nies, H. & Scotto, P. (2003). Temporal and spatial trends in the distribution of 137Cs in surface waters of Northern European Seas—a record of 40 years of investigations. *Deep Sea Research Part II: Topical Studies in Oceanography*, 50 (17-21): 2785-2801. doi: 10.1016/s0967-0645(03)00148-6.

Rainey, M. P., Tyler, A. N., Gilvear, D. J., Bryant, R. G. & McDonald, P. (2003). Mapping intertidal estuarine sediment grain size distributions through airborne remote sensing. *Remote Sensing of Environment*, 86 (4): 480-490. doi: 10.1016/s0034-4257(03)00126-3.

Rajec, P. (1999). Effect of Illite Particle Shape on Cesium Sorption. *Clays and Clay Minerals*, 47 (6): 755-760. doi: 10.1346/ccmn.1999.0470610.

Saiers, J. E. & Hornberger, G. M. (1996). The Role of Colloidal Kaolinite in the Transport of Cesium through Laboratory Sand Columns. *Water Resources Research*, 32 (1): 33-41. doi: 10.1029/95wr03096.

Salbu, B., Lind, O. C. & Skipperud, L. (2004). Radionuclide speciation and its relevance in environmental impact assessments. *Journal of Environmental Radioactivity*, 74 (1-3): 233-242. doi: 10.1016/j.jenvrad.2004.01.008.

Salbu, B. (2007). Speciation of radionuclides – analytical challenges within environmental impact and risk assessments. *Journal of Environmental Radioactivity*, 96 (1-3): 47-53. doi: 10.1016/j.jenvrad.2007.01.028.

Salbu, B. (2009). Fractionation of radionuclide species in the environment. *Journal of Environmental Radioactivity*, 100 (4): 283-289. doi: 10.1016/j.jenvrad.2008.12.013.

Salbu, B. (2016). Environmental impact and risk assessments and key factors contributing to the overall uncertainties. *Journal of Environmental Radioactivity*, 151: 352-360. doi: 10.1016/j.jenvrad.2015.09.001.

Simonsen, M., Saetra, Ø., Isachsen, P. E., Lind, O. C., Skjerdal, H. K., Salbu, B., Heldal, H. E. & Gwynn, J. P. (2017). The impact of tidal and mesoscale eddy advection on the long term dispersion of 99 Tc from Sellafield. *Journal of Environmental Radioactivity*, 177: 100-112. doi: 10.1016/j.jenvrad.2017.06.002.

Simonsen, M., Lind, O. C., Saetra, Ø., Isachsen, P. E., Teien, H.-C., Albretsen, J. & Salbu, B. (2019a). Coastal transport of river-discharged radionuclides: Impact of speciation and transformation processes in numerical model simulations. *Science of The Total Environment*, 669: 856-871. doi: 10.1016/j.scitotenv.2019.01.434.

Simonsen, M., Teien, H.-C., Lind, O. C., Saetra, Ø., Albretsen, J. & Salbu, B. (2019b). Modeling key processes affecting Al speciation and transport in estuaries. *Science of The Total Environment*, 687: 1147-1163. doi: 10.1016/j.scitotenv.2019.05.318.

Skjerdal, H., Heldal, H. E., Gäfvert, T., Gwynn, J., Strålberg, E., Sværen, I., Liebig, P. L., Kolstad, A. K., Møller, B., Komperød, M., et al. (2015). *Radioactivity in the marine environment 2011. Results from the Norwegian National Monitoring Programme (RAME).* Østerås, Norway: Norwegian Radiation Protection Authority.

Skjerdal, H., Heldal, H. E., Rand, A., J., G., Jensen, L. K., Volynkin, A., Haanes, H., Møller, B., Liebig, P. L. & Gäfvert, T. (2020). Radioactivity in the Marine Environment 2015, 2016 and 2017. *Results from the Norwegian Marine Monitoring Programme RAME.*, DSA Report 2020:04.

Skoog, D. A., West, D. M., Holler, F. J. & Crouch, S. R. (2014). *Fundamentals of analytical chemistry*. Ninth ed.: BROOKS/COLE CENGAGE Learning.

Song, J. H., Kim, T. & Yeon, J.-W. (2020). Radioactivity data analysis of 137Cs in marine sediments near severely damaged Chernobyl and Fukushima nuclear power plants. *Nuclear Engineering and Technology*, 52 (2): 366-372. doi: 10.1016/j.net.2019.07.017.

Standring, W. J. F., Oughton, D. H. & Salbu, B. (2002). Potential Remobilization of 137Cs, 60Co, 99Tc, and 90Sr from Contaminated Mayak Sediments in River and Estuary Environments. *Environmental Science & Technology*, 36 (11): 2330-2337. doi: 10.1021/es0103187.

Staunton, S., Dumat, C. & Zsolnay, A. (2002). Possible role of organic matter in radiocaesium adsorption in soils. *Journal of Environmental Radioactivity*, 58 (2-3): 163-173. doi: 10.1016/s0265-931x(01)00064-9.

Stenius, S. (2017). *Revidert flomberegning for Vefsna og Skjerva - Flomsonekartprosjektet*, ISBN: 978-82-410-1569-4. Oslo, Norway: Norges vassdrags- og energidirektorat.

Sutherland, B. R., Barrett, K. J. & Gingras, M. K. (2015). Clay settling in fresh and salt water. *Environmental Fluid Mechanics*, 15 (1): 147-160. doi: 10.1007/s10652-014-9365-0.

Takata, H., Hasegawa, K., Oikawa, S., Kudo, N., Ikenoue, T., Isono, R. S. & Kusakabe, M. (2015). Remobilization of radiocesium on riverine particles in seawater: The contribution of desorption to the export flux to the marine environment. *Marine Chemistry*, 176: 51-63. doi: 10.1016/j.marchem.2015.07.004.

Tanaka, Y., Kojima, T., Takata, Y., Chainani, A., Lovesey, S. W., Knight, K. S., Takeuchi, T., Oura, M., Senba, Y., Ohashi, H., et al. (2010). Determination of structural chirality of berlinite and quartz using resonant x-ray diffraction with circularly polarized x-rays. *Physical Review B*, 81 (14). doi: 10.1103/PhysRevB.81.144104.

Teien, H.-C., Standring, W. J. F. & Salbu, B. (2006). Mobilization of river transported colloidal aluminium upon mixing with seawater and subsequent deposition in fish gills. *Science of The Total Environment*, 364 (1-3): 149-164. doi: 10.1016/j.scitotenv.2006.01.005.

Tessier, A., Campbell, P. G. C. & Bisson, M. (1979). Sequential Extraction Procedure for the Speciation of Particulate Trace Metals. *Analytical Chemistry*, 51 (7): 8.

Topcuoğlu, S. (2001). Bioaccumulation of cesium-137 by biota in different aquatic environments. *Chemosphere*, 44 (4): 691-695. doi: 10.1016/s0045-6535(00)00290-3.

Tsukada, H., Hasegawa, H., Hisamatsu, S. I. & Yamasaki, S. I. (2002). Transfer of 137Cs and stable Cs from paddy soil to polished rice in Aomori, Japan. *Journal of Environmental Radioactivity*, 59 (3): 351-363. doi: 10.1016/s0265-931x(01)00083-2.

Uchida, S. & Tagami, K. (2007). Soil-to-plant transfer factors of fallout 137Cs and native 133Cs in various crops collected in Japan. *Journal of Radioanalytical and Nuclear Chemistry*, 273 (1): 205-210. doi: 10.1007/s10967-007-0737-5.

Uncles, R. J., Stephens, J. A. & Harris, C. (2015). Estuaries of southwest England: Salinity, suspended particulate matter, loss-on-ignition and morphology. *Progress in Oceanography*, 137: 385-408. doi: 10.1016/j.pocean.2015.04.030.

UNSCEAR. (2000). *SOURCES AND EFFECTS OF IONIZING RADIATION - United Nations Scientific Committee on the Effects of Atomic Radiation*, vol. 1: Sources. New York.

VanLoon, G. W. & Duffy, S. J. (2017). *Envitonmental chemistry - A global perspective*. Fourth ed.: Oxford University Press.

Vives I Batlle, J. (2012). Radioactivity in the Marine Environment In, pp. 8387-8425: Springer New York.

Vives I Batlle, J., Aoyama, M., Bradshaw, C., Brown, J., Buesseler, K. O., Casacuberta, N., Christl, M., Duffa, C., Impens, N. R. E. N., Iosjpe, M., et al. (2018). Marine radioecology after the Fukushima Dai-ichi nuclear accident: Are we better positioned to understand the impact of radionuclides in marine ecosystems? *Science of The Total Environment*, 618: 80-92. doi: 10.1016/j.scitotenv.2017.11.005.

von Gunten, H. R. & Benes, P. (1994). Specation of radionucleides in the environment. *Radiochimica Acta* (69): 1-29.

Wada, T., Konoplev, A., Wakiyama, Y., Watanabe, K., Furuta, Y., Morishita, D., Kawata, G. & Nanba, K. (2019). Strong contrast of cesium radioactivity between marine and freshwater fish in Fukushima. *Journal of Environmental Radioactivity*, 204: 132-142. doi: 10.1016/j.jenvrad.2019.04.006.

Walker, C. H., Sibly, R. M., Hopkin, S. P. & Peakall, D. B. (2012). *Principles of ecotoxicology*. Fourth ed.: CRC Press Taylor & Francis Group.

Walseng, B. (1989). Verneplan IV Ferskvannsundersøkelser i 8 vassdrag i midtre deler av Nordland. *NINA Norsk institutt for naturforskning*.

Wilschefski, S. & Baxter, M. (2019). Inductively Coupled Plasma Mass Spectrometry: Introduction to Analytical Aspects. *Clinical Biochemist Reviews*, 40 (3): 115-133. doi: 10.33176/aacb-19-00024.

WTW. (2017). Operating manual - VisoTurb® 900-P. In. Germany.

Zhou, X., Liu, D., Bu, H., Deng, L., Liu, H., Yuan, P., Du, P. & Song, H. (2018). XRD-based quantitative analysis of clay minerals using reference intensity ratios, mineral intensity factors, Rietveld, and full pattern summation methods: A critical review. *Solid Earth Sciences*, 3 (1): 16-29. doi: 10.1016/j.sesci.2017.12.002.

Appendices

A. Statistics

Table A1: *p-values form different t-tests performed for activities of Cs-137 in water, sediments, sequential extraction results and K_d. The t-test uses the mean value of Matrix 1 and Matrix 2 when estimating the p-value. Green cells contain significant p-values. FW=freshwater, SW=seawater.*

Sample type	Matrix 1	Matrix 2	p-value
Water	LMM	coloids	0,002
Sediment	Sand, all sites	Silt, All	0,11
	Silt, all	Clay, all	0,19
	Clay, all	Sand, All	0,16
	Sand, FW	Silt, FW	0,10
	Silt, FW	Clay, FW	0,35
	Clay, FW	Sand, FW	0,29
	Sand, SW	Silt, SW	0,07
	Silt, SW	Clay, SW	0,13
	Clay, SW	Sand, SW	0,07
	Sand, FW	Sand, SW	0,37
	Silt, FW	Silt, SW	0,002
	Clay, FW	Clay, SW	0,04
Sequential extraction	step 6, SW	step 6, FW	0,72
	residue, SW	residue, FW	0,72
	Step 6, clay	Step 6, silt	0,07
	residue, clay	residue, silt	0,07
Kd	sand, FW	Clay, FW	0,22
	silt, FW	sand, FW	0,18
	silt, FW	clay, FW	0,30
	sand, SW	Clay, SW	0,07
	silt, SW	sand, SW	0,38
	silt, SW	clay, SW	0,18
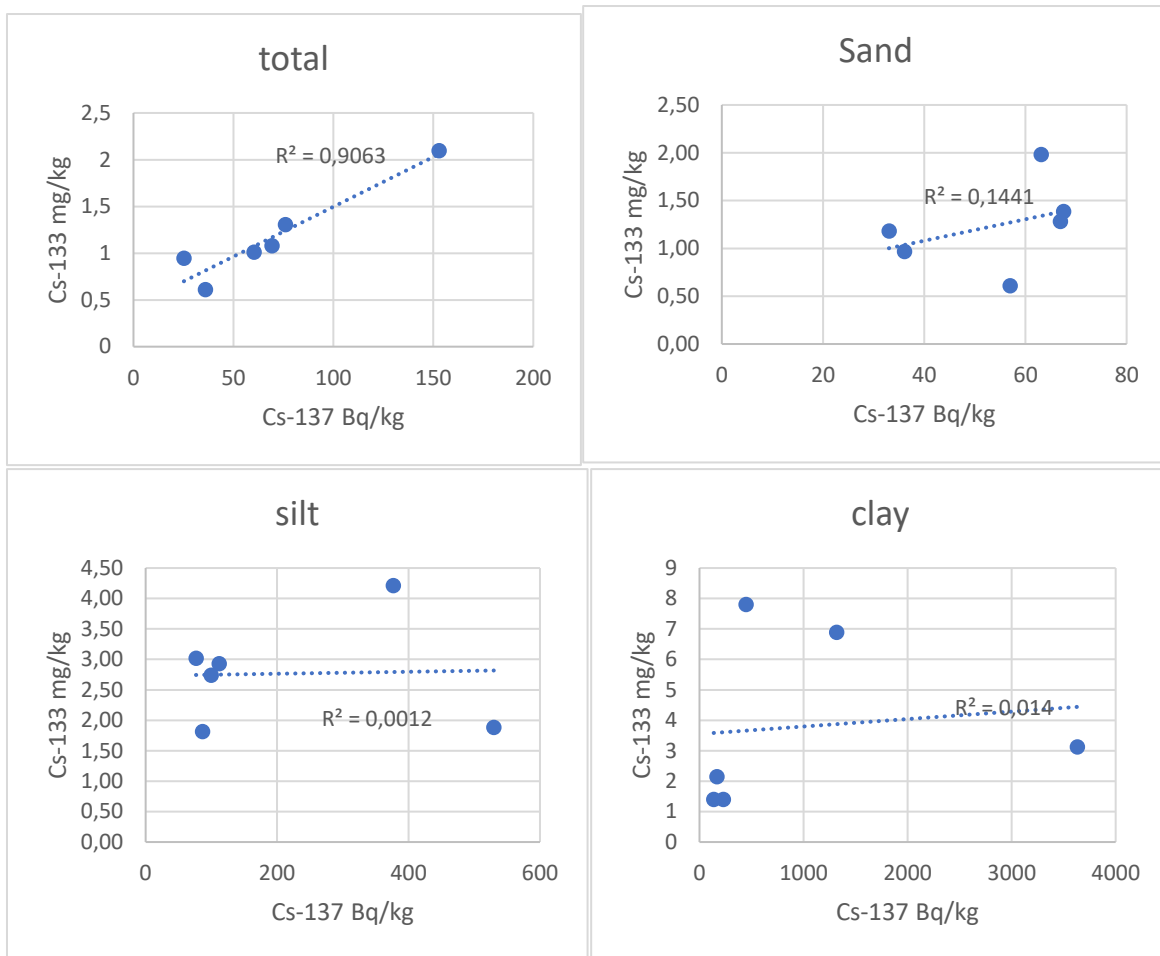
Figure A1*: Linear regression of the concentration of Cs-133 compared to Cs-137 in sediments and sediment fractions. Only total sediment sample showed a correlation between concentration of Cs-133 and Cs-137 in sediments, with R²=0.9.*
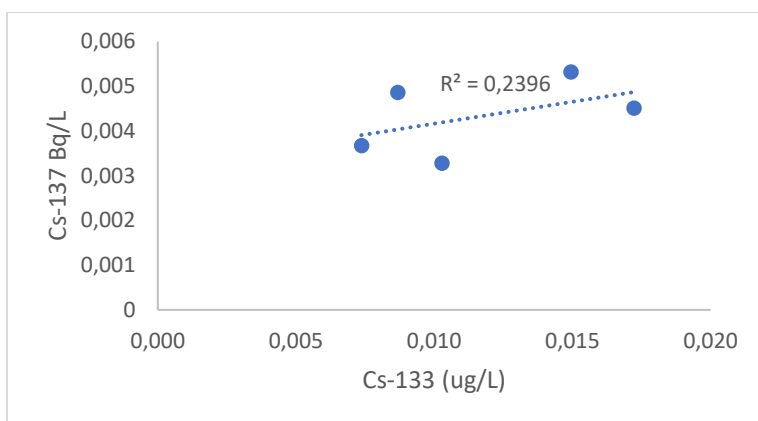
Figure A2: *Plot of Cs-133 (ug/L) against Cs-137 (Bq/L) to look for correlations between the two isotopes in the <0.45 µm fraction.*

B.1 Concentration and distribution of Cs-133 and Ca+ in water
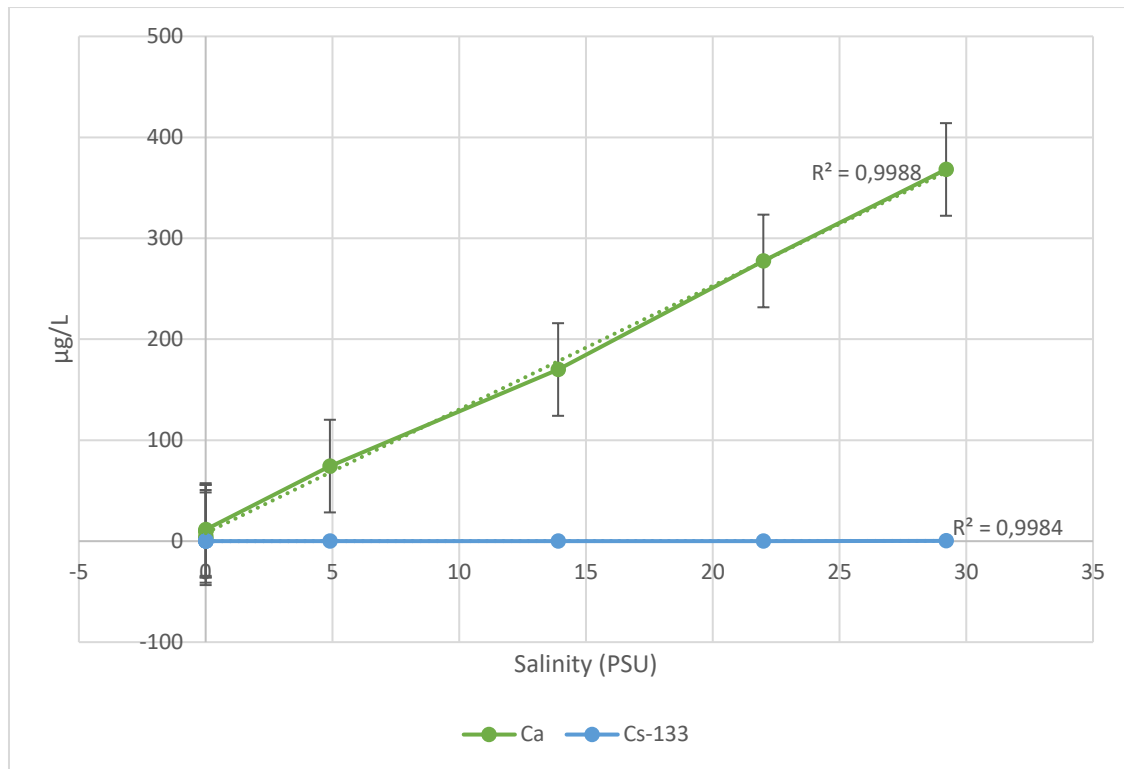
Figure B.1: *Plot of Cs-133 and Ca^{2+} concentrations as a function of salinity. Includes linear regression that illustrates the linearity of the plots, with R^2 vales indicating a good linear fit.*

Table B.1: *Calculation of relationship between cation/calcium based on standard values of seawater with an ionic strength of 35 PSU. The factor equals to theoretical concentration of cation divided by the concentration of measured Ca.*

Cation	standard (mg/kg)	factor (M^{n+}/Ca^{2+})
Ca	400	1
K	380	0,95
Na	10556	26,39
Mg	1262	3,155

Table B.2: *Concentration of Cs-133 (ug/L) (n=3) in LMM, colloids, <0.45 um, particles, and unfiltered fractions in freshwater from Vefsna river.*

Site	Salinity (PSU)	LMM	STD	Colloids	uncertainty	0.45 um	STD	Particles	uncertainty	unfiltered	STD
FW1	0	0,0079	0,00012	0,0008	0,0002	0,009	0,00014		0,001	0,011	0,0010
FW2	0	0,0072	0,00017073	0,0002	0,0002	0,007	0,00015		0,007	0,009	0,0002
FW3	0	NA	-			0,010	0,00014	0,0010	0,0003	0,011	0,0002
FW4	0	NA	-			0,015	0,00015	0,0069	0,002	0,022	0,0016
FW5	0	NA	-			0,017	0,00169	0,0114	0,009	0,029	0,0093
SW1	4,9	0,05	0,0017	0,0020	0,0023	0,054	0,00151		0,003	0,055	0,0018
SW2	13,9	0,13	0,0037	-0,0073	0,0055	0,123	0,00409		0,007	0,132	0,0042
SW3	22	0,20	0,0088	-0,0039	0,0142	0,200	0,01109		0,020	0,203	0,0146
SW4	29,2	0,26	0,0083	0,0010	0,0108	0,261	0,00689		0,012	0,261	0,0063

Table B.3: *Percentage distribution of Cs-133 in LMM, colloids, <0.45 um, and particles in freshwater from Vefsna river and seawater from the Vefsnfjord.*

Site	Salinity (PSU)	LMM	% RU	colloids	%RU	<0.45 um	%RU	particles	%RU
FW1	0	73,4	6,7	7,5	1,4	80,9	7,4		
FW2	0	78,6	2,8	2,3	1,7	80,9	2,7		
FW3	0	ND		ND		91,5	2,1	8,47	2,2
FW4	0	ND		ND		68,4	4,9	31,5	7,5
FW5	0	ND		ND		60,2	20,3	39,7	35,3
SW1	4,9	95,3	4,4	3,6	4,1	99,0	4,3		
SW2	13,9	98,6	4,2			93,1	4,2		
SW3	22	100,1	8,4			98,2	8,9		
SW4	29,2	99,6	3,9			100,0	3,5		

C. Activity and distribution of Cs-137 in water, yield of Cs-134

Table C.1: Yield obtained from measuring Cs-134 tracer.

Activity of yield = 6,282 Bq			
Site /filter size	Cs-134 (Bq)	uncertainty (%)	yield
FW1 <0,45um	4,297	1,02	0,684
FW1 LMM	4,245	1,34	0,676
FW2 <0,45um	4,241	1,23	0,675
FW2 LMM	4,166	1,11	0,663
FW3 <0,45um	4,946	0,7	0,787
FW4 <0,45um	4,626	0,78	0,736
FW5 <0,45um	4,879	1,14	0,777
SW1 <0,45um	4,999	1,21	0,796
SW1 LMM	5,229	0,9	0,832
SW2 <0,45um	4,465	0,9	0,711
SW2 LMM	4,785	1,2	0,762
SW3 <0,45um	4,465	1,01	0,711
SW3 LMM	4,419	1,94	0,703
SW4 <0,45um	4,738	1,45	0,754
SW4 LMM	4,267	0,98	0,679

Table C.2: Percentage LMM Cs-133 and Cs-137 present in the <0.45 um fraction in the Vefsnfjord.

Cs-137			Cs-133		
Sample site	% LMM	uncertainty	Site	% LMM	uncertainty
FW1	82	13	FW1	91	2
FW2	93	16	FW2	97	3
FW3	NA		FW3	NA	
FW4	NA		FW4	NA	
FW5	NA		FW5	NA	
SW1	95	9	SW1	96	2
SW2	102*	9	SW2	106*	5
SW3	137*	12	SW3	102*	4
SW4	116*	8	SW4	100	7

* More than 100% due to counting uncertainties.

Table C.3: *Activity concentration (Bq/kg) of Cs-137 in LMM, colloids, <0.45 um, and particles in water. N=1, uncertainty based on counting uncertainty.*

Site	LMM	Uncertainty	Colloids	Uncertainty	<0,45 um	Uncertainty	Particles	Uncertainty
FW1	0,0040	0,0006	0,00086316	0,00069751	0,00486316	0,00042504	0,0005537	8,72638E-05
FW2	0,0034	0,0005	0,00027328	0,00070319	0,00367328	0,00051279	<LOQ	
FW3					0,00327876	0,0002741	<LOQ	
FW4					0,00532015	0,00031548	<LOQ	
FW5					0,00450954	0,00045005	<LOQ	
SW1	0,0038	0,0004	0,00019299	0,0003693	0,00399299	0,00039411	<LOQ	
SW2	0,0051	0,0004	-9,4997E-05		0,005005	0,00039189	<LOQ	
SW3	0,0042	0,0004	-0,00114096		0,00305904	0,00022086	<LOQ	
SW4	0,0030	0,0002	-0,00042012		0,00257988	0,00034312	<LOQ	

Table C.4: *activity distribution (%) of Cs-137 in freshwater from Vefsna river.*

Sample site	LMM	uncertainty	Coloids	uncertainty	<0.45	uncertainty	Particles	uncertainty
FW1	73,8	14	16	13	90	14	10	2
FW2	92,6	20	7	19	100	18		
FW3					100	12		
FW4					100	8		
FW5					100	12		

Table C.5: *Activity distribution (%) of Cs-137 in seawater from the Vefsnfjord:*

Site	Salinity (PSU)	LMM	% RU	Colloids	%RU	Particles	% RU
FW1	0	74	13	16	2	10	0,2
SW1	4,9	95	12	5	0,4		
SW2	13,9	100	12				
SW3	22	100	13				
SW4	29,2	100	10				

D. Weights of particles and sediments, sediment distribution

Table: Filtered volumes (L) and weight of particles on membrane filter (g)

Site	LMM (L)	<0.45 (L)	Particles (g)
FW1	101,4	102,3	0,3287
FW2	101,3	101,7	0,0013
FW3		106,8	0,0006
FW4		104,5	0,0900
FW5		104,3	0,9829
SW1	102,4	127,9	0,0647
SW2	109,5	98,5	0,3120
SW3	203	195,7	0,5459
SW4	180,3	180,8	0,3971

Table: Weights and distribution (%) of sand, silt and clay from surface sediments.

Site	Weight [g]					Distribution [%]		
	Total	Sand	Silt	Clay + salt	Clay	Sand	Silt	Clay
FW2	507,82	457,60	2,64	0,13	0,13	90	0,5	0,03
FW1	3066	2927,90	10,70	2,48	2,48	95	0,3	0,08
SW1	149,60	71,30	67,30	9,29	1,29	48	45	1
SW4	138,13	48,70	76,40	8,67	0,67	35	55	0
SW5	58,42	6,54	49,50	9,00	1,00	11	85	2
SW6	58,75	2,39	50,30	8,95	0,95	4	86	2

E. Concentration and distribution of Cs-133 in sediments

Table E.1: Concentration of Cs-133 in sediments and sediment fractions of n=3 parallels.

Cs-133 (mg/kg d.w) in sediment fractions							
Site	Total	stdev	sand	stdev	silt	stdev	clay	stdev
FW2	0,61	0,05	0,61	0,04	1,88	0,02	6,88	0,11
FW1	0,95	0,14	1,18	0,05	4,21	0,72	3,13	0,11
SW1	1,01	0,13	1,39	0,10	1,81	0,17	7,80	0,38
SW4	1,08	0,03	0,97	0,07	2,74	0,26	1,39	0,04
SW5	1,31	0,02	1,98	0,06	2,93	0,16	1,40	0,06
SW6	2,10	0,38	1,28	0,03	3,02	0,33	2,14	0,15

Table E.2: Distribution (%) of Cs-133 in sand, silt and clay. N=3

Site	Sand	Uncertainty	Silt	Uncertainty	Clay	uncertainty
FW2	14	0,8	36	0,8	50	1,0
FW1	24	4,0	76	19	49	7,9
SW1	35	3,2	45	4,8	20	2,1
SW4	25	2,7	71	8,6	4	0,3
SW5	37	3,1	60	5,9	3	0,2
SW6	26	1,8	69	5,9	5	0,3

F. Activity and distribution of Cs-137 in sediments

Table F.1*: Sediment samples measured on the Ge-detector. Includes measured net area (counts), time (s), weight of sample (g), activity (Bq) and geometry.*

Site	Bulk/Core	Net area (co	net area +/-	Uncertainty	Time (s)	Weight (g (d	Bq	Bq/kg	Bq/kg +/-	Geometry
SW1	Bulk	17406	173	0,99	77670	151,3	9,11	60,22	0,60	Blue cap bottle 160 mL
SW4 (HI)	Bulk	939	40	4,26	3993	138,1	9,56	69,21	2,95	Blue cap bottle 160 mL
SW6 (HI)	Bulk	1112	54	4,86	10131	58,75	4,47	76,00	3,69	Blue cap bottle 160 mL
SW5 (HI)	Bulk	1070	42	3,93	4873	58,42	8,93	152,86	6,00	1/2 Blue cap bottle 80 mL
FW2	Bulk	12983	151	1,16	64860	251,3	8,14	32,39	0,38	Blue cap bottle 160 mL
FW2	Bulk	675	29	4,30	2975	256,5	9,23	35,98	1,55	Blue cap bottle 160 mL
FW1	Bulk	1794	46	2,56	1409	2057	51,85	25,21	0,65	Marinelli beaker 1000 mL
SW1	core 0-1 cm	4418	124	2,81	80914	15,0063	2,221	148,00	4,15	Plastic vial 20 mL
	core 1-2 cm	24241	286	1,18	429718	14,5266	2,295	157,99	1,86	Plastic vial 20 mL
	core 2-3 cm	5088	131	2,57	88674	15,8408	2,334	147,34	3,79	Plastic vial 20 mL
	core 3-4 cm	1351	64	4,74	23692	17,2862	2,32	134,21	6,36	Plastic vial 20 mL
	core 4-5 cm	14368	242	1,68	341119	8,6829	1,714	197,40	3,32	1/2 Plastic vial 10 mL
FW1	core A 0-1 cm	2405	128	5,32	101894	30,358	0,694	22,86	1,22	Plastic vial 20 mL
	core B 0-1 cm	2105	104	4,94	70276	30,5337	0,882	28,89	1,43	Plastic vial 20 mL
FW2	core 0-1 cm	3858	109	2,83	653525	28,4794	2,339	82,13	2,32	Plastic vial 20 mL
	core 1-2 cm	4617	124	2,69	81570	28,2259	2,3	81,49	2,19	Plastic vial 20 mL
	core 2-3 cm	1554	72	4,63	27503	27,523	2,296	83,42	3,87	Plastic vial 20 mL
	core 3-4 cm	9944	180	1,81	167183	26,096	2,42	92,73	1,68	Plastic vial 20 mL
	core 4-5 cm	22545	283	1,26	420208	25,1063	2,18	86,83	1,09	Plastic vial 20 mL
	core 5-6 cm	3756	117	3,12	75516	25,6765	1,465	57,06	1,78	Plastic vial 20 mL
	core 6-7 cm	4367	131	3,00	85724	23,9587	1,5	62,61	1,88	Plastic vial 20 mL
	Fraction									
FW1	Clay	24925	196	0,79	81079	2,48	9,005	3631,05	28,55	Plastic vial 10 mL
	silt	1003	48	4,79	7295	10,7	4,029	376,54	18,02	Plastic vial 20 mL
	Sand	2720	113	4,15	78650	30,68	1,013	33,02	1,37	Plastic vial 20 mL
FW2	Clay	5519	288	5,22	626384	0,12	0,158	1316,67	68,71	Plastic vial 10 mL
	Silt	3984	124	3,11	86192	2,64	1,3984	529,70	16,49	Plastic vial 10 mL
	Sand	18502	247	1,33	322864	29,46	1,678	56,96	0,76	Plastic vial 20 mL
SW1	Clay	7362	159	2,16	171790	1,29	0,5756	446,20	9,64	Plastic vial 20 mL
	Silt	744	35	4,70	3745	67,3	5,816	86,42	4,07	1/2 blue cap bottle 80 mL
	Sand	1155	45	3,90	7138	70,2	4,738	67,49	2,63	1/2 blue cap bottle 80 mL
SW4	Clay	2717	258	9,50	517736	0,67	0,1537	229,40	21,78	Plastic vial 20 mL
	Silt	790	34	4,30	3070	75,74	7,535	99,49	4,28	1/2 blue cap bottle 80 mL
	Sand	3739	116	3,10	63478	47,78	1,725	36,10	1,12	1/2 blue cap bottle 80 mL
SW5	Clay	1939	231	11,91	416760	1,00	0,1362	136,20	16,23	Plastic vial 20 mL
	Silt	1371	52	3,79	7286	49,25	5,51	111,88	4,24	1/2 blue cap bottle 80 mL
	Sand	11806	350	2,96	865267	6,37	0,4018	63,08	1,87	Plastic vial 10 mL
SW6	Clay	2789	260	9,32	519799	0,95	0,1581	166,42	15,51	Plastic vial 10 mL
	Silt	1152	49	4,25	8644	50,97	3,903	76,57	3,26	1/2 blue cap bottle 80 mL
	Sand	1880	204	10,8510638	346336	2,39	0,1598	66,86	7,26	Plastic vial 10 mL

Table F2*: Activity distribution of Cs-137 in sediments and sediment fractions.*

Site	Sand	% RU	Silt	%RU	Clay	%RU
FW1	66,8	4,8	5,2	5,4	11,6	2,6
FW2	63,6	5,9	8,0	5,3	0,9	6,7
SW1	52,0	4,0	56,8	4,8	6,3	2,3
SW4	18,0	5,2	78,8	6,0	1,6	10,4
SW5	43,7	5,6	61,7	6,1	1,5	12,8
SW6	3,5	11,5	87,3	5,7	3,5	10,1

G. Weights, concentration of Cs-133 and activity of Cs-137 from sequential extraction
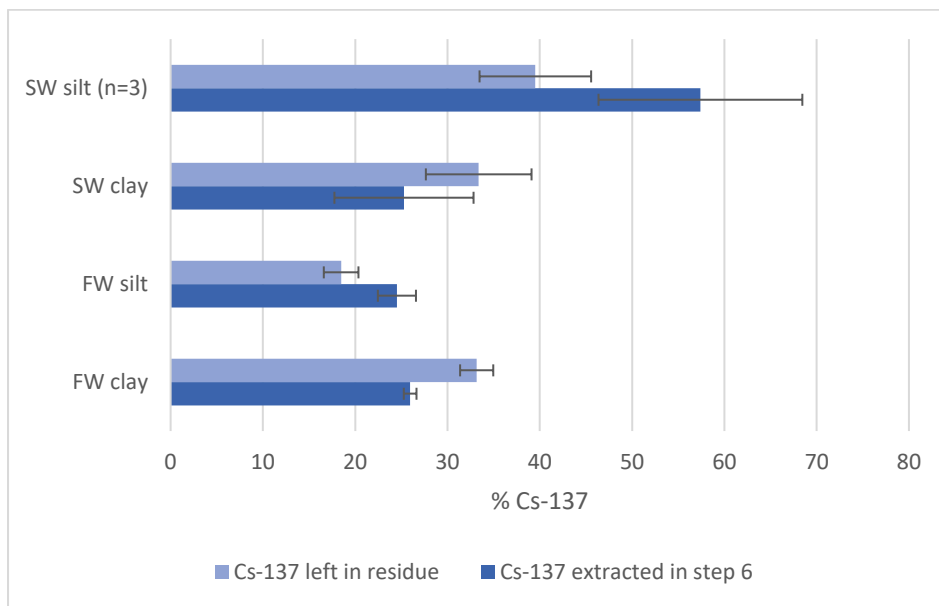
Figure G1: *Percentage Cs-137 extracted in step 6 of sequential extraction, and what is left in residue, based on estimated total activity.*

Table G1*: estimated total activity in samples used for sequential extraction.*

	weight (g)	Bq/kg in sample	Bq/g	Bq in sample	Uncertainty (%)	Bq +/-
FW clay	1,91	3631,0	3,6	6,9	0,8	0,1
FW silt	9,97	376,5	0,4	3,8	4,0	0,2
SW clay	10	210,0	0,2	2,1	9,0	0,2
SW silt, n=3	20,53	93,6	0,1	1,9	4,3	0,1

Table G2: *Initial weights and weights of residue after sequential extraction. The weight of SW clay is much lower than expected, only 1.7 g. However, weight is after weight of glove + filter has been subtracted, and each filter and glove were not weighted individually, causing some error. In addition, the weight of FW clay and SW silt were higher after the extraction, which means it must have been some moisture left in the residue.*

	Initial weight (g)	Residue (g)	vial	glove	filter
FW silt	9,97	8,7	6,4151	4,6	2,35
FW clay	1,91	2,8	6,4052	4,6	2,35
SW clay	30,24*	1,7	6,64431	4,6	2,35
SW silt 1	20,25	24,1	6,4054	4,6	2,35
SW silt 2	20,79	23,5	6,9083	4,6	2,35
SW silt 3	20,55	24,9	6,9519	4,6	2,35

*Total weight with salt.

Table G.3: *Concentration of Cs-133 leach out in step 1-6 of sequential extraction.*

Cs-133 mg/kg						
Sample	step 1	step 2	step 3	step 4	step 5	step 6
blank	<0	<LOD	<LOD	<LOD	<LOD	<LOD
blank	<0	<LOD	<LOD	<LOD	<LOD	<LOD
blank	<0	<LOD	<LOD	<LOD	<LOD	<LOD
FW leire	0,00269	0,0618	0,0949	0,248	0,374	330
FW silt	0,00201	0,0672	0,049	0,12	0,0683	77,5
SW leire	2,85	0,0344	0,00914	0,00254	0,119	21,3
SW silt 1	0,0838	0,024	0,0131	0,0276	0,132	93,2
SW silt 2	0,0746	0,0249	0,0288	0,0279	0,134	84,9
SW silt 3	0,0699	0,022	0,0125	0,0266	0,112	85,2
SW silt, n=3	0,076	0,024	0,018	0,0274	0,13	88
SW silt, +/-	0,0071	0,0015	0,0092	0,00068	0,012	4,7

Table G.4: *Distribution (%) of Cs-133 extracted in each sequential extraction step.*

% Cs-133 extracted						
Sample	step 1	step 2	step 3	step 4	step 5	step 6
FW clay	0,001	0,019	0,029	0,075	0,113	100
FW silt	0,003	0,086	0,063	0,154	0,088	100
SW clay	11,7	0,141	0,038	0,010	0,489	88
SW silt, n=3	0,09	0,027	0,021	0,031	0,143	100
SW silt uncertainty	0,11	0,082	0,512	0,059	0,110	0,08

Table G.5: *Activity of Cs-137 extracted from each step in sequential extraction. LOQ=0.17 Bq.*

Sample	Step 6 (Bq)	uncertainty (Bq)	stdav	Step 5	Step 4	Step 3	Step 2	Step 1	Filter	uncertainty (Bq)	stdav
FW clay	1,80	0,04		<LOQ	<LOQ	<LOQ	<LOQ	<LOQ	2,30	0,12	
FW silt	0,92	0,06		<LOQ	<LOQ	<LOQ	<LOQ	<LOQ	0,69	0,06	
SW clay	0,53	0,15		<LOQ	<LOQ	<LOQ	<LOQ	<LOQ	0,70	0,10	
SW silt (n=3)	1,09	0,20	0,05	<LOQ	<LOQ	<LOQ	<LOQ	<LOQ	0,75	0,11	0,02

Table G.6: *Distribution of Cs-137 in step 6 and residue, based on estimated total activity and calculated total of extract (step 6) + residue.*

	Percentage Cs-137 leached from S.E			
	From estimated total		From total = extract + residue	
Sample	Cs-137 extracted in step 6	Cs-137 left in residue	Cs-137 extracted step 6	Cs-137 left in residue
FW clay	26	33	44	56
FW silt	25	18	57	43
SW clay	25	33	43	57
SW silt (n=3)	57	40	59	41
	Uncertainties (% RU)			
Sample	Cs-137 extracted in step 6	Cs-137 left in residue	Cs-137 extracted step 6	Cs-137 left in residue
FW clay	1	2	2	3
FW silt	2	2	5	4
SW clay	8	6	14	12
SW silt (n=3)	11	6	13	8

H. Calculation of K$_d$ values

Table H.1: *Activity concentration in sediments and water used for calculating K$_d$ values.*

Site	Salinity (PSU)	Conc. Sediments [Bq/kg]	uncertainty (Bq/kg)	Conc. Water (<0.45 um) [Bq/L]	uncertainty (Bq/L)	Kd [L/kg]	Uncertainty
FW1	0	25	0,65	0,0049	0,00043	**5183**	**954**
FW2	0	36	1,55	0,0037	0,00032	**9796**	**472**
SW1	4,9	60	0,60	0,0040	0,00035	**15081**	**1327**
SW4	29,2	69	2,95	0,0026	0,00023	**26827**	**2608**
Cs-137 in sand fraction							
Site	Salinity (PSU)	Conc. Sediments [Bq/kg]		Conc. Water (<0.45 um) [Bq/L]		Kd [L/kg]	
FW1	0	33	1,37	0,0049	0,00043	**6789**	**1371**
FW2	0	57	0,76	0,0037	0,00032	**15506**	**657**
SW1	4,9	67	2,63	0,0040	0,00035	**16903**	**1617**
SW4	29,2	36	1,12	0,0026	0,00023	**13994**	**1298**
Cs-137 in silt fraction							
Site	Salinity (PSU)	Conc. Sediments [Bq/kg]		Conc. Water (<0.45 um) [Bq/L]		Kd [L/kg]	
FW1	0	377	18,02	0,0049	0,00043	**77427**	**13379**
FW2	0	530	16,49	0,0037	0,00032	**144203**	**7715**
SW1	4,9	86	4,07	0,0040	0,00035	**21643**	**2148**
SW4	29,2	99	4,28	0,0026	0,00023	**38562**	**3757**
Cs-137 in clay fraction							
Site	Salinity (PSU)	Conc. Sediments [Bq/kg]		Conc. Water (<0.45 um) [Bq/L]		Kd [L/kg]	
FW1	0	3631	28,6	0,0049	0,00043	**746643**	**36487**
FW2	0	1317	68,7	0,0037	0,00032	**358445**	**65520**
SW1	4,9	446,2	9,6	0,0040	0,00035	**111746**	**10061**
SW4	29,2	229	21,8	0,0026	0,00023	**88919**	**11475**

I. Concentrations and BCF of Cs-133 and Cs-137 in biota

Table I.1: *Measurement of Cs-137 in biota samples in Ge-detector. Read cell contains activity under detection limit.*

Sample	Site	Net area	Net area +/-	Uncertainty	Time	Weight	Activity (Bq)	Bq/kg	Geometry
Sea weed mix	Skjærflesa	2963	252	8,504893689	165541	730	0,5243	0,72	Marinelli beaker
Sea weed mix	Holand	4128	276	6,686046512	184647	1006	0,6549	0,65	Marinelli beaker
Blue mussels	Alterneset	188	157	83,5106383	86331	122	0,06377	0,52	Marinelli beaker
Sea weed mix	Alterneset, halsøya, river outlet	7051	321	4,552545738	243247	820	0,8491	1,04	Marinelli beaker

Table I.2: *Calculation of BCF.*

Sample site	Sea weed (Bq/kg)	Uncertainty (%)	uncertainty (Bq/kg)	Water (Bq/L)	uncertainty	BCF	uncertainty (%RU)
Alterneset, Halsøya, river outlet (mix)	1,04	4,552545738	0,04714106	0,0042	0,0003738	247	24,6
Skjærflesa (PSU ≈ 20)	0,72	8,504893689	0,06108378	0,0042	0,0003738	171	21,1
Holand (PSU ≈ 30)	0,65	6,686046512	0,04352576	0,003	0,0002187	217	21,5

Table I.3: *Concentration of Cs-133 in biota samples.*

	Cs- 133 (mg/kg)				
Site	Seaweed (*F.vesiculosus/L.digitata*)	uncertainty	Blue mussel (*M.edulis*)	uncertainty
River outlet (PSU ≈ 5)	0,086	0,003		
Halsøya (PSU ≈ 10)	0,026	0,00006		
Svarthamran (PSU ≈ 10)	0,023	0,002		
Skjærflesa (PSU ≈ 20)	0,023	0,001	0,018	0,003
Alterneset (PSU ≈ 25)	0,040	0,003	0,033	0,015
Holand (PSU ≈ 30)	0,091	0,007	0,027	0,003

Table I.4: *BCF in biota samples (Cs-133)*

Site	Approx. PSU	Seaweed (F.vesiculosus/L.digitata)	uncertainty	Blue mussel (M.edulis)	uncertainty
River outlet (PSU ≈ 5)	5	1587	71		
Halsøya (PSU ≈ 10)	10	211	7		
Svarthamran (PSU ≈ 10)	10	188	18		
Skjærflesa (PSU ≈ 20)	20	116	7	92	15
Alterneset (PSU ≈ 25)	25	203	19	166	77
Holand (PSU ≈ 30)	30	348	29	105	14

Table J.1: *Peaks used to identify mineral composition of XRD diffractograms.*

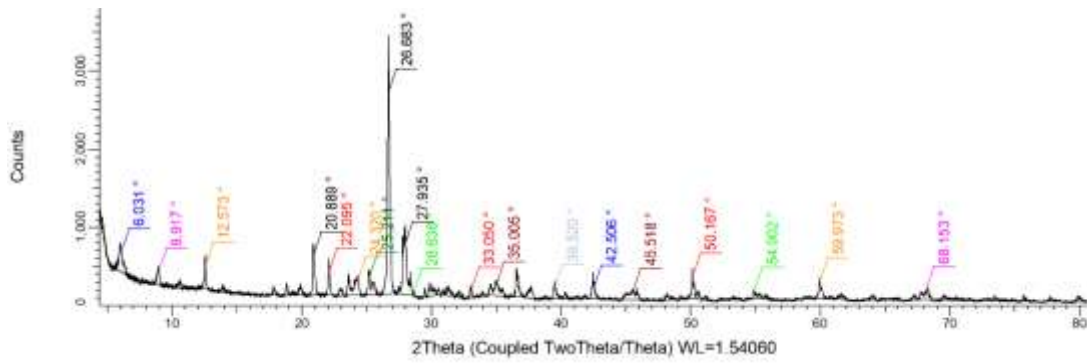| Sample	angle 2θ	Mineral	Sample	Angle	Mineral	Sample	Angle 2θ	Mineral	Sample	Angle 2θ	Mineral	Sample	Angle θ	Mineral	close peak, a
FW silt	6,031		SW silt	6,27		SW4 silt Fres	6,278		SW clay	11,708		SW4 clay freshwater			
	8,917			8,872			8,901			20,832			12,732		
	12,573			10,551			10,516			21,739			20,075	Muscovite	
	20,889	Quartz, Berlinite		12,537			12,533			24,756			21,126		
	22,095	Albite		18,865			13,879			27,739	Halite, SeTm, AgClNaO		25,395	CdCrO4	Muscovite
	24,32	Albite		19,85			17,827			24,756			26,897	As4Ba3Sn2	Muscovite
	25,211			20,889	Quartz, Berlinite		18,839			27,425			28,14		Muscovite
	26,683	Quartz, Berlinite		22,059	Albite		19,849			28,638			30,103		Muscovite
	27,935	Albite		22,91	albite		20,907	Quartz, Berlinite		29,202			31,898		
	28,636			24,346	Albite		22,098	Albite		31,783	Halite, SeTm, AgClNaO		32,273		
	33,05			26,665	Quartz, Berlinite		25,3			32,918			34,787	Muscovite	
	35,005	Albite		25,192			25,545			33,956			36,913		
	39,52	Quartz, Berlinite		27,893	Albite		26,69	Quartz, Berlinite		40,904			37,874		
	42,506	Quartz, Berlinite		29,487			27,953	Albite		45,509	Halite, SeTm, AgClNaO		40		
	45,518			31,727			28,337	Albite		50,652			45,419		Muscovite
	50,167	Quartz, Berlinite		32,065			34,57			53,888	SeTm, AgClNaO		60,09		
	54,902	Quartz		34,98	Albite		35,068	Albite		56,518	Halite, SeTm, AgClNaO		66,126		
	59,973	Quartz		36,573	Quartz		36,623	Quartz, Berlinite		66,248	Halite, SeTm, AgClNaO				
	68,153			37,637			37,74			75,287	Halite, SeTm, AgClNaO				
				39,5	Quartz		39,482	Quartz, Berlinite							
				42,481	Quartz, Berlinite		40,34	Quartz, Berlinite							
				45,454			42,503	Quartz, Berlinite							
				50,137	Quartz, Berlinite		45,08								
				54,895			45,922								
				56,448			48,172								
				59,956	Quartz		50,22	Quartz, Berlinite							
							51,165								
							54,965	Quartz							
							55,876								
							60,004	Quartz							
							61,6	Berlinite							

Figure J.1: *XRD scan of FW silt.*
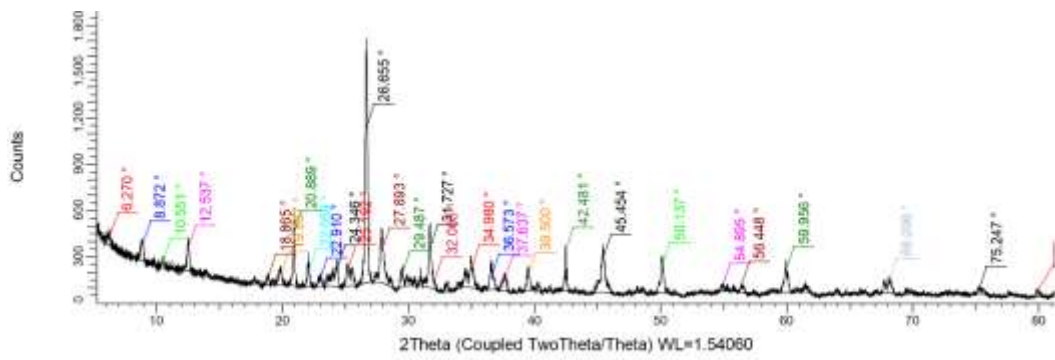

Figure J.2: *XRD scan of SW silt*

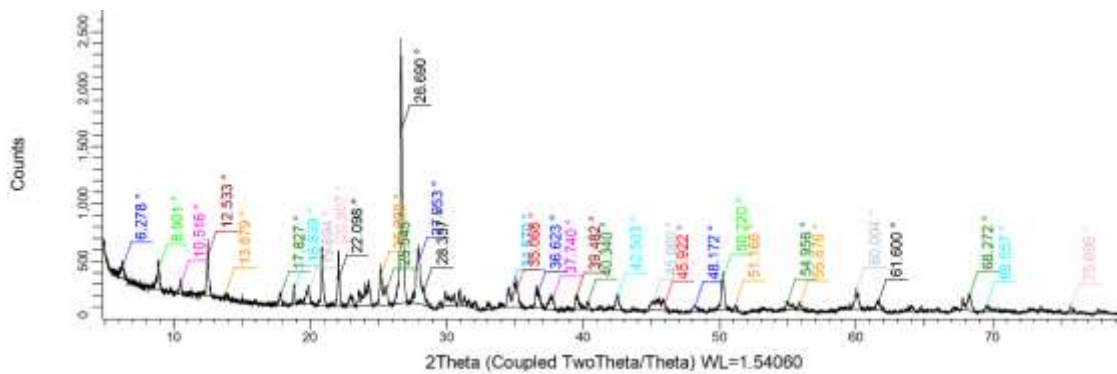***Figure J.3****: XRD scan of SW4 silt freshwater*
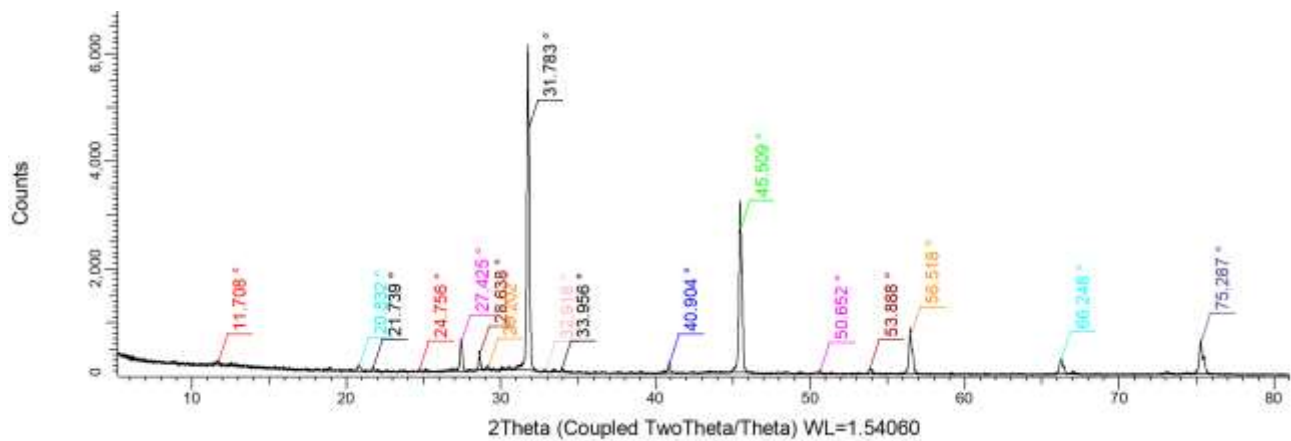
Figure J.4: *XRD scan of SW clay*
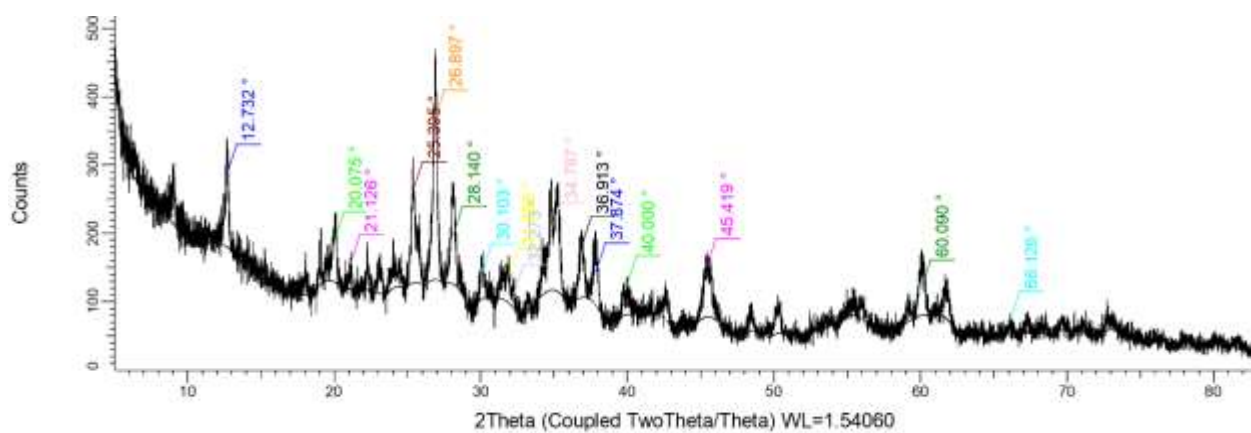
Figure J.5*: XRD scan of SW4 clay freshwater*